Biomolecule Substrate Topography of Inkjet Printed Structures

Liyakat Hamid Mujawar

Thesis committee

Promotor
Prof. Dr. ir. W. Norde
Emeritus Professor of Bionanotechnology
Wageningen University

Co-promotor
Dr. A. van Amerongen
Senior scientist
Food & Biobased Research, Wageningen UR

Other members
Prof. Dr. J.C.T. Eijkel   University of Twente, Enschede
Prof. Dr. R. O'Kennedy   Dublin City University, Ireland
Prof. Dr. J.G.M. Kuerten   Eindhoven University of Technology
Prof. Dr. H.F.J. Savelkoul   Wageningen University

Biomolecule Substrate Topography
of Inkjet Printed Structures

Liyakat Hamid Mujawar

Thesis

submitted in fulfillment of the requirement for the degree of doctor

at Wageningen University

by the authority of the Rector Magnificus

Prof. dr. M. J. Kropff,

in the presence of the

Thesis Committee appointed by the Academic Board

to be defended in public

on Monday 27th May 2013

at 11 a.m. in the Aula.

Dedicated to my dearest parents…………
especially for my beloved Papa……

Contents

1

General Introduction

In this chapter we briefly describe the utilization of inkjet printing technology in producing microarrays. The key aspects, i.e., the influence of substrate porosity and its chemistry on the functionality and distribution of inkjet printed biomolecules are discussed, followed by a brief overview of the experimental chapters. For the readers to get acquainted with the thesis, we have classified our work into three main parts: studies on non-porous substrates, on porous substrates and on the application of inkjet printing technology in the production of functional biochips. In the general discussion we exchange our views with respect to the work performed by other research groups, followed by a future prospect of our endeavour and conclude this thesis with a concise summary.

1.1 Inkjet printing

"Printing" commonly refers to a process of depositing dispersed colloidal particles onto any substrate surface. In the past, this well-designed method was used to deposit colloidal ink onto paper substrates (like newspapers, books, magazines), which is being continued even today by printing press industries. With the advancement of printing technology, engineers have shown that it is possible to print smaller drop volumes (in the micro or pico-litre range) of colloidal dispersions onto any substrate surface. These colloidal particles may be composed of biomolecules which can be deposited onto a substrate in a contact or non-contact mode[1]. Various types of contact and non-contact printing techniques are shown in Table 1.1.

Table 1.1 Various techniques used for depositing solute particles

Contact mode	Non-contact mode
Pin printing[2]	Inkjet printing[3-5]
Micro-stamping[6]	Electro-spray deposition[7]
Dip-Pen Nanolithography[8] (DPN)	Laser writing[9]

In the contact mode of printing, the substrate comes in direct contact with the depositing system (i.e., pin, stamp or pen). Pin-printing is one of the earlier techniques[2] in which solute particles are deposited onto a substrate surface. However, it is not easy to achieve high throughput printing due to uncontrollable drop volume which results in irregular spot size and uniformity[10]. Factors such as sample viscosity, pin contact area, pin surface properties, substrate surface properties mainly influence the spot reproducibility. In order to overcome these problems, researchers have designed solid[11], split[1] and silicon[12] pins to deposit solute particles. However, one of the major drawbacks in pin printing is that the substrate surface is in

direct contact with the stamp or pin due to which the chances of contamination and damaging the substrate and the pin are higher. To overcome the issue of reproducibility, the microstamping technique was designed. It is considered as a potential alternative for printing, in which the colloidal particles are deposited onto a substrate surface in the form of a monolayer[13,14]. Even though this is a robust and inexpensive technique, the major disadvantage is that the volume transferred onto the substrate surface is not reproducible. A more recent advancement in contact printing techniques is the nano-tip pin printing or, more commonly called, dip-pen nanolithography (DPN), based on atomic force microscopy (AFM). The AFM tip is used to produce submicron sized spots with high density of solute particles per spot[8]. The resolution of the spots is influenced by the relative humidity and surface roughness[15]. Even though it is possible to produce nanopatterns, the printing process is slow as compared to microstamping.

Using the non-contact mode of printing, the issues of nozzle damage, contamination, and low reproducibility can easily be eliminated. In this technique, contact with the substrate is completely avoided since the droplet is ejected from a certain distance on to the substrate. There are different ways of non-contact printing, like electro-spray deposition (ESD), laser writing and inkjet printing. In ESD, an activated electrostatic field between the substrate surface and the nozzle causes ejection of the liquid resulting in micron-sized spots. This is a fast mode for printing but the damage occurring to the solute particles (especially biomolecules) due to high shear rates and the activated electrostatic field is high. Moreover, irregular spot size and satellite drops were noticed by Morozov *et al.*[7] which make this technique less common.

Another non-contact printing technique which is familiar nowadays is inkjet printing. This technique permits to deposit small volumes of liquid onto any

substrate surface (porous and non-porous)[5]. The piezoelectric dispensing nozzle along with the robotic system makes inkjet printing a fast method to deposit colloidal particles in a high throughput manner. Even with common problems like droplet smearing and satellite droplets[16], researchers still find this technique more reliable than other available printing methods.

1.2 Inkjet printing of biomolecules

Inkjet printing technology, based on the principle of piezoelectricity, is one of the common non-contact printing techniques, which can deliver small droplets with reproducible volumes. In piezoelectric printers the droplets experience high shear rates while passing through the nozzle and under such conditions the risk of denaturing the biomolecules is high. This is especially the case for proteins, since they are structurally more fragile and, therefore, more sensitive to the extreme conditions of inkjet printing. Studies performed by Allain *et al.* demonstrated that DNA can be spotted with inkjet printers without any damage[5]. Furthermore, Okamoto *et al.* suggested that the elevated temperature of solutions spotted with inkjet printers may enhance DNA reaction times which is an added advantage[17].

Ever since this technology has been implemented, researchers have demonstrated printing of various solute particles like colloidal silver[18], polystyrene latex[19], polymers[20-22] or a range of biomolecules (carbohydrates[23-25], oligo[17,26], DNA[5,27] or antibodies[28,29]). In the middle of the 20th century Fienberg *et al.*[30, 31] demonstrated microdots based immunoassays to detect auto-immune disease. Two decades later Ekins came up with the 'ambient analyte theory' which predicted that in a bioassay miniaturization can lead to an increased detection sensitivity[32]. This theory was explained in detail by Templin *et al.*[33] (see Figure 1.1).
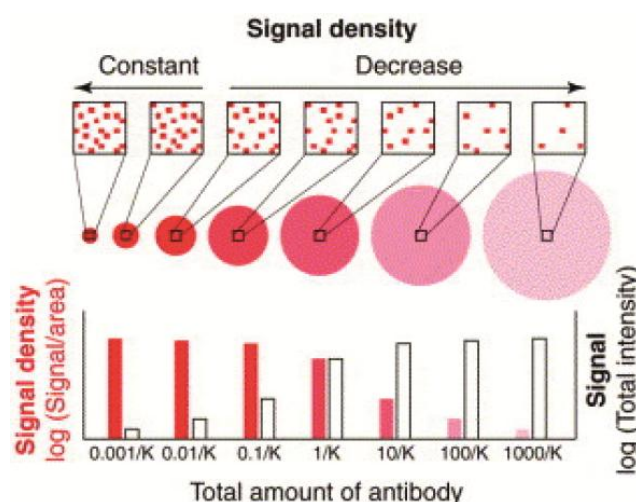
Figure 1.1 Schematic explanation of the 'ambient analyte theory' using signal and signal density in microspots. The signal (total intensity) increases with increasing amount of capture molecules and growing spot size whereas the signal density (signal/area) increases with decreasing amount of capture molecules (decreasing spot size). (*Adapted from Trends in Biotechnology (2002) 20(4): 160-166*.)

Post Ekins' theory, a new term ''microarray'' was coined for an array of various biomolecules produced onto substrate surfaces using inkjet printing technology[34, 35]. Since then, researchers have made immense progress in the field of microarrays, especially in producing DNA microarrays[36, 37]. With the advent of high-throughput molecular biology and DNA microarrays, researchers were trying to focus on producing microarrays for other biomolecules as well, antibodies in particular. With the advancement of immunoassays, researchers believed that there was a need to produce antibody microarrays that could mimic ELISA-like tests on to solid substrates to detect more than one pathogen simultaneously. However, the manufacturing of DNA microarrays cannot be easily translated into the production of protein microarrays due to the fundamental biophysical and biochemical differences between the two classes of biological substances: DNA primarily comprises only four nucleotides whereas proteins are formed from twenty different amino acids. This makes

proteins, being chemically and structurally more complex than nucleic acids, more prone to lose their structure and biochemical activity due to denaturation, dehydration or oxidation. Moreover, the affinities of the printed antibodies to bind antigens (target molecules) were found to be reduced upon immobilization[38]. Despite of these complications, researchers managed to produce microarrays for diagnostic applications[39,40] that can detect multiple analytes on the same substrate[41-46]. This new generation of inkjet printed microarrays (of biomolecules) onto a substrate surface are more familiarly known as biochips.

1.3 Substrate surface used for printing biomolecules

Using inkjet printing technology, it is possible to print various biomolecules on to any substrate surface (porous or non-porous). However, when printing proteins it is important to consider two important parameters; firstly to preserve the folded conformation of a protein biomolecule so that the functionality of the printed biomolecule is maintained and secondly to obtain homogenously distributed protein molecules in the spots on the substrate surface. Both these parameters are mainly influenced by temperature, relative humidity[47-49], substrate chemistry and surface and printing buffer[50] (pH and composition).

1.3.1 Non-porous substrates

With increasing demand of microarrays, researchers managed to develop microarrays for various biomolecules on non-porous substrates like gold[51], non-porous silicon[52], glass[53-55] and plastic[56]. Due to their low costs, glass and plastic are an excellent choice of non-porous substrates for printing biomolecules.

In inkjet printing, glass is considered as one of the first choices as a substrate surface, since it is readily available, chemically inactive and mechanically stable.

The chemistry of immobilizing target biomolecules (proteins) on a glass slide is based on either physical adsorption via non-covalent binding of proteins or covalent bonding between amino acids of the proteins and functional groups on the slide. Native glass slides are functionalized with various silanes which can be used as substrates for printing biomolecules. Most of the glass silanization have been performed by 3-glycidoxypropyltrimethoxy-silane (GPTS), since epoxide groups of the silane react with primary amino groups of the protein forming a covalent bond, as shown by Kusnezow *et al.*[50,57]. They also showed the possibility to bind protein molecules containing free amino or thiol groups on slides modified with NHS ester silane. The improved signal was ascribed to higher binding efficiency of the protein molecule on modified glass substrate as compared to unmodified glass[58]. Apart from modifying the glass with various silanes MacBeath and Schreiber also demonstrated that protein molecules can be bound onto glass slides that were functionalized with aldehyde groups, forming imine-bonds with the primary amino groups of proteins[59]. Haab *et al.* showed that it is possible to perform antibody-antigen assays on glass slides functionalized with poly-L-lysine[60].

The potential alternative for printing biomolecules on a non-porous substrate other than glass is plastic. The main advantage of using plastic is its low production cost and robustness, making it less prone to damage as compared to glass. The use of organic polymers in constructing analytical micro-devices for diagnostics is one of the emerging areas of research[61]. Various forms of plastic-like polymethyl methacrylate[62, 63](PMMA), polycarbonate[64] (PC), polyethylene terephthalate[56] (PET), polystyrene (PS) were demonstrated as a potential material for producing substrates for microarrays. These organic polymer substrates can be easily subjected to modification to produce high throughput microarrays as demonstrated by Moschallski *et al.*[65]. On the non-porous

substrates like glass or polystyrene, optimization of the buffer system is needed to produce high throughput microarrays. Printing of biomolecules (antibodies) onto a polystyrene surface has been demonstrated using various printing buffers like phosphate buffered saline[66] (pH 7.4) and carbonate buffer[67] (pH 9.6).

1.3.2 Porous substrates

Microarrays produced on non-porous substrates have gained a lot of attention, but researchers have showed that binding and correct orientation of bound biomolecules can be improved by producing microarrays on porous substrates[68,69]. It has been demonstrated that biomolecules upon immobilization on non-porous substrate like polystyrene and silicon tend to denature and lose its functional activity[70]. The need to maintain the folded conformation and activity of the immobilized protein molecule on the substrate surface triggered the researchers to produce microarrays on a range of porous substrates like nitrocellulose[69, 71, 72], porous silicon[73-75], porous alumina[76] and hydrogels[65, 77].

Of all the available porous substrates, most of the diagnostic research has been performed on nitrocellulose (NC) membranes. For almost six decades NC has been used as a substrate in biological research[78] and nowadays glass slides coated with a NC membrane in pad-format (~11 μm thick) are used as a substrate for producing microarrays. The 3-D matrix of porous NC membranes increases the effective surface area[79] and helps in efficient binding of the printed biomolecule, which in turn increases the signal-to-noise ratio[69] of the bioassay. It has been shown that assays performed on NC substrates have a lower detection limit as compared to other non-porous substrates[45,80]. Due to the ease in obtaining high throughput signals[71], efforts have been made to produce biochips from NC materials which can be used in diagnostic applications[4,81-83].

1.4 Distribution of biomolecules

Over more than a decade, researchers have shown interest in understanding the distribution of inkjet printed biomolecules onto substrate surfaces. It has been often observed that, upon inkjet printing, the biomolecules within the spot are non-homogenously distributed throughout the spot area, i.e., the biomolecules within the spot tend to concentrate more on the edges[84]. The resulting morphology of the dried spot resembles a "doughnut" and, hence, is called a doughnut-shaped morphology, studied in detail by Deegan *et al.* as the 'coffee-stain' effect[85]. They showed that the pinning of the contact line of the drop during evaporation[79] leads to a higher mass concentration at the edges of the spot (see Figure 1.2-A,B).
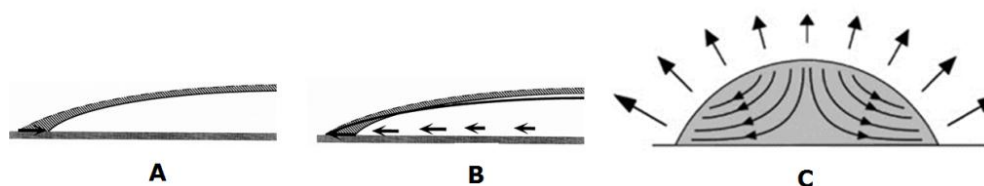

Figure 1.2 Schematic explanation of doughnut-shaped spot formation. (A) The result of evaporation without flow: the droplet shrinks. (B) The compensating flow needed to keep the contact line fixed. *(Adapted from Nature, 2000, 389, by Deegan et al.)* (C) Evaporation-driven convection that leads to ring analyte deposition on planar substrates with pinned drop contact line. *(Adapted from Biotechnology Annual Review, 2007, 13, by Ressine et al.)*

Later, Ressine *et al.* explained this non-homogenous distribution phenomenon by the evaporation-driven internal convection that takes place within a droplet with a pinned contact line[75]. The convection flow from the center of the droplet drives the biomolecules more to the edges, especially in droplets with a low contact angle. The resulting morphology of the spot is visible as a 'coffee-stain' or 'doughnut-like shape' (see Figure 1.2-C).

Irrespective of the substrate used, doughnut-shaped spot morphology was observed on both porous and non-porous substrates. Various strategies have been implemented to eliminate this spot morphology. Incorporating various additives like DMSO[86], CHAPS[87] or polyvinyl alcohol[88] can help to overcome doughnut-shaped spot morphology on the substrate surface. Earlier, Deng *et al.* showed that by incorporating Triton-X 100 in the printing buffer, the doughnut-shaped spots can be eliminated and an evenly distributed spot morphology can be obtained[89] (see Figure 1.3-A,B). Wu *et al.* showed that printing biomolecules in the presence of betaine results in a microarray with better spot homogeneity[90].
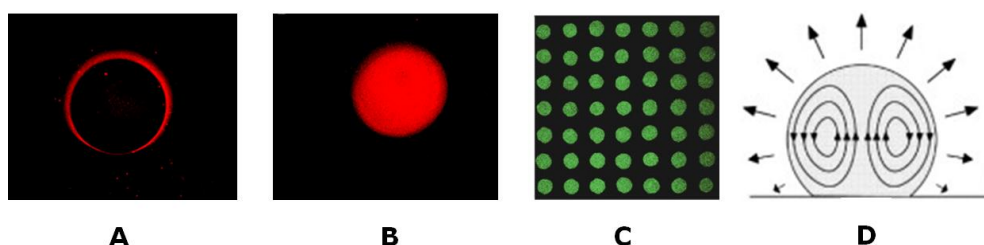

A **B** **C** **D**

Figure 1.3 (A) Doughnut-shaped spots of fluorophore labelled biomolecules on amino silanized glass slide. (B) Homogeneous spot by incorporation of Triton-X 100. *(A and B are adapted from* Journal of the American Chemical Society, 2006, 128 *by Deng et al.)* (C) Homogeneous spots on macro-porous silicon (D) Schematic representation of the advection process resulting in a homogeneous distribution of an analyte in the high contact angle droplet on an ultra-hydrophobic substrate *(C and D are adapted from* NanoBiotechnology, 2008, 4, *by Ressine et al.)*

Ressine *et al.* have shown that instead of incorporating any form of additive in the printing buffer, which may influence the functionality of the biomolecule, a homogenous distribution of inkjet printed spots can be obtained on ultra-hydrophobic nanoporous silicon substrates[74] (see Figure 1.3-C). They showed that on such substrates the high contact angle of a sessile drop causes a circulating convection flow (due to Maragoni stress) within the droplet that results in an intensive mixing of the analyte during the process of evaporation

thus balancing the convection flow of the analytes to the edges (i.e., eliminating the coffee-stain effect) (see Figure 1.3-D). Moreover, recently Eral *et al.* demonstrated that the particles in the sessile drop distribute homogenously by using a process of electro-wetting[91].

1.5 Aim and scope of the thesis

The importance of droplet evaporation in inkjet printing is very clear since it substantially increases the viscosity of the fluid and the concentration of solute. In (protein) microarrays, this process has a large influence on the shape of the deposited droplet and the distribution of (bio)molecules on the substrate. In this project we intend to understand the influence of various parameters on the evaporation of solvent from a droplet and on the distribution of (bio)molecules on (non-porous) and in (porous) various substrates. Especially the substrate properties like wettability and porosity may play an important role in the functionality of printed microarrays. Porous substrates are often used as microarray substrates due to their high surface/volume ratio, which results in a higher binding capacity of the capture probes per unit substrate surface area. In case of a porous substrate, various properties like porosity, pore size and pore size distribution may also play a significant role in the interaction of (bio)molecules with the substrate and the 3-dimensional distribution of the probes.

Therefore, our aim was to understand the phenomena that determine the distribution of the biomolecules in the printed spots and how these influence the functionality of the biomolecules on the various substrate surfaces.

In **Chapter 2** we describe the influence of buffers of varying compositions and pH on the distribution and spot morphology of biomolecules on a polystyrene substrate. Atomic force microscopy was used to characterize the morphological

patterns on printed biomolecule spots, whereas the distribution of the protein molecules was analyzed by confocal fluorescence microscopy. We also compared the influence of the printing buffer composition on the performance of a diagnostic assay and evaluated the compatibility of the buffer system for polystyrene-based biochips.

In **Chapter 3** we report on the influence of substrate hydrophobicity on the distribution of the inkjet printed biomolecules. Pristine glass slides were modified using various silanes resulting in surfaces with varying hydrophobicities with water contact angles (θ) of 49°, 61°, 75°, 88° and 103°, respectively. Microarrays of the biomolecules produced on the silanized glass substrates were compared with those produced on pristine (untreated) glass and (θ <10°) and on HTA polystyrene slide (θ ~92°). Finally, a diagnostic antibody assay was carried out on these non-porous substrates to assess the influence of substrate hydrophobicity on the performance of the bioassay.

In **Chapter 4** we present a mathematical model for the fluid dynamics and the distribution of the solute molecules at different humidities (40% / 50% / 60% / 70% and 80%). The theoretical results on mass distribution in the dried spot were compared to the experimental data obtained by printing fluorophore labeled biomolecules on non-porous substrates. Using confocal laser scanning microscopy, we analyzed the spot morphology and distribution profile of the biomolecules in the spots upon drying at various relative humidities.

In Chapter 5, 6 and 7 we describe the inkjet printed microarrays on porous nitrocellulose substrate.

In **Chapter 5** we illustrate the difference in protein biomolecules distribution in the nitrocellulose membrane pads of slides from three different manufacturers, i.e., GE Whatman (FAST), Sartorius-Stedim Biotech (Unisart) and Grace-Biolabs (Oncyte-Avid). The morphology and distribution of the biomolecules down

into the nitrocellulose membrane were analyzed by using confocal laser scanning microscopy in the 'Z' stack mode. Various properties of the nitrocellulose membranes like the wettability and the fluid flow dynamics were investigated by monitoring the droplet with high-speed cameras installed at three positions on a microscope (side, top and bottom-view).

In **Chapter 6** we present the influence of an additive, Pluronic F127, on inkjet printed spots. The influence of the additive concentration on the distribution as well as the functionality of the printed antibody molecules was also investigated. By performing a diagnostic assay, the influence on the final assay fluorescence signal, as characterized by confocal laser scanning microscopy at 10x magnification and 'Z' stack mode, was determined as well.

In **Chapter 7** we describe the application of the inkjet printing technology in developing diagnostic biochips. In a nucleic acid microarray immunoassay (NAMIA), double-tagged PCR amplicons were sandwiched between printed tag-specific antibodies and carbon nanoparticles having an alkaline phosphatase-neutravidin conjugate at their surface in an one-step incubation. The final assay signal was read by a flatbed scanner or via naked eyes. The assay spots were further analyzed by image analysis to measure the signal intensity in pixel gray volume (PGV).

Finally, in **Chapter 8** we present a general discussion of our studies followed by an outlook of the value of our results on the advancement of the inkjet printing technology. The summary of our work is presented at the end of this thesis.

References

1.   I. Barbulovic-Nad, M. Lucente, Y. Sun, M. Zhang, A. R. Wheeler and M. Bussmann, *Critical Reviews in Biotechnology*, 2006, **26**, 237-259.

2.   M. Schena, D. Shalon, R. W. Davis and P. O. Brown, *Science*, 1995, **270**, 467-470.

3.   T. Fan-Gang, K. Chang-Jin and H. Chih-ming, *Microelectromechanical Systems, Journal of*, 2002, **11**, 437-447.

4.   P. S. Noguera, G. A. Posthuma-Trumpie, M. van Tuil, F. J. van der Wal, A. d. Boer, A. P. H. A. Moers and A. van Amerongen, *Analytical Chemistry*, 2011, **83**, 8531-8536.

5.   L. Allain, M. Askari, D. Stokes and T. Vo-Dinh, *Fresenius Journal of Analytical Chemistry*, 2001, **371**, 146-150.

6.   Y. Xia and G. M. Whitesides, *Angew. Chem. Int. Ed.*, 1998, **37**, 550-575.

7.   V. N. Morozov and T. Y. Morozova, *Analytical Chemistry*, 1999, **71**, 3110-3117.

8.   K.-B. Lee, S.-J. Park, C. A. Mirkin, J. C. Smith and M. Mrksich, *Science*, 2002, **295**, 1702-1705.

9.   B. R. Ringeisen, P. K. Wu, H. Kim, A. Piqué, R. Y. C. Auyeung, H. D. Young, D. B. Chrisey and D. B. Krizman, *Biotechnol Progress*, 2002, **18**, 1126-1129.

10.   D. Rose, *Microfluidic technologies and instrumentation for printing DNA microarrays*, Eaton Publishing, Natick, MA 2000.

11.   M. L. Mace, J. Montagu, S. D. Rose and G. M. McGuinness, *Novel microarray printing and detection technologies*, Eaton Publishing, Natick, MA 2000.

12.   J. Tsai and K. Chang Jin, A silicon micromachined pin for contact droplet printing, 2002.

13.   A. Kumar and G. M. Whitesides, *Applied Physics Letters*, 1993, **63**, 2002-2004.

14.   X.-M. Zhao, Y. Xia and G. M. Whitesides, *Journal of Materials Chemistry*, 1997, **7**, 1069-1074.

15.   R. D. Piner, J. Zhu, F. Xu, S. Hong and C. A. Mirkin, *Science*, 1999, **283**, 661-663.

16.   T. Fan-Gang, K. Chang-Jin and H. Chih-ming, *Microelectromechanical Systems, Journal of*, 2002, **11**, 427-436.

17.   T. Okamoto, T. Suzuki and N. Yamamoto, *Nature Biotechnology*, 2000, **18**, 438-441.

18.   H. H. Lee, K. S. Chou and K. C. Huang, *Nanotechnology*, 2005, **16**, 2436-2441.

19.   Y. Mori and K. Zaitsu, *Journal of Chemical Engineering of Japan*, 2004, **37**, 657-661.

20.   H. Sirringhaus, T. Kawase, R. H. Friend, T. Shimoda, M. Inbasekaran, W. Wu and E. P. Woo, *Science*, 2000, **290**, 2123-2126.

21.   E. Tekin, P. J. Smith and U. S. Schubert, *Soft Matter*, 2008, **4**, 703-713.

22.   H. Yan, Z. Chen, Y. Zheng, C. Newman, J. R. Quinn, F. Dötz, M. Kastler and A. Facchetti, *Nature*, 2009, **457**, 679-686.

23. B. T. Houseman and M. Mrksich, *Chemistry & Biology*, 2002, **9**, 443-454.

24. O. Michel and B. J. Ravoo, *Langmuir*, 2008, **24**, 12116-12118.

25. D. Wang, S. Liu, B. J. Trummer, C. Deng and A. Wang, *Nature Biotechnology*, 2002, **20**, 275-281.

26. A. P. Blanchard, R. J. Kaiser and L. E. Hood, *Biosensors and Bioelectronics*, 1996, **11**, 687-690.

27. T. Goldmann and J. S. Gonzalez, *Journal of Biochemical and Biophysical Methods*, 2000, **42**, 105-110.

28. J. Delehanty and F. Ligler, *Biotechniques*, 2003, **34**, 380-385.

29. J. B. Delehanty and F. S. Ligler, *Analytical Chemistry*, 2002, **74**, 5681-5687.

30. J. G. Feinberg, *Nature*, 1961, **192**, 985-986.

31. J. G. Feinberg and A. W. Wheeler, *Journal of Clinical Pathology*, 1963, **16**, 282-284.

32. R. P. Ekins, *Journal of Pharmaceutical and Biomedical Analysis*, 1989, **7**, 155-168.

33. M. F. Templin, D. Stoll, M. Schrenk, P. C. Traub, C. F. Vöhringer and T. O. Joos, *Trends in Biotechnology*, 2002, **20**, 160-166.

34. R. Ekins and F. W. Chu, *Trends in Biotechnology*, 1999, **17**, 217-218.

35. R. P. Ekins, *Clinical Chemistry*, 1998, **44**, 2015-2030.

36. T. Nakanishi, T. Oka and T. Akagi, *Acta Med Okayama*, 2001, **55**, 319 - 328.

37. S. Taylor, S. Smith, B. Windle and A. Guiseppiâ€◉Elie, *Nucleic Acids Research*, 2003, **31**, e87.

38. R. A. Vijayendran and D. E. Leckband, *Analytical Chemistry*, 2000, **73**, 471-480.

39. C. A. K. Borrebaeck, *Immunology Today*, 2000, **21**, 379-382.

40. M. Hartmann, J. Roeraade, D. Stoll, M. F. Templin and T. O. Joos, *Analytical and Bioanalytical Chemistry*, 2009, **393**, 1407-1416.

41. B. Schweitzer, S. Roberts, B. Grimwade, W. Shao, M. Wang, Q. Fu, Q. Shu, I. Laroche, Z. Zhou, V. T. Tchernev, J. Christiansen, M. Velleca and S. F. Kingsmore, *Nature Biotechnology*, 2002, **20**, 359-365.

42. M. T. McBride, S. Gammon, M. Pitesky, T. W. O'Brien, T. Smith, J. Aldrich, R. G. Langlois, B. Colston and K. S. Venkateswaran, *Analytical Chemistry*, 2003, **75**, 1924-1930.

43. H. Du, W. Yang, W. Xing, Y. Su and J. Cheng, *Biomedical Microdevices*, 2005, **7**, 143.

44.   G. P. Anderson, R. Matney, J. L. Liu, A. Hayhurst and E. R. Goldman, *BioTechniques*, 2007, **43**, 806-811.

45.   D. A. Fici, W. McCormick, D. W. Brown, J. E. Herrmann, V. Kumar and Z. L. Awdeh, *Journal of Immunological Methods*, 2010, **363**, 60-66.

46.   L. G. Mendoza, P. McQuary, A. Mongan, R. Gangadharan, S. Brignac and M. Eggers, *Biotechniques*, 1999, **27**, 778-788.

47.   V. H. Chhasatia, A. S. Joshi and Y. Sun, *Applied Physics Letters*, 2010, **97**, 231909-231903.

48.   C. Liu, E. Bonaccurso and H.-J. Butt, *Physical Chemistry Chemical Physics*, 2008, **10**, 7150-7157.

49.   M. J. Mackel, S. Sanchez and J. A. Kornfield, *Langmuir*, 2006, **23**, 3-7.

50.   W. Kusnezow, A. Jacob, A. Walijew, F. Diehl and J. D. Hoheisel, *Proteomics*, 2003, **3**, 254-264.

51.   P. Pavlickova, N. M. Jensen, H. Paul, M. Schaeferling, C. Giammasi, M. Kruschina, W.-D. Du, M. Theisen, M. Ibba, F. Ortigao and D. Kambhampati, *Journal of Proteome Research*, 2002, **1**, 227-231.

52.   R. Lenigk, M. Carles, N. Y. Ip and N. J. Sucher, *Langmuir*, 2001, **17**, 2497-2501.

53.   H. Zhu, M. Bilgin, R. Bangham, D. Hall, A. Casamayor, P. Bertone, N. Lan, R. Jansen, S. Bidlingmaier, T. Houfek, T. Mitchell, P. Miller, R. A. Dean, M. Gerstein and M. Snyder, *Science*, 2001, **293**, 2101-2105.

54.   B. Joos, H. Kuster and R. Cone, *Analytical Biochemistry*, 1997, **247**, 96-101.

55.   Y.-H. Rogers, P. Jiang-Baucom, Z.-J. Huang, V. Bogdanov, S. Anderson and M. T. Boyce-Jacino, *Analytical Biochemistry*, 1999, **266**, 23-30.

56.   Y. Liu, C. M. Li, W. Hu and Z. Lu, *Talanta*, 2009, **77**, 1165-1171.

57.   W. Kusnezow and J. D. Hoheisel, *Journal of Molecular Recognition*, 2003, **16**, 165-176.

58.   R. L. DeRosa, J. A. Cardinale and A. Cooper, *Thin Solid Films*, 2007, **515**, 4024-4031.

59.   G. MacBeath and S. L. Schreiber, *Science*, 2000, **289**, 1760-1763.

60.   B. Haab, M. Dunham and P. Brown, *Genome Biology*, 2001, **2**, research0004.0001 - research0004.0013.

61.   J. S. Rossier, A. Schwarz, F. Reymond, R. Ferrigno, F. Bianchi and H. H. Girault, *ELECTROPHORESIS*, 1999, **20**, 727-731.

62.   F. Fixe, M. Dufva, P. Telleman and C. B. V. Christensen, *Nucleic acids research*, 2004, **32**, e9.

63.   F. Fixe, M. Dufva, P. Telleman and C. B. V. Christensen, *Lab on a Chip*, 2004, **4**, 191-195.

64.   Y. Li, Z. Wang, L. M. L. Ou and H. Z. Yu, *Analytical Chemistry*, 2007, **79**, 426-433.

65.   M. Moschallski, J. Baader, O. Prucker and J. Rühe, *Analytica Chimica Acta*, 2010, **671**, 92-98.

66.   H. Sølling and B. Dinesen, *Clinica Chimica Acta*, 1983, **130**, 71-83.

67.   K. Sollier, C. A. Mandon, K. A. Heyries, L. J. Blum and C. A. Marquette, *Lab on a Chip*, 2009, **9**, 3489-3494.

68.   E. J. Irvine, A. Hernandez-Santana, K. Faulds and D. Graham, *Analyst*, 2011, **136**, 2925-2930.

69.   J.-G. Walter, F. Stahl, M. Reck, I. Praulich, Y. Nataf, M. Hollas, K. Pflanz, D. Melzner, Y. Shoham and T. Scheper, *Eng. Life Sci.*, 2010, **10**, 103-108.

70.   J. E. Butler, *Methods*, 2000, **22**, 4-23.

71.   B. A. Stillman and J. L. Tonkinson, *BioTechniques*, 2000, **29**, 630-635.

72.   R. M. L. van Lieshout, T. van Domburg, M. Saalmink, R. Verbeek, R. Wimberger-Friedl, M. P. van Dieijen-Visser and C. Punyadeera, *Analytical Chemistry*, 2009, **81**, 5165-5171.

73.   R. D. Das, S. Maji, S. Das and C. RoyChaudhuri, *Applied Surface Science*, 2010, **256**, 5867-5875.

74.   A. Ressine, D. Finnskog, G. Marko-Varga and T. Laurell, *NanoBiotechnology*, 2008, **4**, 18-27.

75.   A. Ressine, G. r. Marko-Varga, T. Laurell and M. R. El-Gewely, in *Biotechnology Annual Review*, Elsevier, 2007, vol. Volume 13, pp. 149-200.

76.   S. Y. Kim, J. Yu, S. J. Son and J. Min, *Ultramicroscopy*, 2010, **110**, 659-665.

77.   K. Derwinska, L. A. Gheber and C. Preininger, *Analytica Chimica Acta*, 2007, **592**, 132-138.

78.   J. L. Tonkinson and B. A. Stillman, *Frontiers in bioscience* 2002, **7**, c1-12.

79.   M. Dufva, *Biomolecular Engineering*, 2005, **22**, 173-184.

80.   M. Reck, F. Stahl, J. G. Walter, M. Hollas, D. Melzner and T. Scheper, *Biotechnolgy Progress*, 2007, **23**, 1498-1505.

81.   T. Kukar, S. Eckenrode, Y. Gu, W. Lian, M. Megginson, J.-X. She and D. Wu, *Analytical Biochemistry*, 2002, **306**, 50-54.

82.   J. Petrik, *Transfusion Medicine*, 2006, **16**, 233-247.

83.   J. Lin, N. Renault, H. Haas, G. Schramm, S. Vieths, L. Vogel, F. H. Falcone and M. J. C. Alcocer, *Clinical and Experimental Allergy*, 2007, **37**, 1854-1862.

84.   R. Blossey and A. Bosio, *Langmuir*, 2002, **18**, 2952-2954.

85.   R. D. Deegan, O. Bakajin, T. F. Dupont, G. Huber, S. R. Nagel and T. A. Witten, *Nature*, 1997, **389**, 827-829.

86.   M. K. McQuain, K. Seale, J. Peek, S. Levy and F. R. Haselton, *Analytical Biochemistry*, 2003, **320**, 281-291.

87.   D. S. Rickman, C. J. Herbert and L. P. Aggerbeck, *Nucleic acids research*, 2003, **31**.

88.   P. Wu and D. W. Grainger, *Journal of Proteome Research*, 2006, **5**, 2956-2965.

89.   Y. Deng, X. Y. Zhu, T. Kienlen and A. Guo, *Journal of the American Chemical Society*, 2006, **128**, 2768-2769.

90.   F. Diehl, S. Grahlmann, M. Beier and J. D. Hoheisel, *Nucleic acids research*, 2001, **29**.

91.   H. B. Eral, D. M. Augustine, M. H. G. Duits and F. Mugele, *Soft Matter*, 2011, **7**, 4954-4958.

2

Influence of buffer composition on the distribution of inkjet printed protein molecules

Abstract

Producing high quality protein microarrays on inexpensive substrates like polystyrene is a big challenge in the field of diagnostics. Using a non-contact inkjet printer we have produced microarrays on polystyrene slides for two different biotinylated biomolecules, bovine serum albumin (BSA-biotin) and immunoglobulin-G (IgG-biotin) and studied the influence of buffer (composition and pH) on the spot morphology and signal intensity. Atomic force microscopy revealed the morphological pattern of the (biomolecule) spots printed from phosphate buffer (pH 7.4), phosphate buffered saline (pH 7.4) and carbonate buffer (pH 9.6). The spots showed an irregular crust-like appearance when printed in phosphate buffered saline (pH 7.4), mainly due to the high NaCl content, whereas spots of biomolecules printed in carbonate buffer (pH 9.6) showed a smooth morphology. In addition, the rinsing of these dried spots led to the loss of a considerable fraction of the biomolecules, leaving behind a small fraction that is compatible with the (mono) layer. It was confirmed by confocal laser microscopy that the quality of the spots with respect to the uniformity and distribution of the biomolecules therein was superior when printed in carbonate buffer (pH 9.6) as compared to other buffer systems. Particularly, spotting in PBS yielded spots having a very irregular distribution and morphology.

2.1 Introduction

Microarrays of various biomolecules (DNA, antibodies, serum albumin) have gained a lot of attention in the scientific world due to a wide range of potential applications[1, 2]. Inexpensive sources of substrates like glass and plastics[3, 4] are most commonly used for printing biomolecules. Printing with a non-contact microarrayer causes the biomolecules to physically adsorb onto these non-porous substrates, e.g., a polystyrene slide. Adsorption of a protein onto such substrate surface is influenced by various factors like temperature, humidity[5], pH[6] and composition. The charge of the biomolecule may also vary depending on the pH and the ionic strength of the medium, which may further influence the process of adsorption. In studying protein microarrays, two factors play an important role: firstly, the immobilization of the biomolecule onto the substrate, and secondly, the effect of immobilization on the functionality of the biomolecule. It has been reported that adsorption and functionality are interrelated such that the biomolecule which is more strongly adsorbed onto the surface has a higher activity[7]. However, by studying various conditions in the preparation of protein microarrays this assumption could not be confirmed[8-10]. The printing buffer used to print biomolecules could be modified with additives like Triton-X-100[11], glycerol[12, 13] and trehalose[14]. End results showed that high density of protein immobilization and superior quality of the microspots were obtained when the printing buffer had an optimal concentration of glycerol (10%) and Triton-X-100 (0.003%), respectively. Printing of biomolecules (antibodies) onto a polystyrene surface has been performed with phosphate buffered saline (pH 7.4)[15] and carbonate buffer (pH 9.6)[16] whereas printing of proteins like BSA has been previously done with carbonate buffer[17, 18]. Yet, no clear evidence is available as to why a certain buffer system is to be preferred over others and this raises many unanswered questions.

In this research we addressed the first important factor in the preparation of protein microarrays, i.e., the immobilization of the biomolecule onto the substrate. The main objective was to analyze and compare the influence of buffers of varying compositions and pH on the distribution and spot morphology of different biomolecules on a polystyrene substrate. Atomic force microscopy was used to characterize the morphological pattern on the spot of printed biomolecules, and the distribution of the biomolecules over the spot was analyzed with confocal fluorescence microscopy studies. On these polystyrene slides we also compared the influence of printing buffers on a nucleic acid microarray immunoassay (NAMIA) and evaluated the compatibility of these buffers (based on spot characteristics and signal intensity) for biochip production and performance.

2.2 Materials and methods

2.2.1 Reagents

Bovine serum albumin biotin conjugated (BSA-biotin) was purchased from Thermo Scientific and biotin-SP-conjugated affinipure goat antimouse immunoglobulin (IgG-biotin) was from Jackson ImmunoResearch Laboratories. Anti-Digoxigenin was purchased from Roche (Germany) whereas anti-Dinitrophenyl, anti-Fluroisothiocynate and anti-Texas red were from Invitrogen. DNA template for the *Corynebacterium bovis* and *Staphylococcus aureus* was provided by GD, Deventer, (The Netherlands). The details of the PCR amplification are explained in Appendix 2.5.1. HTA polystyrene (PS) slides were purchased from Greiner BioOne (Kremsmuenster, Austria). Carbon-alkaline phosphatase-neutravidin conjugate was prepared as described[19]. The substrate for the alkaline phosphatase was from Sigma (SigmaFAST BCIP/NBT). Streptavidin-Alexa-633 conjugate for labeling the biotinylated proteins was obtained from Invitrogen. 100 mM phosphate buffer saline (PBS)

pH 7.4, phosphate buffer (PB) pH 7.4, and carbonate buffer (CB) pH 9.6 were prepared in Milli-Q water with resistivity of 18.2 MΩ cm^{-1}. Running buffer (100 mM borate buffer containing 1% BSA and 0.05% Tween20) was used as a diluent for the conjugates and also during the intermediate washing steps.

2.2.2 Apparatus

2.2.2.1 Microarrayer

Biomolecules were arrayed on the HTA-PS surface with a non-contact spotter, sciFLEXARRAYER S3 (Scienion AG, Berlin, Germany). The printer was placed in a hood to maintain constant temperature and humidity. Spotting of the biomolecules was performed at room temperature and ~70% humidity. The voltage and pulse of the piezo-dispensing capillary (PDC) was optimized to print a droplet of ~300 pL. The volume was kept constant throughout the entire process of spotting.

2.2.2.2 Reflectometry

Adsorption of BSA-biotin in various buffers was studied by reflectometry. The setup of the reflectometer has been explained in detail[20]. Si wafer strips (1cm x 5 cm) were cleaned with ethanol followed by piranya treatment (1 part 30 % H_2O_2 and 2 parts concentrated H_2SO_4) to remove any impurities from the surface. Finally, the wafers were rinsed with Milli-Q water and dried under N_2. A thin layer of PS was grafted onto the Si surface as described before[21]. The thickness of the PS layer (60-70 nm) was measured by ellipsometry.

2.2.2.3 AFM measurement

Spot morphology of printed biomolecules was characterized with atomic force microscopy, AFM (Veeco, NY, USA), in tapping mode (in air). For each spot 256 lines were scanned at a frequency of 0.4 Hz. Height data was compared to analyze morphological changes in the biomolecule printed using various

buffers. The average thickness of the spot at various positions was obtained through section analysis (Nanoscope Analysis software).

2.2.2.4 CLSM imaging

Spots of biotinylated proteins were labeled with streptavidin-Alexa-633 conjugate and analyzed by confocal laser scanning microscopy (CLSM) to compare the distribution of the biomolecules in various buffers when printed on HTA-PS surface. Flurophore labeled biomolecules were analyzed using a confocal microscope (Carl Zeiss Axiovert 200 microscope, Zeiss, Jena, Germany) equipped with a LSM 5 Exciter. The configuration of the objective was LD Plan-Neofluar 40x /0.6 Korr Ph2 M27. A He-Ne laser set at 633 nm was used. The size of the pinhole was 182 µm whereas the transmission was 11%. The dimension of the scanner was X: 160.40 µm, Y: 160.40 µm, respectively. Further analysis was carried out by the "Zen 2008" software.

2.2.3 Printing and labeling of BSA-biotin

The wells of the HTA-PS slide (see Appendix 2.5.2) were flushed with N_2 and mounted on the deck of the microarrayer. BSA-biotin (200 µg/mL) was prepared in PBS or CB and 20 µL of the diluted BSA-biotin was carefully placed into the wells of a Genetix 384 microtiter plate that was mounted on the deck as a reagent reservoir. Air bubbles, if present, were removed to prevent any interference during spotting. The microarrayer was programmed to print an array of one drop of BSA-biotin in different buffers on the HTA slide. After printing, the slide was incubated for 1 hour in the sciPROCLIMATE unit at 37°C and 70% humidity. Biotinylated BSA was incubated with 1% carbon - alkaline phosphatase-neutravidin conjugate (prepared in running buffer) for 1 hour. The slide was rinsed 3 times with running buffer, followed by substrate incubation for 10 minutes. Finally, the slide was rinsed 3 times with Milli-Q water and air-dried.

2.2.4 Scanning and image analysis

Biomolecules labeled with carbon conjugates were scanned on an Epson 3200 Photo scanner (Seiko Epson, Nagano, Japan) with a resolution of 4800 dpi and 16 bit gray-scale and the images were saved as *.TIFF files. Spot intensity was measured by the TotalLab image analysis software, by placing a marker ring at the circumference of the spot. The total intensity or pixel gray volume of 16 replicate spots was calculated and compared with the spots printed in other buffers.

2.3 Results and discussion

2.3.1 Analysis of scanned images

Spots of carbon labeled biotinylated BSA printed in PBS and carbonate buffer showed differences in the appearance and signal intensity (see Figure 2.1). In PBS, spots of biotinylated BSA showed a tail-like appearance, commonly known as the spot-smearing effect[22], whereas in CB (pH 9.6) such tails were absent.
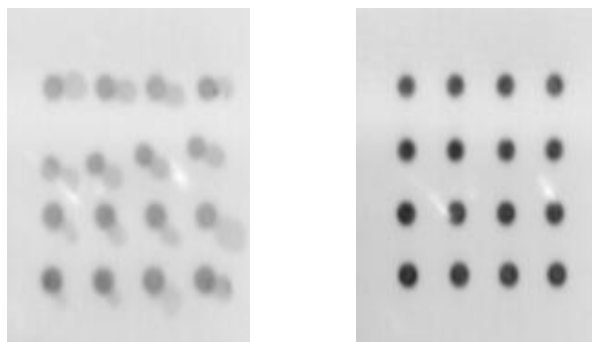
Figure 2.1 Scanned image of HTA polystyrene slide. (left) BSA-biotin spotted in PBS (pH 7.4) and (right) BSA-biotin spotted in carbonate buffer (pH 9.6).

The overall signal intensity of BSA-biotin in PBS was low as compared to those observed in carbonate buffer. These differences in spot appearance and intensity maybe due to weak binding of the BSA-biotin molecules onto the PS

surface so that they were partly removed during the rinsing step or to a suboptimal conformation of the protein with respect to the binding of biotin by neutravidin in the subsequent step.

2.3.2 Reflectometry

To investigate the different spot formation of BSA-biotin in PBS and CB in more detail, reflectometry experiments were performed to study the adsorption of biotinylated BSA (2 µg/mL) onto PS in PBS (pH 7.4) and CB (pH 9.6). Experimental data showed that the adsorption of BSA-biotin in PBS (pH 7.4) reached 1.3 mg/m^2, which was much higher than that in CB (pH 9.6), 0.08 mg/m^2 (see Figure 2.2). A possible explanation for this observation could be the high saline content (137 mM NaCl) of PBS that may result in higher adsorption of BSA-biotin in this buffer. Therefore, the influence of NaCl was studied by comparing the adsorption in PBS with the adsorption in PB (PBS without NaCl; see Figure 2.2). The results clearly demonstrate that in the absence of NaCl the adsorption of BSA-biotin was less. Still the adsorption saturation in PB was much higher than in CB. The above results show that buffer pH along with the presence of saline plays an important role in the adsorption of protein onto the PS surface. The initial increase in the signal reflects the affinity of the protein for the substrate. Although the PS surfaces in the reflectometry experiment and the printing experiments are not identical, the results suggest that the signal intensity of the BSA-biotin in the printed spots (see Figure 2.2) is not directly related to the adsorbed amount (see Figure 2.2). The strong adsorption of these biotinylated BSA molecules in PBS may interfere with the binding of streptavidin in the subsequent step due to steric hindrance.
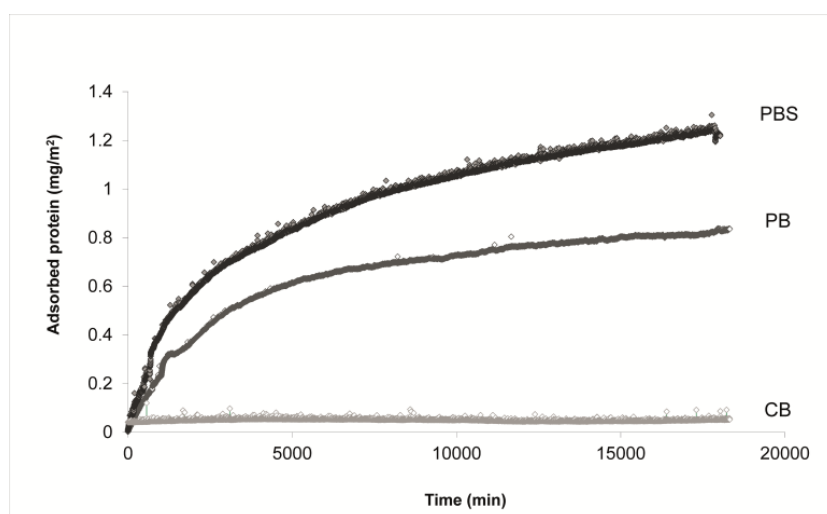
Figure 2.2 Reflectometry data showing adsorbed amount of BSA-biotin in PBS (pH 7.4), PB (pH 7.4) and CB (pH 9.6) on PS substrate.

2.3.3 AFM analysis

To further study the discrepancy between signal intensity and the adsorbed amount of protein, spots of biotinylated BSA printed onto HTA-PS surfaces in PBS or CB were analyzed by AFM in tapping mode (in air). AFM images showed the differences in the spot morphology of BSA-biotin printed in PBS and CB, respectively (see Figure 2.3-A). In carbonate buffer the dried spot had an even distribution with a thickness of 120 nm. In PBS, the distribution of biotinylated BSA showed an irregular pattern with clearly visible high crust-like regions (see Figure 2.3-A, 3D topography). The height of the BSA-biotin spot in PBS was 530 nm, which is 4.4 times higher than the observed thickness for the same protein in CB. It was hypothesized that the appearance of the high crust-like regions on the spot could be due to the presence of the high NaCl content in PBS buffer (137 mM NaCl). The salt could cause the biomolecules to aggregate[23] and could further interfere with an even distribution of the biomolecules on the surface of HTA-PS slide. The influence of the saline content in PBS was investigated by printed spots of BSA-biotin in PB (PBS without

NaCl) on the same PS surface. The thickness of the dried spot in PB was 110 nm, which is almost 5 times less than in PBS. Spots of BSA-biotin in PB showed a different distribution pattern as compared to BSA-biotin in PBS. Both PB and CB do not have a high saline content and the spots of biotinylated BSA had similar dimensions with respect to the diameter and thickness for these two buffers, although a more even distribution was observed across the spot printed in CB. Interestingly, the buffer pH and salt composition hardly had any influence on the spreading of the drop on the PS surface. As shown in the figure, the diameter of the spot did not vary much. For PBS, CB and PB the diameter of the spot was 90 µm, 100 µm and 100 µm, respectively.
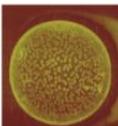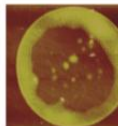
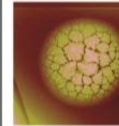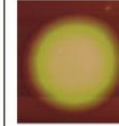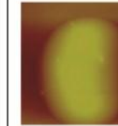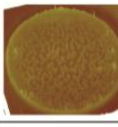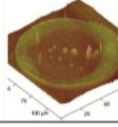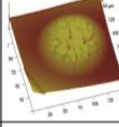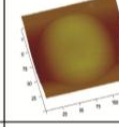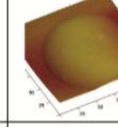| AFM DATA	(A) BSA-biotin			(B) IgG-biotin		
	PBS (pH 7.4)	CB (pH 9.6)	PB (pH 7.4)	PBS (pH 7.4)	CB (pH 9.6)	PB (pH 7.4)
2D Topography						
3D Topography						
Height (nm)	900	120	110	400	100	146
Diameter (µm)	90	100	100	100	100	120

Figure 2.3 AFM images for (A) BSA-biotin and (B) IgG-biotin in PB, PBS and CB printed on HTA polystyrene surface.

Antibodies are often used as ligands in immunoassays. Therefore, we also studied spots of a polyclonal goat IgG preparation by AFM. The printing conditions, the printing buffers and the substrate were the same as to those used for BSA-biotin. AFM images of the IgG-biotin spots also showed differences in the morphology and the thickness when printed in PB, PBS and CB. Here, also the pH and buffer composition did not influence the spreading of the drop as the diameter of IgG-biotin in PB, PBS and CB was between 100

μm and 120 μm (see Figure 2.3-B). The thickness of the IgG-biotin spot in PBS was higher (400 nm) than in PB (146 nm) and CB (100 nm). Again, in PBS the appearance of the spot was rough with a crackled appearance, whereas in CB and PB the dried spot showed a much smoother and more uniform distribution on the surface of the PS slide.

2.3.4 Influence of rinsing on the spots of BSA-biotin and IgG-biotin

The height data obtained from AFM analyses suggested that the spots of biotinylated biomolecules printed on the PS surface was not only made up of just protein, especially if printed in PBS (see Figure 2.3-A). It was shown that the omission of salt substantially reduced the spot height, as shown in the spot printed in PB. Therefore, the structures appearing upon drying the spot most probably consisted of both protein and salt. We studied whether these structures were tightly or loosely bound by rinsing the HTA slide with Milli-Q water, followed by air-drying. Subsequently, the spots were again analyzed by AFM to observe any change in the thickness.

After rinsing the spots of biotinylated biomolecules, the height appeared to be reduced by more than 85%. The change in the thickness of the spots before and after rinsing for biotinylated proteins in PB, PBS and CB is shown in Table 2.1. The dimensions for BSA[24], IgG[25] and biotin[26] are shown in Appendix 2.5.3.

The calculated thickness of the protein (see Appendix 2.5.3) and salt components present in 300 pL PBS printed on an area of ~0.8 x 10^{-8} m^2 would be approximately 206 nm after drying. However, as can be seen in Figure 2.3-A (BSA-biotin in PBS) that 40% of the spot area was occupied by non-proteinaceous components whereas the remaining 60% was still empty (Evaluated by ImageJ software and MatLab). It implies that the average height of the salt deposits on 40% of the spot area amounts to 515 nm which is close to our experimental value of 530 nm.

Table 2.1 Change in the thickness of the spot of BSA-biotin and IgG-biotin in different buffers (before and after rinsing), based on AFM analysis (height data)

Buffer	Before rinse		After rinse		Loss in thickness (%)	
	BSA-bt	IgG-bt	BSA-bt	IgG-bt	BSA-bt	IgG-bt
PB	110 nm	146 nm	10 nm	13 nm	91	91
PBS	530 nm	400 nm	11 nm	16 nm	99	96
CB	120 nm	100 nm	18 nm	13 nm	85	87

Based on the concentration of protein (200 µg/mL) in the PBS, the volume of the drop to be spotted (300 pL) and the area of the spot after drying (~0.8x10^{-8} m^2) the surface concentration of the protein deposited on the spot was calculated to be 7.5 mg/m^2. Assuming a packing density of 0.7 in the dried protein layer and taking a protein density of 1.37 g/cm^3, the thickness of a spot consisting of protein only would amount to 9.2 nm, assuming a protein spot coverage of only 60%. (The dimensions of various biomolecules and various components of the printing buffers are explained in Appendix 2.5.3 and 2.5.4).

Even after allowing for a large uncertainty in the assumptions underlying the calculation of the thickness of a spot solely consisting of protein and for a considerable experimental error in determining the thickness by AFM, it is obvious that the thicknesses of BSA-bt and IgG-bt spots before rinsing contain a large fraction of non-proteinaceous components. These components cannot be other than the salts from the buffer; indeed, the largest thickness before rinsing is observed for the spots in the buffer of high salinity, i.e., PBS. The influence of high saline content on the spot morphology has also been observed by Ressine *et al.*, where they showed a salt crystallization effect[22] on the spot of the biomolecule when printed in PBS buffer. After rinsing the thicknesses of the

spots were different but in the same range as the one calculated for pure protein layers on 60% of the spot area i.e., 9.2 nm. Moreover, these values are comparable with the dimensions of the protein molecules (see Table 2.1). These considerations strongly suggest that upon rinsing most of the salt is removed from the spots, leaving behind spots of which 60% of the spot area is covered by a (mono) layer mainly made up of protein.

Data in Table 2.1 shows the height of the dried spot (before rinsing) for BSA-biotin and IgG-biotin in three different buffers. The non-proteinaceous components present in the buffer along with the protein form structures with a final height of 400-500 nm (in PBS) and 100-150 nm in PB and CB. These structures are loosely bound onto the surface and tend to be washed away during the intermediate rinsing step, thus leaving behind a thin layer of protein on the PS surface. The average thickness of that layer was less than 20 nm which is compatible with a monolayer of albumin and immunoglobulin on the PS surface[27].

Based on the above observations, it is clear that the choice of printing buffer is very crucial for printing biomolecules onto a non-porous substrate like PS. The buffer composition (See Appendix 2.5.4) and pH play a vital role in packing of the biomolecules within the drying/dry spot. Use of a common buffer like PBS that has a high saline content (137 mM) results in high crust-like structures following drying of the printed droplet (see Figure 2.3) as compared to the same protein printed in the same buffer but without saline.

2.3.5 CLSM analysis

Following Alexa-633-streptavidin labelling of the immobilized biotinylated biomolecules the spots were scanned with a 40x objective at 633 nm wavelength. The PMT settings were kept the same for all the measurements. For the BSA-biotin spot in carbonate buffer, the fluorescence distribution was

uniform throughout the spot as compared to BSA-biotin spots in PB and PBS, where the spots had an uneven distribution pattern (see Figure 2.4). CLSM images of BSA-biotin in PBS showed empty regions where no fluorescence was observed. Comparison with AFM data (see Figure 2.3-A) showed the influence of the high saline content on the distribution of the BSA-biotin on the dried spot. The CLSM image for BSA-biotin in PBS was exactly the mirror image of the AFM data (Compare with Figure 2.3-A, BSA-biotin in PBS), which could be explained as follows: when a drop of BSA-biotin in PBS comes in contact with the PS surface, the surface area of the spot is not completely occupied with the BSA-biotin molecules, instead some portion of the surface is covered with buffer-salt moieties, especially NaCl which is in excess. Drying of the spot leads to the formation of a multilayer structure mainly composed of non-proteinaceous components which tend to be washed off during rinsing, leaving behind an empty space in the spot. Since Alexa-streptavidin molecules couple only to the biotinylated biomolecules, the empty regions present within the spot of BSA-biotin in PBS showed no fluorescence.

BSA-biotin in PB showed a doughnut appearance with a strong fluorescence at the edges and a weak signal at the interior of the spot, whereas in CB the distribution pattern was more regular with an uniform fluorescence intensity throughout the spot (see Figure 2.4). IgG-biotin in all the three buffer systems showed less variation as compared to BSA-biotin. However, in carbonate buffer the distribution pattern was again more uniform than observed for the same biomolecule in PB and PBS (see Figure 2.4). The observations based on CLSM data reveal the distribution of biotinylated biomolecules on the PS surface and illustrated the influence of a high salt content on the final outcome. IgG-biotin printed in PB and PBS had a better distribution pattern throughout the spot as compared to BSA-biotin when printed in the same buffers.
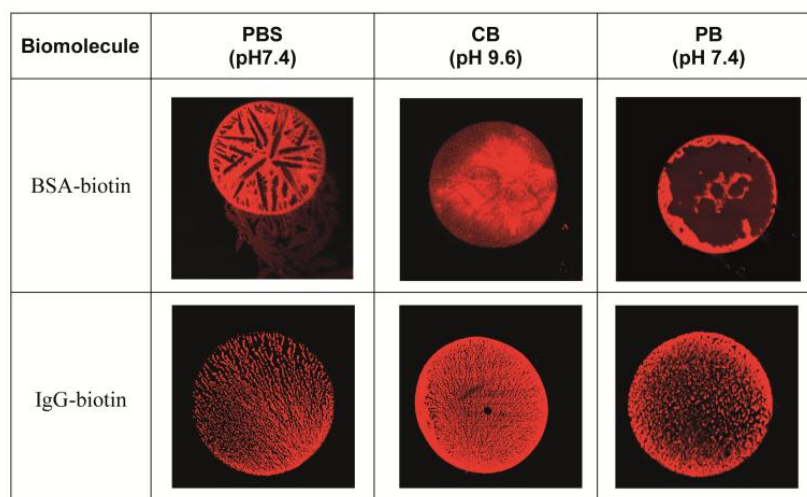
Biomolecule	PBS (pH7.4)	CB (pH 9.6)	PB (pH 7.4)
BSA-biotin			
IgG-biotin			

Figure 2.4 CLSM images for *(upper lane)* BSA-biotin and *(lower lane)* IgG-biotin in PB, PBS and CB printed on HTA polystyrene surface.

2.3.6 Influence of printing buffer on the assay performance on HTA-PS slide

In order to analyze the influence of buffer on a real antibody assay, a one-step NAMIA [19] (nucleic acid microarray immunoassay) was performed on the HTA-PS slide (see Figure 2.5-A). The layout of the microarray is shown in Figure 2.5-B. The antibodies specific for different tags (anti-DIG, anti- FITC, anti-DNP and anti-TR) were printed along with BSA-biotin (positive control) in PBS (pH 7.4) and CB (pH 9.6).

A double labeled PCR amplicon (*C.bovis*) with FAM (Fluorescein amidite) at one end and biotin at the other end was incubated with a carbon-alkaline phosphatase-neutravidin conjugate. A similar incubation with another PCR amplicon for *S.aureus*, containing a DIG (digoxygonin) tag, was also used in a similar manner. The double-labeled amplicon was sandwiched in one-step incubation for 1 hour between these carbon nanoparticles conjugates and the immobilized antibodies resulting in black spots. On HTA-PS and when printed with CB (pH 9.6), the NAMIA spots had a more regular and defined shape without any spot-smearing effect (see Figure 2.5-C, D). In PBS (pH 7.4),

however, the NAMIA spots as well as the control spots showed a clear spot smearing (tailing appearance), thus reducing the overall quality of the biochip.
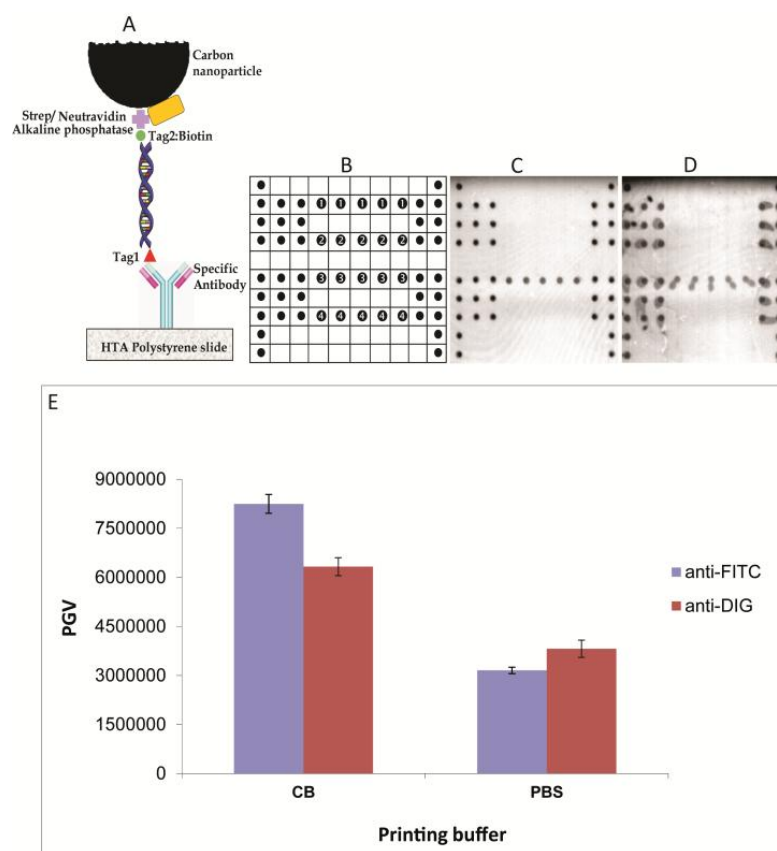

Figure 2.5 (A) Schematic representation for the detection principle of NAMIA. (B) Layout of the NAMIA on HTA-PS slide: 1=anti-DIG *(S.aureus)*, 2=anti-DNP *(Streptococcus spp.)*, 3=anti-FITC *(C.bovis)*, 4=anti-TR *(M.bovis)* •=BSA-biotin control. (C) Scanned iamge of HTA slide showing a antibody assay (anti-FITC) performance in CB (pH 9.6) and (D) in PBS (pH 7.4). (E) NAMIA results for anti-FITC (against *C.bovis*) and anti-DIG (against *S.aureus*) when printed on HTA-PS slide in two different buffers.

The average pixel gray volume (PGV) was calculated for five NAMIA spots. It was found that when anti-FITC and anti-DIG were printed with CB (pH 9.6), the PGV (assay signal) was higher as compared to the same biomolecule when printed with PBS (pH 7.4). The PGV of the NAMIA spots for anti-FITC in PBS (pH 7.4) was ~38% less as compared to CB (pH 9.6) (see Figure 2.5-E). On the

other hand the PGV of the NAMIA for anti-DIG in PBS was ~60% lower as compared to CB. As explained in section 3.4, in the presence of PBS the spot coverage of the biomolecule was ~40%, leaving 60% of the spot area unoccupied. Therefore, the reduced spot coverage in PBS atleast partly explains the reduced signals upon printing with PBS (pH 7.4) as compared to CB (pH 9.6).

2.4 Conclusion

 In this study we have demonstrated the influence of printing buffers on distribution and spot morphology of the different biomolecules using a hydrophobic polystyrene slide as a substrate. Based on our experimental data we recommend that, upon printing onto a hydrophobic substrate, the printing buffer should be CB (pH 9.6). This will result in even spot morphology with a superior signal to noise ratio as compared to that of PBS, where our observations showed that the distribution of biomolecules and spot morphology were highly irregular. Due to the presence of a high NaCl content in PBS buffer, the spots show spot-smearing[22] and salt crystallization which is not acceptable for diagnostic purposes, as non-homogeneous signal intensity reduces the (data) output quality. On these hydrophobic polystyrene substrates, we also demonstrated and compared the performance of NAMIA for different buffers. Higher signal intensity and superior spot quality were achieved when CB (pH 9.6) was used instead of PBS (pH 7.4) as a printing buffer.

References

1.   P. Angenendt, *Drug Discovery Today*, 2005, **10**, 503-511.

2.   M. Cretich, F. Damin, G. Pirri and M. Chiari, *Biomolecular Engineering*, 2006, **23**, 77-88.

3.   M. Dufva, *Biomolecular Engineering*, 2005, **22**, 173-184.

4.   M. Moschallski, J. Baader, O. Prucker and J. Rühe, *Analytica Chimica Acta*, 2010, **671**, 92-98.

5.   M. D. Kurkuri, C. Driever, G. Johnson, G. McFarland, H. Thissen and N. H. Voelcker, *Biomacromolecules*, 2009, **10**, 1163-1172.

6.   W. Kusnezow, A. Jacob, A. Walijew, F. Diehl and J. D. Hoheisel, *Proteomics*, 2003, **3**, 254-264.

7.   G. MacBeath and S. L. Schreiber, *Science*, 2000, **289**, 1760-1763.

8.   B. B. Haab, *Current Opinion in Biotechnology*, 2006, **17**, 415-421.

9.   G. Klenkar and B. Liedberg, *Analytical and Bioanalytical Chemistry*, 2008, **391**, 1679-1688.

10.   B. Lu, M. R. Smyth and R. O'Kennedy, *The Analyst*, 1996, **121**, 29R - 32R.

11.   Y. Liu, C. M. Li, W. Hu and Z. Lu, *Talanta*, 2009, **77**, 1165-1171.

12.   N. Nath, R. Hurst, B. Hook, P. Meisenheimer, K. Q. Zhao, N. Nassif, R. F. Bulleit and D. R. Storts, *Journal of Proteome Research*, 2008, **7**, 4475-4482.

13.   E. W. Olle, J. Messamore, M. P. Deogracias, S. D. McClintock, T. D. Anderson and K. J. Johnson, *Experimental and Molecular Pathology*, 2005, **79**, 206-209.

14.   A. Wolter, R. Niessner and M. Seidel, *Analytical Chemistry*, 2007, **79**, 4529-4537.

15.   H. Sølling and B. Dinesen, *Clinica Chimica Acta*, 1983, **130**, 71-83.

16.   K. Sollier, C. A. Mandon, K. A. Heyries, L. J. Blum and C. A. Marquette, *Lab on a Chip*, 2009, **9**, 3489-3494.

17.   M. Mrksich, *Chemical Society Reviews*, 2000, **29**, 267-273.

18.   Z. Yong, *Colloids and Surfaces B: Biointerfaces*, 2006, **48**, 95-100.

19.   P. S. Noguera, G. A. Posthuma-Trumpie, M. van Tuil, F. J. van der Wal, A. d. Boer, A. P. H. A. Moers and A. van Amerongen, *Analytical Chemistry*, 2011, **83**, 8531-8536.

20.   J. C. Dijt, M. A. Cohen Stuart and G. J. Fleer, *Advances in Colloid Interface Science*, 1994, **50**, 79-101.

21.   J. H. Maas, M. A. Cohen Stuart, A. B. Sieval, H. Zuilhof and E. J. R. Sudhölter, *Thin Solid Films*, 2003, **426**, 135-139.

22.   A. Ressine, G. r. Marko-Varga, T. Laurell and M. R. El-Gewely, in *Biotechnology Annual Review*, Elsevier, 2007, vol. Volume 13, pp. 149-200.

23.   V. B. Galazka, D. Smith, D. A. Ledward and E. Dickinson, *Food Chemistry*, 1999, **64**, 303-310.

24.   A. K. Wright and M. R. Thompson, *Biophysical Journal*, 1975, **15**, 137-141.

25. K.-B. Lee, S.-J. Park, C. A. Mirkin, J. C. Smith and M. Mrksich, *Science*, 2002, **295**, 1702-1705.

26. P. Hu, T. Tanii, G.-J. Zhang, T. Hosaka and I. Ohdomari, *Sensors and Actuators B: Chemical*, 2007, **124**, 161-166.

27. R. J. Green, J. Davies, M. C. Davies, C. J. Roberts and S. J. B. Tendler, *Biomaterials*, 1997, **18**, 405-413.

2.5 Appendix

PCR protocol and details of tagged primers used for PCR reaction

The PCR protocol was optimized to 30 minutes using Phire Hot Start polymerase (Finnzymes) and the Piko thermal cycler (Finnzymes). The PCR tube contained 0.4 µL Phire Hot Start DNA Polymerase, 4µL 1x Phire reaction buffer (final concentration $MgCl_2$: 1.5 mM), 4 µL dNTPs (200 µM), 1 µL each forward and reverse primer (0.5 µM) and 2 µL template in a total volume of 20 µL. The protocol consisted of an initial denaturation step at 98°C for 30 s followed by 35 cycles at 98°C for 5 s, 60°C for 5 s, 72°C for 10 s, and a final extension step at 72°C for 1 min. *C.bovis* template was amplified using primers Cb-F2 and Cb-R3, where the forward primer was labeled with FAM and reverse primer with biotin. Similarly, *S.aureus* template was amplified using primers Au-F and Au-R, where the forward primer was labeled with DIG and the reverse primer was biotin respectively.

Tag specific antibody	Microorganism	Primer	Sequence (5'-3')	Forward tag	Amplicon size (bp)
Anti -FITC	*Corynebacterium bovis*	Cb-F2	CGTGCTTTAGTGTGTGCG	FAM	652
		Cb-R3	GGCACGGAAATCGTGGAAG	Biotin	
Anti-DIG	*Staphylococcus aureus*	Au-F	TTCGTACCAGCCAGAGGT	DIG	227
		Au-R	TTCAGCGCATCACCAAT	Biotin	

2.5.2 HTA polystyrene slide with 12 spotting wells

2.5.3 Dimension of various biomolecules.

Biomolecule	Dimension (nm³)
BSA	14.0 x 4.0 x 4.0
IgG	14.5 x 8.5 x 4.0
Biotin	0.5 x 1.0 x 2.1

2.5.4 Dimension of various biomolecules.

Compound	Mw	Density (gms/cm³)	grams/L	Mass (gms)
KH_2PO_4	136.00	2.34	0.24	7.2×10^{-11}
Na_2HPO_4	141.00	1.00	1.44	43.2×10^{-11}
NaCl	58.44	2.16	8.00	240×10^{-11}
KCl	74.55	1.98	0.20	6×10^{-11}

3

Spot morphology of inkjet printed biomolecules on a range of hydrophobic substrates

Abstract

Non-contact inkjet printing technology is one of the most promising tools for producing microarrays. The quality of the microarray depends on the type of substrate used for printing biomolecules. Various porous and non-porous substrates have been used in the past, but due to low production cost and easy availability, non-porous substrates like glass and plastic are preferred over porous substrates. On these non-porous substrates, obtaining spot uniformity and a high signal to noise ratio is a big challenge. In our research work, we have modified pristine glass slides using various silanes to produce a range of hydrophobic glass substrates. The hydrophobicities of the slides expressed in the contact angle (θ) of a sessile drop of water were 49°, 61°, 75°, 88° and 103°, respectively. Using a non-contact inkjet printer, microarrays of biotinylated biomolecules (BSA and IgG) were produced on these modified glass substrates, pristine (untreated) glass and also on HTA polystyrene slide. The uniformity of the spots, reflecting the distribution of the biomolecules in the spots, was analyzed and compared using confocal laser scanning microscopy (CLSM). The quality of the spots was superior on the glass slide with contact angle ~75°. We also investigated the influence of the hydrophobicity of the substrate on a two-step, real diagnostic antibody assay. This nucleic acid microarray immunoassay (NAMIA) for the detection of Staphylococcus aureus showed that on highly hydrophilic (θ <10°) and hydrophobic substrates (θ >100°) the assay signal was

low, whereas an excellent signal was obtained on the substrates with intermediate contact angle, θ ~61° and θ ~75°, respectively.

3.1 Introduction

The use of microarrays on biochips for diagnostics purposes is well known[1, 2], and inkjet printing is one of the most promising tools for preparing arrays[3]. In order to produce such biochips porous and non-porous substrates have been selected. Porous substrates like nitrocellulose membrane[4, 5] and hydrogels[6, 7] film slides have been used to produce high quality microarrays. These substrates have a high signal to noise ratio but due to the high cost of these porous substrates, researchers have made efforts to produce microarrays onto non-porous substrates like glass[8-10] and plastic[6, 11, 12]. It is a big challenge to attain high quality microarrays on non-porous substrates as the spot morphology and signal to noise ratio depend on parameters such as substrate material and buffer (pH and composition)[13, 14]. Due to its easy availability and inexpensive nature, glass is an excellent choice as a substrate material. However on hydrophilic glass, the spots of printed biomolecules are irregular in shape due to minimum initial binding of the biomolecules with the surface[15]. To improve spot morphology and to obtain a better signal, efforts have been made in the past to modify glass by coating with silanes[15-17]. It has been shown that the binding of biomolecules is increased on silanized glass as compared to pristine glass[18].

In our research work, we have produced a range of modified non-porous glass substrates to study the influence on microarray performance. Different silanes have been used to modify glass resulting in surfaces with varying hydrophobicity, having water contact angles ranging between 49° to 103°. An untreated glass and an HTA polystyrene slide with a contact angle of less than 10° and ~92°, respectively, were used as control substrates. By inkjet printing a microarray of model biomolecules like biotinylated BSA and polyclonal IgG

was applied on these silanized glass substrates. The biomolecules were tagged with a fluorophore label and their distribution on the non-porous substrates was studied by confocal laser scanning microscopy.

Finally, a real diagnostic two-step assay was performed on these non-porous substrates. A preliminary test method was developed, by combining a rapid PCR method with a user-friendly and fast antibody microarray, the nucleic acid microarray immunoassay (NAMIA)[5, 14]. The double-labeled amplicons were sandwiched in an one-step incubation between carbon nanoparticles-neutravidin conjugates and immobilized antibodies. Sandwiched amplicons were visible as black spots on a white background. The signal could be further enhanced by a short incubation with a solution containing a substrate for alkaline phosphatase that had been immobilized onto the carbon nanoparticles as a fusion protein with neutravidin. Quantitative data were obtained by analyzing the total pixel gray volume of the spots with TotalLab image analysis software.

3.2 Materials and methods

3.2.1 Reagents

3-cyanopropyltriethoxy silane[15], 3-glycidyloxypropyltrimethoxy silane[19], phenylethylchloro silane[20], hexamethyldisilazane, dichlorodimethyl silane were purchased from Aldrich (Seelze, Germany). Streptavidin-Alexa-633 conjugate for labelling the biotinylated proteins was obtained from Invitrogen (Bleiswijk, The Netherlands). 150 mM phosphate buffer saline (PBS) pH 7.4 and 100mM carbonate buffer (CB) pH 9.6 were prepared in Milli-Q water with resistivity of 18.2 MΩ cm^{-1}. A borate buffer (100 mM borate buffer containing 1% BSA and 0.05% Tween20) was used as diluent for the conjugates / labels and also during the intermediate washing steps. Pluronic F127 purchased from Sigma-Aldrich

(St. Louis, USA) was diluted to 0.1% in borate buffer (pH 8.8) and was used as a blocking agent.

3.2.2 Biomolecules

Immunopure biotinylated biotin (BSA-biotin) was purchased from Thermo scientific (Rockford, USA). Biotin-SP-conjugated affinipure goat antimouse (IgG-biotin) was from Jackson Immunoresearch (West Grove, PA, USA). Anti-Digoxigenin was purchased from Roche Diagnostics GmBH (Mannheim, Germany), anti-Fluoroisothiocynate from Bioconnect (Huissen, The Netherlands) whereas anti-Dinitrophenyl and anti-Texas red were from Invitrogen (Oreagon, USA). The DNA template for *Staphylococcus aureus* was provided by the Animal Health Service (Deventer, The Netherlands). These biomolecules were diluted (200 µg/mL) in PBS (pH 7.4) and CB (pH 9.6) and loaded into the wells of Genetix microtiter plate (Genetix X7020, Berkshire, United Kingdom).

3.2.3 Substrates used for printing biomolecules

Two different types of surface were used i.e., glass (microscopic glass slide from Thermo) and polystyrene (PS) (HTA slides from Greiner-BioOne, (Kremsmuenster, Austria).

3.3 Instrumentation

3.3.1 Contact angle measurement

The hydrophobicity of the surfaces was analyzed by measuring the contact angle (θ) of a sessile water droplet using a Krüss contact angle measuring system (G10, Hamburg, Germany). The water droplet was analyzed by an in-built CCD video camera (Sony XC-77CE). The contact angle (θ) of the water droplet was measured with the drop analysis software (DSA-1).

3.3.2 Microarrayer

Inkjet printing of biomolecules on various non-porous substrates was performed by a non-contact spotter, sciFLEXARRAYER S3 (Scienion AG, Berlin, Germany). The spotter was enclosed in a hood to maintain temperature and humidity at 21°C and ~70%, respectively. The voltage and pulse of the piezo-dispensing capillary (PDC) were optimized such that the volume of the droplet was ~300 pL.

3.3.2 Confocal Laser Scanning Microscopy

To study the distribution of biomolecules on the substrates, the inkjet printed biotinylated biomolecules were labelled with streptavidin-Alexa-633 conjugate. These labelled biomolecules were analyzed with a confocal laser scanning microscope (Carl Zeiss Axiovert 200 microscope, Zeiss, Jena, Germany) equipped with a LSM 5 Exciter. The configuration of the objective was LD Plan-Neofluar 10x/0.30 Korr M27. A He-Ne laser set at 633 nm was used. The size of the pinhole was 182 μm whereas the transmission was 11%. The dimension of the scanner was X: 1270.31 μm, Y: 1270.31 μm, respectively. Spot analysis was subjected to various gain settings (1000 to 600) in order to study the distribution pattern of the biomolecules on the various surfaces. Image analysis was performed by "Zen 2008" software.

3.4 Experimental setup

3.4.1 Surface modification (silanization)

Prior to the modification process, glass slides were cleaned with ethanol sonication (2 min), rinsed with MQ water and plasma-treated for further 2 min. The plasma-treated slides were modified by various silanes:

- 3-Cyano Propyl Triethoxy Silane (CPTS)-Slides were incubated in a solution of 2.5% CPTS in ethanol for one hour, rinsed with ethanol and MQ water, and further dried with N_2.

- 3-Glycidyloxy Propyl)Trimethoxy Silane (GPTS)-Slides were incubated in a solution of 2.5% GPTS in ethanol for 4 hours, rinsed with ethanol and baked in an oven at 100°C for one hour. After cooling down the slides were used for printing.

- Phenyl Ethyl Chloro Silane (PhECS)-Slides were incubated for one hour in a solution of 1% PhECS in toluene, rinsed with toluene and ethanol, further dried with N_2.

- Hexa Methyl DiSilazane (HMDS)-The glass was silanized by vapor deposition where 5mL of HMDS was loaded into a small petri plate placed inside desiccators. Glass slides were placed in the desiccators for overnight incubation. After incubation, the slides were rinsed with toluene, ethanol and dried with N_2.

- Dichloro dimethyl silane (DCDMS)-Slides were incubated for one hour in a solution of 1% DCDMS in toluene rinsed with toluene and ethanol, and further dried with N_2.

3.4.2 Printing of biotinylated BSA and IgG on various non-porous surfaces

Biotinylated BSA and IgG (200 μg/mL) were prepared in PBS (pH 7.4), or CB (pH 9.6) and 20 μL of the diluted samples was loaded into the wells of a Genetix microtiter plate. The proteins were arrayed onto the various substrates mentioned above. After printing, all the slides were dried for one hour at 70% humidity. Subsequently, the slides were stored in a sealed aluminium pouches.

3.4.3 Nucleic Acid Microarray Immunoassay (NAMIA)

To check the acceptability of the non-porous surface in a real assay, antibodies specific for a digoxigenin (DIG) tag were prepared in CB (pH 9.6) and printed

on various non-porous substrates[14]. Mastitis-causing *S.aureus* template was subjected to PCR reaction with a specific forward primer with a DIG tag and a specific reverse primer with a biotin tag, both coupled to the 5-end'. Specific binding was detected by a conjugate of carbon nanoparticles and neutravidin-alkaline phosphatase, a fusion protein consisting of neutravidin and alkaline phosphatase. The double-labeled amplicons were sandwiched in an one-step incubation between these carbon nanoparticle conjugates and the anti-DIG antibody on the substrates (see Figure 3.1).

The carbon-neutravidin-alkaline phosphatase conjugate (2.5%) was prepared in borate buffer and incubated together with the amplicons for one hour[14, 21]. The signal could be further enhanced by a short (5 min) incubation with alkaline phosphatase substrate solution.
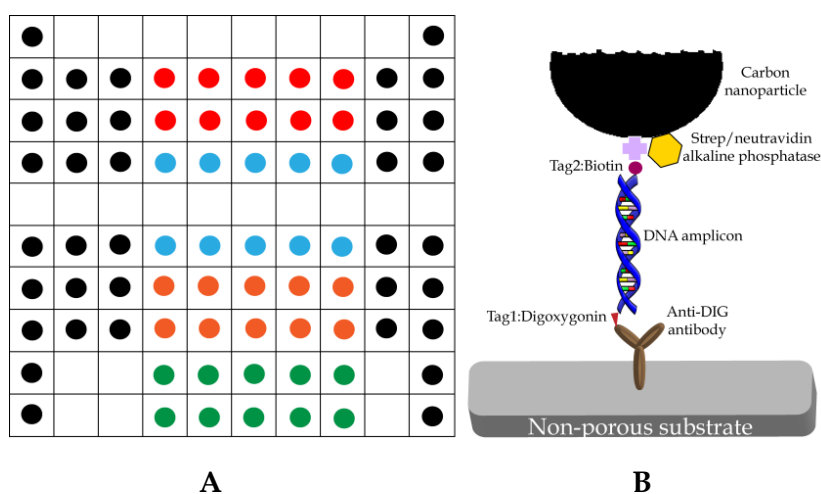

A   **B**

Figure 3.1 (A)Layout of the Mastitis NAMIA, ● =Anti-Digoxigenin , ● =Anti-DNP, ● =Anti-FITC, ● =Anti-Texas Red, ● =BSA-biotin (control*). (B) Schematic representation of NAMIA.

3.4.4 Incubation of the biomolecules with the labels (fluorophore and carbon conjugates)

Silanized slides printed with biotinylated BSA and IgG were incubated with Streptavidin-Alexafluor-633 conjugate for one hour. These fluorophore-labelled biomolecules were analyzed under CLSM to observe their distribution on the surfaces. Slides printed with mastitis specific anti-DIG antibodies were labelled with carbon-alkaline phosphatase-streptavidin conjugate. Further incubation with the alkaline phosphatase substrate resulted in additional staining of the printed spots.

3.4.5 Scanning and image analysis

Biomolecules labelled with carbon conjugates were scanned on an Epson 3200 Photo scanner (Seiko Epson, Nagano, Japan) with a resolution of 4800 dpi and 16 bit gray-scale and the images were saved as TIFF-files. Spot intensities were obtained by placing a marker ring at the circumference of the spot and determining the total pixel gray volume using TotalLab image analysis software. Data are given as the mean of 10 replicate spots. The mean pixel gray volume per unit spot area, i.e., the intensity, was also calculated and compared for all the non-porous substrates.

3.5 Results and discussion

3.5.1 Contact angle measurement

The hydrophobicity of the silanized glass was analyzed by measuring the contact angle (θ) of a sessile drop of water using a goniometer. Ten measurements on various locations of the slide were performed and the standard deviation was calculated. The average contact angle for these

Table 3.1 Goniometer data

Silane	Contact angle (θ)	SD
CPTS	49.4°	1.8
GPTS	61.2°	2.1
PhECS	75.2°	0.7
HMDS	88.2°	1.2
DCDMS	102.6°	1.2

ten measurements and the standard deviation showed that the slides were modified in a uniform pattern as the standard deviation for the entire silanized glass surface was less than 2.2 and of all the modified glass surfaces, the PhECS silanized substrate showed the least variation (see Table 3.1). Superior reproducibility was obtained for images of the water droplet on the silanized glass substrates are shown in Figure 3.2. These glass slides were used as substrate for printing biomolecules.

Silane used	Water droplet image on a goniometer	Contact angle (θ)
Untreated glass		<10°
CPTS		~49°
GPTS		~61°
PhECS		~75°
HMDS		~88°
DCDMS		~103°

Figure 3.2 Goniometer images of a water droplet (1 µL) placed on glass surfaces of varying hydrophobicites.

3.5.2 Microarray of biotinylated BSA and IgG on silanized glass surface

The distribution of biomolecules on the non-porous substrates was studied using two different model biomolecules, both biotinylated. BSA and IgG were inkjet-printed onto the non-porous substrates in two different buffers, PBS (pH 7.4) and CB (pH 9.6). The printed biotinylated biomolecules were incubated with streptavidin-Alexa-633 fluorophore and scanned at 10x magnification using a confocal microscope. The labeled biomolecules were scanned at various gain settings, from 1000 to 600. During scanning, all photomultiplier tube (PMT) settings were kept constant. The fluorophore labeled biomolecules were

scanned at gain values of 850 and 750, respectively. When scanned at gain values above 850, the fluorophore labeled biomolecules showed a very strong intensity on all substrates with a high background. This may lead to misleading results such as the conclusion that a spot shows a homogeneous distribution of biomolecules. However, reducing the gain setting may reveal doughnut-like distribution patterns (see Figure 3.3).

3.5.2.1 Biotinylated BSA and IgG on non-porous substrate

Spots of BSA-biotin in PBS printed on the various non-porous substrates showed differences in spot size and distribution. At a gain value of 850, spots of BSA-biotin did not show any fluorescence on a highly hydrophilic substrate like untreated glass (θ <10°) as well as on highly hydrophobic glass (θ >100°) (see Figure 3.3-A). Obviously, BSA molecules were only loosely bound to these surfaces and washed away upon addition of the solution with the streptavidin-fluorophore conjugate. In the series of substrates of varying hydrophobicity, the optimum total fluorescence was observed for the spots printed on the substrate having a water contact angle of 61°. The spot diameter was inversely proportional to the contact angle of the substrate (see Figure 3.4-B). Spots on the glass substrate with contact angle 49° showed higher fluorescence intensity with tailing appearance, commonly called as "spot smearing" effect[14, 22]. Substrates with contact angle 61° and 75° also showed higher fluorescence and a more uniform morphology as compared to the spots on other non-porous surfaces (see Figure 3.3-A). Substrates with contact angle larger than 75° showed spots with reduced fluorescence intensity and irregular spot morphology. When these spots were scanned at gain setting of 750, the overall signal intensity was lower with still some fluorescence on glass substrates with a contact angle of 49°-75°, but on the other substrates no fluorescence signal was observed at all (see Figure 3.3-A).

Gain value	(A) BSA-biotin printed on various non-porous substrates with PBS (pH 7.4)						
	UNTREATED θ<10°	CPTS θ~49°	GPTS θ~61°	PhECS θ~75°	HMDS θ~88°	HTA θ~92°	DCDMS θ~103°
850							No image
750	No image				No image	No image	No image
	(B) BSA-biotin printed on various non-porous substrates with CB (pH 9.6)						
850							
750							No image

Figure 3.3 CLSM images for BSA-biotin printed in (A) PBS (pH 7.4) and (B) CB (pH 9.6) scanned at two different gain values, 850 and 750

In carbonate buffer (pH 9.6), the total fluorescence intensity for labeled BSA-biotin spots on the non-porous substrates was higher compared to PBS (see Figure 3.4-A). These labeled spots were also scanned at the same PMT settings with a similar set of gain values (750 and 850). At gain value 850, BSA-biotin showed a fluorescence signal on all non-porous substrates (see Figure 3.3-B). The spot morphology was also uniform in carbonate buffer without any spot smearing. Spots were more compact and uniform in shape than observed in PBS buffer. On untreated glass, the printed droplet spread unevenly, which gave an irregular shape to the spot whereas on silanized glass substrates, the spots had a uniform shape except for the BSA-biotin printed on DCDM silanized substrate (θ ~103°) (see Figure 3.3-B).
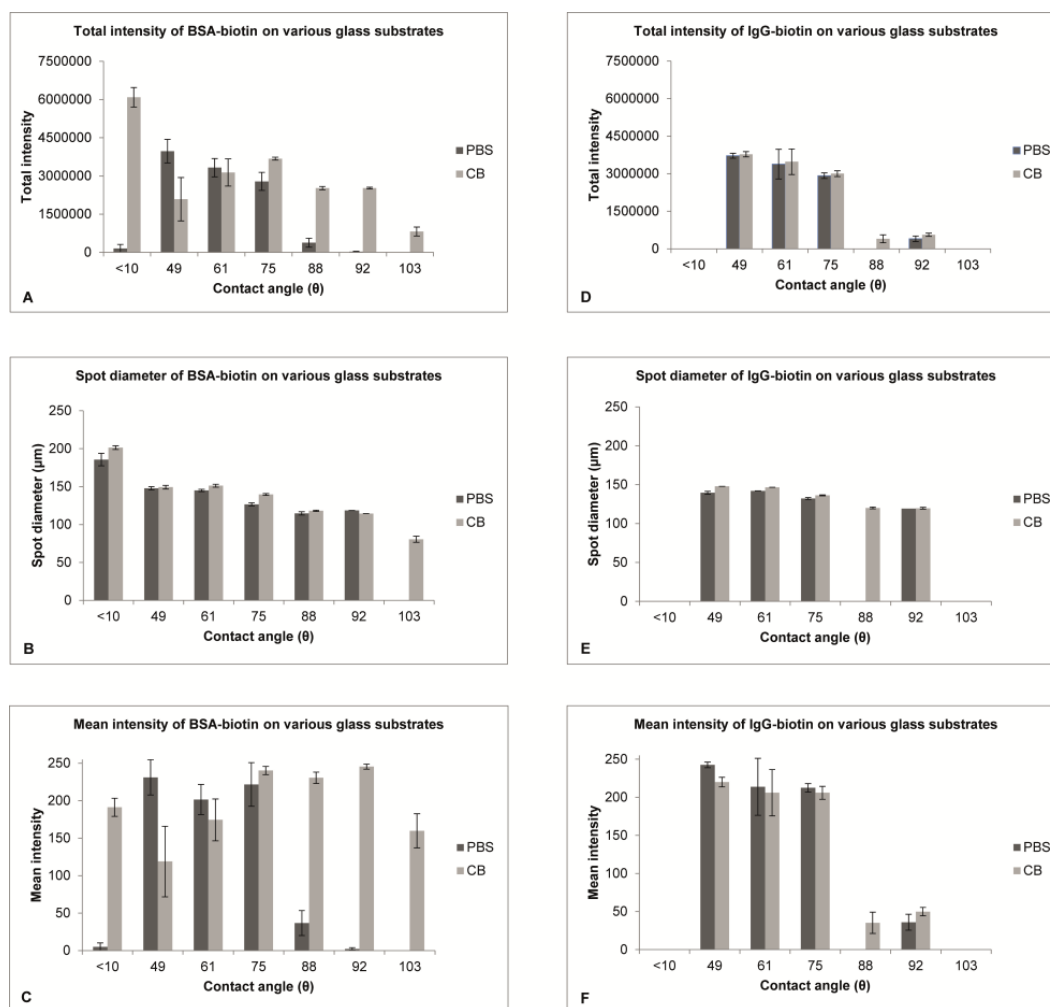
Figure 3.4 CLSM data on for BSA-biotin (A) Total intensity (B) spot diameter (C) mean intensity when scanned at gain value of 850 and (D) Total intensity (E) spot diameter (F) mean intensity for IgG-biotin when scanned at gain value of 1050.

Variation in the total intensity and the distribution of the biomolecule was observed on the non-porous substrates when these spots were scanned at a gain setting of 750 (see Figure 3.3-B). The total signal intensity of the printed spots was low on all surfaces except for those printed on PhECS silanized glass (θ ~75°) and HTA polystyrene slide. Doughnut-effects were clearly visible on all silanized surfaces except for PhECS silanized glass (θ ~75°). Even though the difference in water contact angle between HTA polystyrene slide (θ ~92°) and HMDS (θ ~88°) silanized glass was small, the total fluorescence intensity on

HMDS silanized glass was low as compared to the HTA polystyrene slide. This demonstrated that the substrate material also plays a role in total fluorescence intensity, i.e., by having particular binding characteristics towards the biomolecules. For BSA-biotin in CB, the mean intensity was almost similar on all the substrates whereas in PBS, the mean intensity was optimal on the substrate with a contact angle between 49°-75° (see Figure 3.4-C).

Similar experiments were also performed for biotinylated IgG printed on the non-porous substrates using same printing buffers; PBS (pH 7.4) and CB (pH 9.6). The spot size, total intensity and mean intensity of the labeled IgG showed variations depending on the substrate hydrophobicity (see Figure 3.4-D, E, F). On a highly hydrophilic substrate like untreated glass ($\theta < 10°$) and on a substrate with a contact angle of more than 75° the total fluorescence intensity was low, reflecting a weak binding of IgG molecules onto these surfaces. IgG-biotin printed on substrates with a contact angle between 49°-75° showed a higher total fluorescence signal as compared to the other substrates. The difference in the total fluorescence intensity between PBS and CB was very small.

As shown above (see Figure 3.3, 3.4) the uniformity of the spots as well as the reproducibility of the staining of the spots (in terms of standard deviation) was superior on the substrate with the contact angle ~75° (PhECS silanized). With respect to surface hydrophobicity this modified surface also demonstrated the best homogeneity (lowest standard deviation as shown in Table 3.1), which positively contributes to the experimental results. As shown previously, the binding efficiency of the biomolecules is increased sufficiently on the functionalized glass as compared to native glass[9, 16]. On such modified substrates a real diagnostic test like ELISA[23] and protein binding studies can be performed as well as high throughput signal can be achieved[24].

However, irrespective of the substrate used during CLSM imaging, the signal-to-noise ratio's vary in accordance to the set gain values. Preferably, the laser gain value should be optimized in such a way that the background is not illuminated (i.e. a black background). This ensures that the sample spot is not over-exposed, i.e., that the distribution of biomolecules within the spot is clearly visible. Improper setting at too high gains may hamper the correct interpretation of the results such as missing the doughnut-shaped distribution of the biomolecules over the spot area.

3.5.3 NAMIA for anti-DIG on various substrates

A NAMIA was performed with anti-DIG antibodies printed on the various non-porous substrates. Incubation with DIG-/biotin-tagged amplicons and carbon-alkaline phosphatase-neutravidin conjugate, simultaneously, showed an excellent signal-to-noise ratio for all the non-porous substrates except for hydrophilic glass (θ <10°) (see Figure 3.5-top). The average pixel gray volume (PGV) of ten spots was used to compare the substrates. It was found that the highest signals were obtained on substrates with a contact angle of 61° and 75°. On substrates with a contact angle higher than 75° the total PGV was lower than observed for the substrates with a contact angle lower than 75°(see Figure 3.5-left).

In the previous section it was shown that the spot size and the substrate hydrophobicity were inversely proportional. Therefore, the mean signal was also calculated based on the total signal per unit spot area. As shown (see Figure 3.5-right), the mean PGV was not proportional to the hydrophobicity of the surface. The mean PGV was higher for spots printed on the HTA polystyrene substrate and on the glass substrates with a contact angle of 61° and 75°, as compared to those observed on glass substrates with a contact angle

of 49° and 88°. Whereas the DCDMS treated substrate (θ ~103°) showed a higher mean PGV as compared to others (Figure 3.5-right).
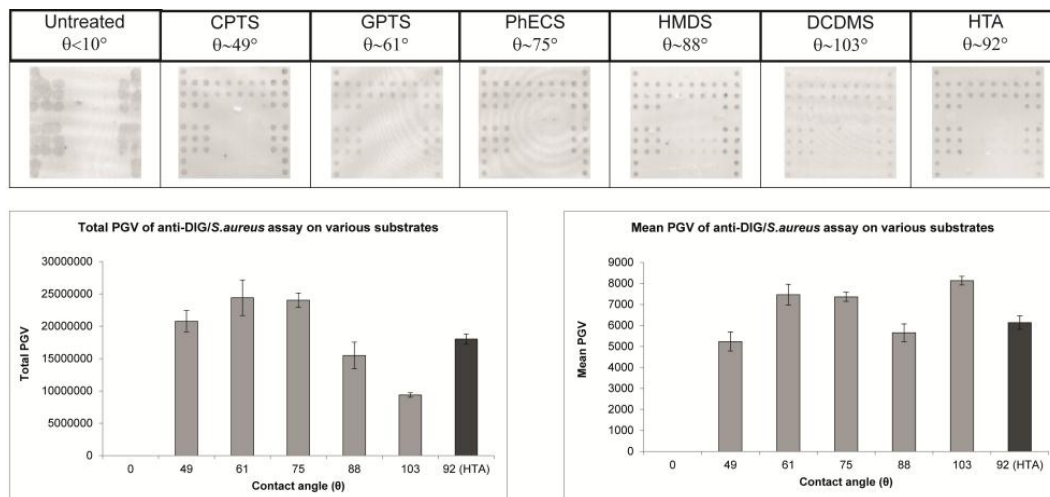

Figure 3.5 (top) Scanned images of the Nucleic Acid Microarray ImmunoAssay for the detetion of Staphylococcus aureus performed on various hydrophobic substrates. Total PGV (left). Mean PGV of the scanned NAMIA results (right).

Even though the functionality of the anti-DIG antibody, as reflected by total and mean fluorescence, on GPTS and PhECS silanized substrate was similar, the standard deviation of both total and mean pixel gray volumes was smaller on the PhECS silanized glass slide. A similar conclusion was drawn from the experiments in which BSA and IgG were printed on the various non-porous substrates (see Figure 3.4 and 3.5).

3.6 Conclusions

Following inkjet printing of BSA and IgG on a series of modified glass and polystyrene substrates with a range of hydrophobicities (contact angle 49°-103°) the distribution of these biomolecules, the total fluorescence intensity and the spot uniformity were analyzed. Based on confocal microscopy and image analysis of the pixel gray volumes of printed spots the HTA polystyrene slide and the glass substrate silanized with PhECS (θ ~75°) were superior as

compared to the other non-porous substrates. Analysis of the spot morphology by confocal microscopy requires a proper gain setting to prevent misinterpretation by over-exposure. These results can be used to rationalize and optimize the development of diagnostic protein microarrays.

References

1.   H. Zhu and M. Snyder, *Current Opinion in Chemical Biology*, 2003, 7, 55-63.

2.   K. Abe, K. Kotera, K. Suzuki and D. Citterio, *Analytical and Bioanalytical Chemistry*, 2010, 398, 885-893.

3.   I. Barbulovic-Nad, M. Lucente, Y. Sun, M. Zhang, A. R. Wheeler and M. Bussmann, *Critical Reviews in Biotechnology*, 2006, 26, 237-259.

4.   B. A. Stillman and J. L. Tonkinson, *BioTechniques*, 2000, 29, 630-635.

5.   P. S. Noguera, G. A. Posthuma-Trumpie, M. van Tuil, F. J. van der Wal, A. d. Boer, A. P. H. A. Moers and A. van Amerongen, *Analytical Chemistry*, 83, 8531-8536.

6.   M. Moschallski, J. Baader, O. Prucker and J. Rühe, *Analytica Chimica Acta*, 2010, 671, 92-98.

7.   A. Y. Rubina, A. Kolchinsky, A. A. Makarov and A. S. Zasedatelev, *Proteomics*, 2008, 8, 817-831.

8.   P. Angenendt, J. Glökler, D. Murphy, H. Lehrach and D. J. Cahill, *Analytical Biochemistry*, 2002, 309, 253-260.

9.   R. L. DeRosa, J. A. Cardinale and A. Cooper, *Thin Solid Films*, 2007, 515, 4024-4031.

10.   M. Rober, J. Walter, E. Vlakh, F. Stahl, C. Kasper and T. Tennikova, *Analytica Chimica Acta*, 2009, 644, 95-103.

11.   K. Sollier, C. A. Mandon, K. A. Heyries, L. J. Blum and C. A. Marquette, *Lab on a Chip*, 2009, 9, 3489-3494.

12.   Y. Liu, C. M. Li, W. Hu and Z. Lu, *Talanta*, 2009, 77, 1165-1171.

13.   C. Preininger, U. Sauer, J. Dayteg and R. Pichler, *Bioelectrochemistry*, 2005, 67, 155-162.

14.   L. Mujawar, A. van Amerongen and W. Norde, *Talanta*.

15.   K. Stadtherr, H. Wolf and P. Lindner, *Analytical Chemistry*, 2005, 77, 3437-3443.

16.   B. Joos, H. Kuster and R. Cone, *Analytical Biochemistry*, 1997, 247, 96-101.

17.   C. M. Halliwell and A. E. G. Cass, *Analytical Chemistry*, 2001, 73, 2476-2483.

18.   K. E. Sapsford and F. S. Ligler, *Biosensors and Bioelectronics*, 2004, 19, 1045.

19.   S.-K. Chiu, M. Hsu, W.-C. Ku, C.-Y. Tu, Y.-T. Tseng, W.-K. Lau, R.-Y. Yan, J.-T. Ma and C.-M. Tzeng, *Biochem. J.*, 2003, 374, 625-632.

20.   G. A. Diaz-Quijada, R. Peytavi, A. Nantel, E. Roy, M. G. Bergeron, M. M. Dumoulin and T. Veres, *Lab on a Chip*, 2007, 7, 856-862.

21.   P. S. Noguera, G. A. Posthuma-Trumpie, M. van Tuil, F. J. van der Wal, A. d. Boer, A. P. H. A. Moers and A. van Amerongen, *Analytical Chemistry*, 2011, 83, 8531-8536.

22.   A. Ressine, G. r. Marko-Varga, T. Laurell and M. R. El-Gewely, in *Biotechnology Annual Review*, Elsevier, 2007, vol. Volume 13, pp. 149-200.

23.   L. G. Mendoza, P. McQuary, A. Mongan, R. Gangadharan, S. Brignac and M. Eggers, *Biotechniques*, 1999, 27, 778-788.

24.   G. MacBeath and S. L. Schreiber, *Science*, 2000, 289, 1760-1763.

4

Influence of relative humidity on the spot morphology of inkjet printed spots

Abstract

During the drying of inkjet printed droplets, the solute particles (biomolecules) in the drop may distribute unevenly on the substrate resulting in a "coffee-stain" or "doughnut-shape" spot morphology. The drying of the droplet depends on the relative humidity and, therewith, on the rate of evaporation. In our study, we investigated the influence of the relative humidity on the distribution of inkjet printed biomolecules on a polystyrene substrate. A theoretical model for an evaporating droplet was developed in order to predict the changes in the spot diameter, height and volume of a drying droplet. An experiment was performed at relative humidity of ~19% where a sessile droplet was monitored using a CCD camera installed on a goniometer and a good agreement was found between experimental results and simulation data. Further, we also developed pinned contact line model and predicted the changes in the spot morphology for an inkjet printed microarray spot for various relative humidities (40%, 50% 60%, 70% and 80%). The simulation results were confirmed by experimental analysis where fluorophore labeled IgG molecules were printed and dried at various relative humidities. Spot morphology of the dried spots was analyzed by confocal laser microscopy. At lower relative humidity (i.e., <60%), a non-homogeneously distributed spot morphology resembling a doughnut was prominent, whereas a more homogeneous distribution was observed when droplets were printed and dried at a higher relative humidity (~70%).

4.1. Introduction

Inkjet printing is one of the most versatile techniques used for depositing a range of polymers and colloid materials onto various substrates[1-4]. In the past, researchers have demonstrated the application of inkjet printing to produce microarrays[5-7] of various biomolecules onto non-porous substrates like glass[8-11] and plastic[12, 13]. Such non-porous substrates are preferred over porous substrates since they are cost-durable and easily available. However, printing of biomolecules (for e.g., producing biochips) on non-porous substrates is a challenge because the distribution of the biomolecules is influenced by parameters like temperature, relative humidity[14-16] (RH) and solvent[13, 17] (pH and composition). The most commonly observed non-homogeneous distribution of inkjet printed spots, often termed 'coffee-stain' effect or 'doughnut-shape' spot, was studied in detail by Deegan *et al.*[18-20]. Deegan's approach is based on the in-homogeneity of the substrate surface such that the contact line of the drop remains pinned during evaporation. This implies that the dynamics of the solvent is dominated by the surface tension of the droplet driving the solution to the outward direction, thereby causing the coffee-stain effect. An extension to this model was proposed by Fischer[21], where the shape of the droplet is not assumed to be spherical during the evaporation process. Van Dam and Kuerten[22] proposed an extension for the calculation of the curvature of the droplet shape in order to incorporate a less flat micro-scale droplet than was assumed in the previous model.

While printing, controlled evaporation of the droplet[14] (by maintaining a constant relative humidity) is of crucial importance. In our research, we have demonstrated the influence of various relative humidities (40±1% / 50±1% / 60±1% / 70±1% and 80±1%) on the distribution of inkjet printed biomolecules. Using a non-contact microarrayer, fluorophore-labeled antibody molecules

(IgG-Alexa-635) were printed and dried under similar conditions and the spot morphology of the biomolecules in the dried spots was analyzed by confocal laser scanning microscopy. From the observed profiles of the spots we could determine the distribution pattern of the biomolecules printed and dried at various relative humidities.

Further, we present a mathematical model for the fluid dynamics and the distribution of the solute molecules. The model is based on considering three major aspects: flow of the liquid due to evaporation, convection and diffusion of the solute, and binding of the solute molecules to the substrate.

4.2 Materials and methods

4.2.1 Mathematical Model

The mathematical model covers the dynamics of the solvent due to evaporation, the change in concentration of the solute and the binding of the solute molecules to the surface. Figure 4.1 depicts an axially symmetric droplet on a horizontal substrate, where *h* denotes the height of the droplet.
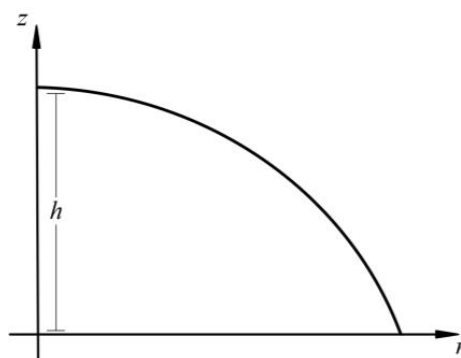

Figure 4.1 Schematic representation of a spherical droplet on an impermeable substrate.

A complete model for the flow inside the droplet is provided by the three-dimensional Navier-Stokes equation and the continuity equation for an incompressible fluid. However, a study of the order of the magnitude of the

terms in these equations reveals that the model can be simplified by the lubrication approximation[21-24]. The most important assumption in this simplified model is that the height of the droplet is small compared to its radius. This assumption leads to a simplified form of the Navier-Stokes equation. In this approach, the radial velocity component can explicitly be determined from the pressure difference between the inside and the outside of the droplet at the liquid-air interface.

The dynamics of a sessile droplet is driven by the pressure p in the droplet, which is strongly influenced by the surface tension σ and by the radius of curvature of the interface. The shape of the droplet $h(r)$ is determined by conservation of mass, which incorporates changes in shape due to the flow inside the droplet driven by the pressure and due to evaporation.

$$\frac{\partial h}{\partial t} = \frac{1}{3\mu}\frac{1}{r}\frac{\partial}{\partial r}\left(rh^3\frac{\partial p}{\partial r}\right) - J(r) \tag{1}$$

where t is the time, r denotes the radial coordinate, μ is the dynamic viscosity and $J(r)$ indicates the evaporation velocity, which may depend on the radial coordinate. Evaporation of the droplet is induced by a normal gradient of vapor pressure at the droplet-liquid interface. The vapor pressure gradient depends on the relative humidity in the ambient air and on the temperature-dependent saturation pressure. An evaporation model by Popov[25] and Siregar *et al.*[26] is applied to describe the mass transfer over the liquid-air interface.

The pressure within the droplet is dominated by the surface tension. At the liquid–air interface, the pressure difference between the droplet and the air is given by the Laplace pressure:

$$p = -\sigma \ \frac{1}{r}\frac{\partial}{\partial r} \left(\frac{r}{\sqrt{1+\left(\frac{\partial h}{\partial r}\right)^2}} \frac{\partial h}{\partial r} \right) \tag{2}$$

The term in the denominator accounts for the exact radius of curvature of an axially symmetric drop. It allows for extending the range of validity of the lubrication approximation to the case with a larger ratio between height and radius. In case the contact line of the droplet is not pinned to the substrate, the dynamics of the contact line is incorporated in the model by adding the disjoining pressure to (2)[26]. The disjoining pressure, which accounts for the molecular interaction near the contact line, is only unequal to zero in a small region near the contact line and keeps the contact angle constant.

During the evaporation process, the change in solute concentration is determined by three physical phenomena: the loss of solvent by evaporation, the dynamics of the fluid due to the surface tension, and the adsorption of solute molecules to the substrate. The loss of solvent not only increases the solute concentration but also leads to transport of solute by diffusion. Adsorption leads to a local decrease of solute concentration in the region near the liquid-substrate interface. Hence, the concentration distribution of the solute is governed by a two dimensional convection-diffusion equation:

$$\frac{\partial C}{\partial t} = -\frac{1}{r}\frac{\partial}{\partial r}(rCu) - \frac{\partial}{\partial z}(Cw) + D\frac{1}{r}\frac{\partial}{\partial r}\left(r\frac{\partial C}{\partial r}\right) + D\frac{\partial^2 C}{\partial z^2} - F\delta(z) \tag{3}$$

where C is the solute concentration in the droplet, u and w are radial and axial velocity components, respectively, and D is the diffusivity of the solute particles. The function F describes the mass loss of the solute in mass per unit area due to the binding between molecules and surface. This process takes place only on the surface of the substrate. Furthermore, we have to define the

function *F* due to adsorption and also quantify the amount of adsorbed biomolecules on the surface.

The adsorption of the solute determines the surface coverage and influences the functioning of the biomolecule. Here we make use of a model by Kurrat *et al.* [27] where the adsorption of biomolecules may happen in a reversible and an irreversible way. This model describes the dependency of the mass adsorption rate on the concentration of the solute particles near the liquid-substrate interface C_s. The region where the solute concentration influences the adsorption rates depends on the choice of the numerical discretization of the mathematical model[28]. We indicate the reversibly and irreversibly adsorbed mass per unit area by M_r and M_i, respectively[30]. The rates of adsorption for the reversible and irreversible processes are given by:

$$\frac{\partial M_r}{\partial t} = k_a C_s \emptyset - \frac{k_d M_r}{\sqrt{\emptyset}} \tag{4}$$

$$\frac{\partial M_i}{\partial t} = k_s C_s \emptyset \tag{5}$$

where k_a and k_s are the rate constants for reversible and irreversible adsorption, respectively, and k_d is the rate constant for desorption. These constants can be determined experimentally and depend on the type of molecule, on the buffer that is used and on the properties of the substrate. The variable ϕ defines the fraction of surface area that is available to become occupied by the solute particles. Using conservation of solute mass, the rate of solute mass loss *F* defined in the concentration model Eq. (3) is given as the sum of the rates for reversible and irreversible adsorption from Eqs. (4) and (5):

$$F = k_a C_s \emptyset - \frac{k_d M_r}{\sqrt{\emptyset}} + k_s C_s \emptyset \tag{6}$$

4.2.2 Experimental

4.2.1.1 Substrate and reagents

For the experimental studies, a non-porous HTA polystyrene (PS) slide was used which was purchased from Greiner BioOne (Kremsmuenster, Austria). For printing onto the polystyrene substrate, a 100 mM carbonate buffer (CB) pH 9.6 was prepared in Milli-Q water with resistivity of 18.2 MΩ cm^{-1}.

4.2.1.2 Biomolecules

Microarrays were produced on HTA polystyrene slide by printing IgG-Alexa-635 which was purchased from Invitrogen (Oregon, USA). The stock was diluted to (200 µg/mL) in 0.1 M CB (pH 9.6) and loaded into the wells of Genetix microtiter plate (Genetix X7020, Berkshire, United Kingdom).

4.2.2.3 Printing of biomolecules

Biomolecules were printed on the HTA polystyrene slides with a non-contact spotter, sciFLEXARRAYER S3 (Scienion AG, Berlin, Germany). The voltage and pulse of the piezo dispensing capillary (PDC) were optimized to print a droplet of ~250 pL. The temperature was maintained at 21°C. On these HTA slides, IgG-Alexa-635 was printed at different relative humidities, i.e. 40%, 50%, 60%, 70% and 80%.

While printing under various relative humidities, other printing conditions like temperature (~21°C), voltage (88V) and pulse (49µs) were kept constant. Prior to printing, the hood of the printer was allowed to be conditioned for 15 minutes at the set humidity value. After printing, the substrate was incubated and dried under the same conditions for one hour and stored in a sealed aluminium pouch. After overnight drying, the printed spots were analyzed by CLSM to study the spot morphology and the distribution of the biomolecules in the spot.

4.3 Instrumentation

4.3.1 Goniometer

The influence of relative humidity on the drying of the droplet was analyzed by monitoring the change in contact angle (θ), diameter (D), the volume (V) and the height (h) of a liquid droplet using a Krüss contact angle measuring system (G10, Hamburg, Germany). A 2 µL MQ water droplet was placed on the surface of a polystyrene slide and analyzed by an in-built CCD video camera (Sony XC-77CE). All the parameters were measured with the drop analysis software (DSA-1).

The change in contact angle (θ) and volume (V) for a droplet of IgG-Alexa (200µg/mL) was monitored at two different relative humidity levels, ~19% and ~75% respectively. The measurements at 19% relative humidity were performed in a room where the default humidity was 19±1%. For the measurements at 75% relative humidity the HTA PS slide was placed inside a transparent home-made chamber which was pre-saturated with water. Prior to placing the droplet on the HTA polystyrene surface, the relative humidity inside the chamber was monitored for one hour using a portable thermo-hygrometer (Testo AG, Lenzkirch, Germany). The relative humidity was found to be 75±1%. This transparent chamber was positioned on the stage of the goniometer and using a micropipette a droplet was placed on the HTA polystyrene surface.

4.3.2 Confocal laser scanning microscopy (CLSM) imaging

The distribution of the fluorophore-labelled biomolecules printed at various humidities on the non-porous HTA PS slide was analyzed by confocal laser scanning microscopy (Carl Zeiss Axiovert 200 microscope, Zeiss, Jena, Germany), equipped with a LSM 5 Exciter. The spots were scanned at 10x magnification and the configuration of the objective was LD Plan-Neofluar 10x/0.30 Korr M27. The CLSM was set at 633 nm with a He-Ne laser, the size of

the pinhole was 206 nm and the transmission was 11%. The dimensions of the scanner were X: 1272.79 μm, Y: 1272.79 μm, respectively. The mean intensity of the spots was analyzed by "Zen 2008" software, and the homogeneity of the spots was investigated using ImageJ software. The CLSM images files (*.lsm) were uploaded into ImageJ software and a cross-section profile plot for each of the nine spots was calculated; the final plot data were made after averaging these values along with the standard deviation. The total intensity for each spot was also calculated as the product of the mean intensity and the surface area of the spots.

4.4 Results and Discussion

4.4.1 Numerical validation

The validation of the lubrication approach and of the evaporation model is presented in this subsection. Numerical results are compared with experimental results from an experiment in which a droplet of MQ water was evaporated at a relative humidity of ~19%.

Figure 4.2 shows the comparison between the numerical and experimental results during the evaporation. The experimental results clearly indicated that the contact line is not pinned: the diameter monotonically decreased during the evaporation due to which the contact angle remains constant in time. Therefore, we included the disjoining pressure in the model with a constant contact angle of 90°.

Figure 4.2-B shows the droplet volume as a function of time. During the whole evaporation process the experimental results agreed very well with the model results and showed the typical behavior for an unpinned contact line, in which the rate of mass loss is proportional to the radius of the droplet. In Figure 4.2-A it can be seen that the experimentally measured diameter was almost constant

during the first stages of the evaporation process, after which it started decreasing at the same rate as in the model. This indicates that the contact line was pinned during the first stages and then started retracting. The results for the droplet height, displayed in Figure 4.2-C, are consistent with this explanation: initially the measured decrease in height is larger than predicted by the model, after 2-3 minutes they decrease at the same rate.
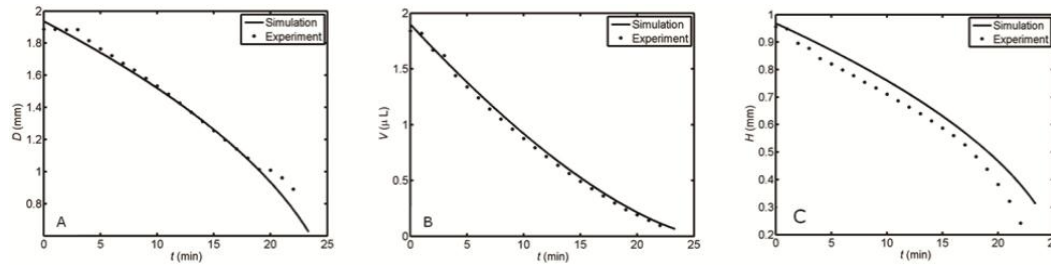

Figure 4.2 Comparison between numerical and experimental results for a droplet with initial volume 2 μL and relative humidity *RH*=0.19. The numerical simulation is performed with the model for the droplet with an unpinned contact line on PS surface. The comparison shows the droplet (A) diameter (B) volume and (C) height, as functions of time.

4.4.2 Experimental analysis of drying of a liquid droplet at two different humidities (~19% and ~75%)

As shown in section 4.1, an unpinned situation was observed for a pure liquid droplet drying on a non-porous substrate. We also studied the influence of two different relative humidities i.e., ~19% and ~75% on the drying of a droplet of IgG-Alexa-635 (200 μg/mL) by monitoring the change in contact angle (θ_t) and volume (V).
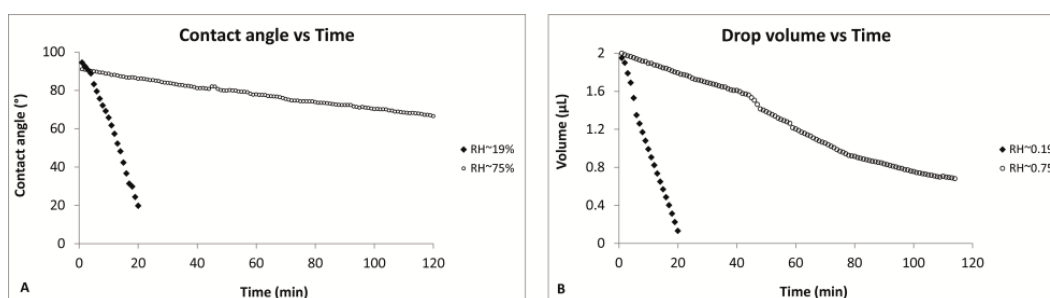
Figure 4.3 The influence of humidity on the drying of a droplet containing IgG-Alexa-635 monitored by a goniometer; (A) change in contact angle (θ) and (B) change in volume at two different relative humidities; ~19% and ~75%.

It was found that irrespective of the relative humidity used, the initial contact angle (θ_0) for a sessile droplet on a PS surface was ~93°. The change in contact angle (θ) during the drying process was faster at lower RH: in 20 seconds θ decreased to 46° at *RH* ~19%, whereas at *RH* ~75% it decreased to 86° (Figure 4.3-A). These observations are in agreement with studies performed earlier by Lages *et al.* who used modified gold surfaces and observed the change in contact angle (θ) for aqueous solutions under controlled conditions[29]. Irrespective of the relative humidity used for drying, the contact angle changed with time (see Figure 4.3-A), thus implying that, in contrast to a droplet of MQ water, the contact line of a liquid droplet containing biomolecules was pinned.

The influence of the relative humidity on the drop volume history was also significant; at *RH* 19% evaporation of the initial volume (2 µL) to 0.6 µL occurred in less than 20 minutes, whereas at *RH* ~75% it took 120 minutes (Figure 4.3-B). Our observations are in line with those presented by Liu[15] *et al.* who, at a lower humidity (47%), observed a significant decrease in sessile drop volume of pure water as compared to the same experiment at a higher humidity (80%).

4.4.3 Influence of relative humidity on mass distribution on non-porous substrates

In this subsection the influence of the relative humidity on the deposited solute mass is described. The relative humidity determines the magnitude of the evaporation term compared to the convective term in the evolution equation for the droplet height Eq. (1). Due to the small diffusion coefficient, the solute transport within the droplet is mainly driven by convection. In this study, we choose relative humidity values ranging between 0.3 and 0.9 and considered a droplet with a pinned contact line, an initial volume of 250 pL and a diameter of 100 μm. The consideration of a pinned contact line model can be well understood with the results explained in Section 4.2. We choose higher rate constants for adsorption and desorption than Kurrat *et al*.[27], in order to take into account the effect of the hydrophobicity[30] of the substrate in our case.

The maximum possible adsorbed mass density equals 3.7 mg/m^2, whereas the initial concentration leads to an average deposited mass density of 6.4 mg/m^2. This implies that not all molecules present in the solution can be adsorbed. After the liquid has completely evaporated there will still be molecules unbound to the substrate.

Figure 4.4-A shows the profiles of the total deposited mass density, including both the adsorbed and the unbound molecules, and Figure 4.4-B shows the profiles of the adsorbed mass density. The most important effect of the relative humidity is the total evaporation time. For lower relative humidities the evaporation rate is larger and this results in a higher convection velocity in the droplet and a lower evaporation time. Therefore, in the center of the droplet only a small fraction of the molecules can be adsorbed before they move with the liquid toward the edges of the droplet. Consequently, the concentration becomes higher near the edges of the drop and after total evaporation there will

still be a large number of unbound molecules close to the edge of the droplet. At low relative humidity both the total deposited mass density and the adsorbed mass density show the doughnut shape. At the highest relative humidity considered here (0.9) the evaporation rate and hence the convection velocity toward the edges are so low, that the substrate is almost completely covered with adsorbed molecules in the center region of the droplet. The unbound molecules are still transported to the edges, but the resulting total deposited mass density profile is more uniform.
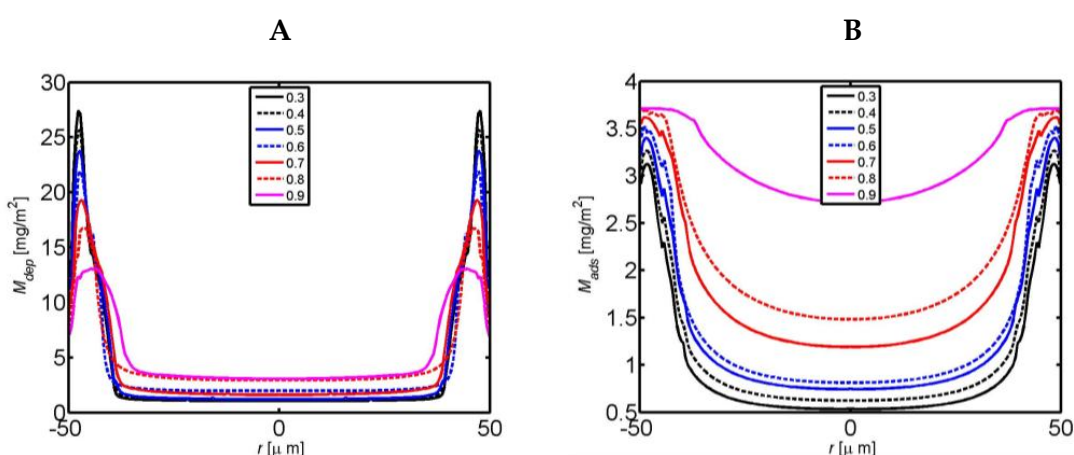
A   **B**

Figure 4.4 Total deposited mass density (A) and adsorbed mass density (B) as functions of the radial.

4.4.4 Experimental analysis of the influence of relative humidity on the fluorescence of inkjet printed biomolecules

Spots of fluorophore-labeled biomolecules printed and dried on a non-porous surface showed variations in the spot morphology and fluorescence intensity depending on the ambient relative humidity. The average mean intensity and total intensity of the inkjet printed spots had a maximum when the biomolecules were printed and dried at a relative humidity of 60% (see Figure 4.5-A, B).
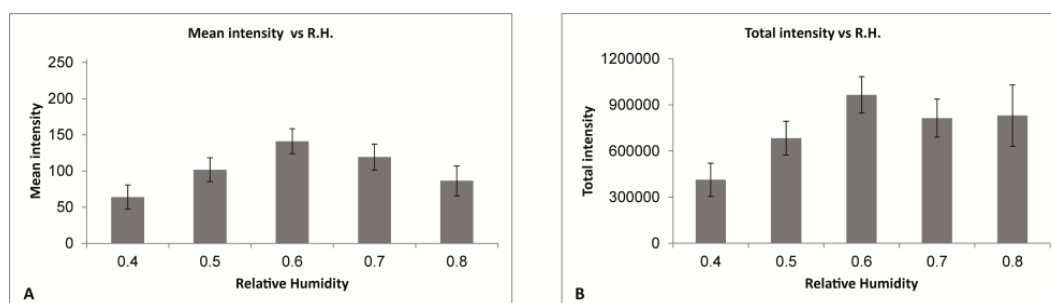
Figure 4.5 Based on CLSM data average mean intensity (A) and average total intensity (B) of the IgG-Alexa-635 spots printed on non-porous surface at various relative humidity.

At low humidity (~0.4), the morphology pattern of the spots of IgG-Alexa-635 showed a non-homogeneous distribution, which resembles a doughnut-shape or a coffee-stain (see Figure 4.5-A). The intensity profile plot clearly shows a higher fluorescence at the edge of the spot as compared to the overall spot area, thus confirming an inhomogeneous distribution. The higher fluorescence intensity observed at the edge of the spot is due to a higher locally deposited mass of biomolecules, as observed in the results of the model of total mass distribution (see Figure 4.4-A). This uneven distribution results from the pinning of the contact line of the evaporating droplet[18] which in turn causes internal convection within the droplet creating an outward flow of the biomolecules towards the edge of the spot[19].

When printing was performed at high relative humidities (>40%), the overall uniformity of the spots increased with increasing humidity. As shown in the profile diagram, the fluorescence intensity was higher at the edge of the spot when the drop was dried at 40% and 50% relative humidity, with a very low fluorescence intensity in the central part of the spot (see Figure 4.6-A,B). Upon raising the relative humidity to 60%, (RH~0.6), the drying time further increased and the doughnut-effect reduced as compared to the drying of similar droplets at lower relative humidities (see Figure 4.6-C). A better and more homogeneous

distribution was observed when the biomolecules were printed at 70% (RH~0.7) where the profile plot was much more uniform (see Figure 4.6-D). This situation may be explained by the fact that at higher relative humidity, the droplet has a longer drying time and hence shows less internal convection. This allows the biomolecules present within the sessile droplet to settle on the substrate rather than being transported to the edges. Moreover, at higher relative humidity the effect of diffusion, which counteracts high local solute concentrations, becomes more prominent. However, although the spot morphology at RH ~0.7 was better than at RH ~0.6, both the mean and total fluorescence intensities were higher at RH~0.6. This may indicate that the conditions for binding of the biomolecule at the surface may be more favorable at RH ~0.6 as compared to ~0.7. Further increase in the humidity (up to RH~0.8) resulted in an increased spreading of the droplet which was clearly demonstrated by the larger spot diameter (117 μm) as compared to 96 μm observed for IgG-Alexa spots printed and dried at 40% humidity (see Figure 4.6-E). Also at RH ~0.8 the spot morphology was quite uniform, although the total intensity was less than at RH ~0.6 (see Figure 4.6, right panel). The results of the numerical simulations for the case of a pinned contact line also showed a similar behavior as was observed in the experiments (see Figure 4.3-A), i.e., when a sessile drop was allowed to evaporate at lower relative humidity the contact line was pinned and the resulting mass distribution was non-homogeneous which was confirmed by experimental results as well.

Based on the plot profile diagram in Figure 4.6, it can be concluded that the overall spot morphology was irregular when the biomolecule was printed and dried at lower humidities (<60°), whereas fluorescence intensity was distributed more evenly when higher relative humidities (>60°) were applied. The mechanism behind the non-homogeneous distribution of biomolecules at lower humidity had already been demonstrated for colloidal polystyrene particles by

Chhasatia[14] *et al.*. Using a CCD camera they showed that at lower humidity the outward migration of the colloidal particles was higher, giving rise to a doughnut-shaped spot, whereas with increasing relative humidity the distribution of the colloidal particles was more uniform. Similar studies on the relation between a pinned contact line and ring formation at lower humidity have been reported by Deegan *et al.*[20].

In our study we focused on establishing optimal humidity conditions for obtaining a more homogeneous distribution of printed biomolecules on the non-porous substrate HTA. The experimental results were in line with theoretical simulations. To overcome the coffee-stain effect, Eral *et al.* demonstrated the process of electrowetting[31]; they showed that the applied electrostatic forces prevented the three phase contact line and generated an internal flow field thereby preventing the accumulation of solutes along the contact line.

Additionally, researchers have shown that incorporation of additives to the printing buffer can also improve the non-homogeneous distribution in an inkjet printed spot[32-36]. The influence of a pluronic additive to improve the functionality, i.e. the antigen binding capacity, of printed antibody molecules is the subject of our next chapter (Chapter 6).
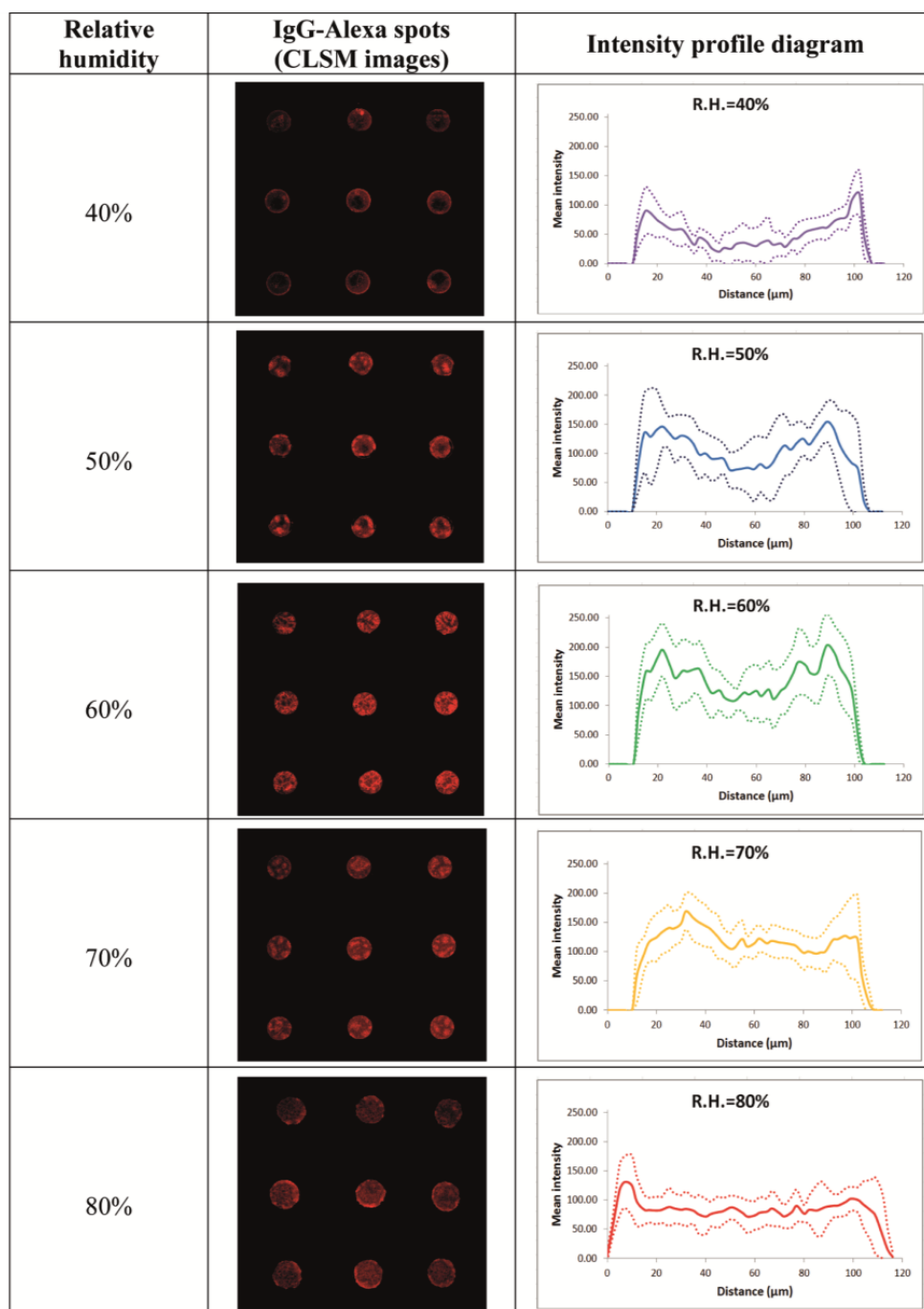
Relative humidity	IgG-Alexa spots (CLSM images)	Intensity profile diagram
40%		
50%		
60%		
70%		
80%		

Figure 4.6 CLSM images of IgG-Alexa-635 printed and dried at (A) ~40%, (B) ~50%, (C) ~60%, (D) ~70% and (E) ~80% at relative humidity, Also shown in the extreme right column the intensity plot profile for these spots at the respective humidities along with the standard deviation.

4.5 Conclusions

By numerical simulations and experiments we have demonstrated the influence of the relative humidity on the mass distribution of inkjet-printed biomolecules on non-porous substrates. It was found that at low humidity, the printed biomolecules are non-homogeneously distributed, thus resulting in doughnut-shaped spots. With increasing relative humidity, the doughnut-like appearance decreased and a more homogeneously distributed spot morphology was achieved. The best morphological results were obtained at a relative humidity of 0.7, but with respect to mean and total fluorescence intensities we conclude that the optimum relative humidity for printing biomolecules onto non-porous substrates is between 60-70% relative humidity. The results compare favorably with results of a numerical model in which it is assumed that the contact line of the droplet is pinned during the evaporation process.

References

1.   H. Sirringhaus, T. Kawase, R. H. Friend, T. Shimoda, M. Inbasekaran, W. Wu and E. P. Woo, *Science*, 2000, **290**, 2123-2126.

2.   H. Yan, Z. Chen, Y. Zheng, C. Newman, J. R. Quinn, F. DÃ¶tz, M. Kastler and A. Facchetti, *Nature*, 2009, **457**, 679-686.

3.   P. Calvert, *Chemistry of Materials*, 2001, **13**, 3299-3305.

4.   H. H. Lee, K. S. Chou and K. C. Huang, *Nanotechnology*, 2005, **16**, 2436-2441.

5.   P. Arenkov, A. Kukhtin, A. Gemmell, S. Voloshchuk, V. Chupeeva and A. Mirzabekov, *Analytical Biochemistry*, 2000, **278**, 123-131.

6.   S. Choudhuri, *Journal of Biochemical and Molecular Toxicology*, 2004, **18**, 171-179.

7.   I. Barbulovic-Nad, M. Lucente, Y. Sun, M. Zhang, A. R. Wheeler and M. Bussmann, *Critical Reviews in Biotechnology*, 2006, **26**, 237-259.

8.   L. H. Mujawar, W. Norde and A. van Amerongen, *Analyst*, 2013, **138**, 518-524.

9.   R. L. DeRosa, J. A. Cardinale and A. Cooper, *Thin Solid Films*, 2007, **515**, 4024-4031.

10.   M. Dufva, *Biomolecular Engineering*, 2005, **22**, 173-184.

11.   W. Kusnezow and J. D. Hoheisel, *Journal of Molecular Recognition*, 2003, **16**, 165-176.

12.   Y. Liu, C. M. Li, W. Hu and Z. Lu, *Talanta*, 2009, **77**, 1165-1171.

13.   L. H. Mujawar, A. van Amerongen and W. Norde, *Talanta*, 2012, **98**, 1-6.

14.   V. H. Chhasatia, A. S. Joshi and Y. Sun, *Applied Physics Letters*, 2010, **97**, 231909-231903.

15.   C. Liu, E. Bonaccurso and H.-J. Butt, *Physical Chemistry Chemical Physics*, 2008, **10**, 7150-7157.

16.   M. J. Mackel, S. Sanchez and J. A. Kornfield, *Langmuir*, 2006, **23**, 3-7.

17.   W. Kusnezow, A. Jacob, A. Walijew, F. Diehl and J. D. Hoheisel, *Proteomics*, 2003, **3**, 254-264.

18.   R. D. Deegan, O. Bakajin, T. F. Dupont, G. Huber, S. R. Nagel and T. A. Witten, *Nature*, 1997, **389**, 827-829.

19.   R. D. Deegan, O. Bakajin, T. F. Dupont, G. Huber, S. R. Nagel and T. A. Witten, *Physical Review E*, 2000, **62**, 756.

20.   R. D. Deegan, *Physical Review E*, 2000, **61**, 475.

21.   B. J. Fischer, *Langmuir*, 2001, **18**, 60-67.

22.   D. B. van Dam and J. G. M. Kuerten, *Langmuir*, 2007, **24**, 582-589.

23.   S. Howison, *Cambridge University Press, UK*, 2005, **1**.

24.   J. G. M. Kuerten and D. P. Siregar, *Wiley-VCH*, 2012.

25.   Y. O. Popov, *Physical Review E*, 2005, **71**, 036313.

26.   D. P. Siregar, J. G. M. Kuerten and C. W. M. van der Geld, *Journal of Colloid and Interface Science*.

27.   R. Kurrat, J. J. Ramsden and J. E. Prenosil, *Journal of the Chemical Society, Faraday Transactions*, 1994, **90**, 587-590.

28.   D. P. Siregar, Doctorate Thesis Eindhoven University of Technology, 2012.

29.   C. Lages and E. Mèndez, *Analytical and Bioanalytical Chemistry*, 2007, **388**, 1689-1692.

30.   P. Van Dulm and W. Norde, *Journal of Colloid and Interface Science*, 1983, **91**, 248-255.

31.   H. B. Eral, D. M. Augustine, M. H. G. Duits and F. Mugele, *Soft Matter*, 2011, **7**, 4954-4958.

32. Y. Deng, X. Y. Zhu, T. Kienlen and A. Guo, *Journal of the American Chemical Society*, 2006, **128**, 2768-2769.

33. F. Diehl, S. Grahlmann, M. Beier and J. D. Hoheisel, *Nucleic acids research*, 2001, **29**.

34. M. K. McQuain, K. Seale, J. Peek, S. Levy and F. R. Haselton, *Analytical Biochemistry*, 2003, **320**, 281-291.

35. K. Pappaert, H. Ottevaere, H. Thienpont, P. Van Hummelen and G. Desmet, *Biotechniques*, 2006, **41**, 609-616.

36. P. Wu and D. W. Grainger, *Journal of Proteome Research*, 2006, **5**, 2956-2965.

5

Distribution and morphological patterns of inkjet printed biomolecules on porous substrates

Abstract

The main focus of our research was to study the distribution of inkjet printed biomolecules in porous nitrocellulose membrane pads of different brands. We produced microarrays of fluorophore-labelled IgG and BSA on FAST, Unisart and Oncyte-Avid slides and compared the spot morphology of the inkjet printed biomolecules. The distribution of these biomolecules within the spot embedded in the nitrocellulose membrane was analyzed by confocal laser scanning microscopy in the 'Z' stacking mode. By applying a 'concentric ring' format the distribution profile of the fluorescence intensity in each horizontal slice was measured and represented in a graphical colour-coded way. Furthermore, a real one-step diagnostic antibody assay was performed with a primary antibody, double-labelled amplicons and fluorophore-labelled streptavidin in order to study the functionality and distribution of the immune-complex in the nitrocellulose membrane slides. Under the conditions applied, the spot morphology and distribution of the primary labelled biomolecules was non-homogenous and doughnut-like on the FAST and Unisart nitrocellulose slides, whereas a better spot morphology with more homogeneously distributed biomolecules was observed on the Oncyte-Avid slide. Similar morphologies and distribution patterns were observed when the real diagnostic one-step nucleic acid microarray immunoassay was performed on these nitrocellulose slides. We also investigated possible reasons for the differences in the observed spot morphology by monitoring the dynamic behaviour of a

liquid using high speed cameras. The spreading of the liquid droplet was comparable for the FAST and Unisart slides, but different, i.e., slower, for the Oncyte-Avid slide. The results of the spreading of the droplet and the penetration behaviour of the liquid in the nitrocellulose membrane may (partly) explain the distribution of the biomolecules in the different slides.

5.1 Introduction

Porous materials like nitrocellulose[1, 2], hydrogel[3, 4], alumina[5], and silicon[6] have been used as substrates for producing microarrays. As compared to non-porous substrates like glass[7] and polystyrene[8], these porous substrates provide a 3-D network that increases the effective surface area for biomolecules to bind. Of all the available porous substrates nitrocellulose is most widely used due to its three dimensional fibre matrix, which is known to result in high quality microarrays[9, 10]. Based on the high signal-to-noise ratio obtained with these substrates, nitrocellulose membranes have been used extensively in immuno-diagnostic applications[1, 11, 12]. It has been shown previously that the assays performed with these substrates have a lower limit of detection as compared to 2-D substrates[13].

The distribution of the biomolecules across the printed spot in the porous nitrocellulose membrane is an interesting area of research. As a result of inkjet printing, the biomolecules often distribute non-homogeneously, i.e. resulting in a doughnut-shaped morphology of the spot[14]. This phenomenon, also known as the 'coffee-stain' effect, was studied in detail on a non-porous substrate like glass by Deegan[15, 16] *et al*. However, the issue as to the distribution of inkjet printed biomolecules in porous nitrocellulose membranes and its impact on the functionality of the assay are still unanswered.

Therefore, we undertook a study where we produced a microarray of fluorophore-labeled biomolecules (IgG-FITC and BSA-Alexa) on slides with

nitrocellulose membrane pads of three different manufacturers, i.e., GE Whatman (FAST), Sartorius-Stedim Biotech (Unisart) and Grace-Biolabs (Oncyte-Avid). The morphology and distribution of the biomolecules were analyzed and compared by using confocal laser scanning microscopy in the 'Z' stack mode. A real one-step diagnostic antibody assay[1, 7, 8] (anti-FITC as a primary antibody) was performed on the nitrocellulose slides and the distribution as well as the functionality of the primary antibody, as judged from the distribution of the fluorescence signal of the final assay, was investigated and compared using CLSM ('Z' stacking) and concentric ring overlay method. Various properties of the nitrocellulose membranes like the wettability and the fluid flow dynamics were investigated by monitoring the droplet with high-speed cameras installed at three positions on a microscope (side-, top- and+ bottom-view).

5.2 Materials and methods

5.2.1 Reagents

Streptavidin-Alexa-633 conjugate for labelling the biotinylated amplicons was obtained from Invitrogen (Bleiswijk, The Netherlands). 150 mM phosphate buffered saline (PBS) pH 7.4 was prepared in Milli-Q water with a resistivity of 18.2 MΩ cm^{-1}. A borate buffer (100 mM borate buffer containing 1% BSA and 0.05% Tween20) was used as diluent for the conjugates / labels and also during the intermediate washing steps.

5.2.2 Biomolecules

BSA-Alexa-643 was purchased from Invitrogen (Oregon, USA) and IgG-Fluoroisothiocyanate (IgG-FITC) from Sigma (Missouri, USA). Anti-Fluoroisothiocyanate was purchased from Bioconnect (Huissen, The Netherlands) and the DNA template of *Corynebacterium bovis* was provided by

the GD Animal Health Service (Deventer, The Netherlands). The biomolecules were diluted (200 µg/mL) in PBS (pH 7.4) and loaded into the wells of a Genetix microtiter plate (Genetix X7020, Berkshire, United Kingdom).

5.2.3 Substrates for printing biomolecules

Nitrocellulose (NC) coated slides from three different manufacturers were used and compared. Unisart slides were purchased from Sartorius (Göttingen, Germany), FAST slides 16 were from GE Whatman (Freiburg, Germany) and ONCYTE® AVID 16 slides were from Grace-Biolabs (Oregon, USA). All these slides were in 16 pad format where each pad had a dimension of 6x6 mm.

5.2.4 Printing

All the biomolecules (IgG-FITC, BSA-Alexa-643 and anti-FITC antibody) were printed on various NC membrane slides using a non-contact inkjet printer, sciFLEXARRAYER S3 from Scienion AG (Berlin, Germany). The printer was placed in a hood to maintain a relative humidity of ~70%. Spotting of the biomolecules was performed at room temperature. The voltage and pulse of the piezo-dispensing capillary (PDC) was optimized to print a droplet of ~250 pL throughout the experiment. Printed substrates were dried under controlled temperature (37°C) and humidity (70%) in the Scienion sciProCLIMATE (Berlin, Germany) for 1 hour. The slides were stored overnight in a sealed aluminium pouch with a silica desiccant.

5.2.5 Confocal laser scanning microscopy

The spot morphology and the distribution of the biomolecules in the porous NC membranes was analyzed by confocal laser scanning microscopy (CLSM; Carl Zeiss Axiovert 200 microscope, Zeiss, Jena, Germany) which was equipped with a LSM 5 Exciter. The flurophore labeled spots were first scanned at 10x magnification (overall surface fluorescence), where the configuration of the

objective was LD Plan-Neofluar 10x/0.30 Korr M27. For BSA-Alexa-643 the He-Ne laser set at 633 nm was used, whereas for the IgG-FITC an Ar laser was used set at 488 nm. The size of the pinhole was 182 μm and the transmission was 11%. The dimension of the scanner was X: 1272.8 μm and Y: 1272.8 μm.
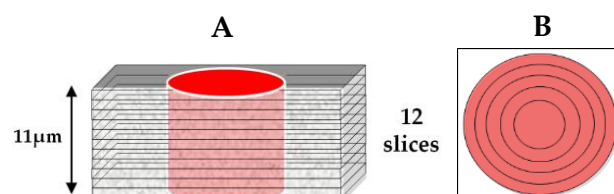

Figure 5.1 (A) Schematic representation of the 'Z' stacking method. (B) Schematic view of the 5 concentric ring model to calculate the distribution of the mean intensity of the concentric rings in each slice of the spot.

The distribution of the biomolecules in the membrane was studied by 'Z' stacking using an oil-immersion lens (100x magnification). The configuration of the objective was LD Plan-Neofluar 100x/0.6 Korr Ph2 M27. The dimension of the scanner was X: 127.3 μm and Y: 127.3 μm. Each spot of biomolecule on NC membranes was sliced horizontally into 12 parts of 1 μm each (see Figure 5.1-A). Furthermore, each slice was divided in five concentric-rings (the distance between each ring was constant and was equal to the radius of the inner ring). The mean intensity of each ring was determined to assess the (in)homogeneity of the spots (see Figure 5.1-B).

5.2.6 High speed camera analyses

The influence of properties of the various NC membrane slides like the wettability and time of penetration (t_{pen}) (i.e. the time required for a droplet to reach the bottom of the membrane from the moment it touched the top) on the fate of the droplet were investigated by high-speed cameras (HSC). All experiments were performed with IgG-FITC (200 μg/mL) prepared in PBS buffer (pH 7.4).

A 'side-view' HC was used to analyze the effect of wettability on the spreading of the droplet on and penetration of the liquid in the NC membrane slides. A droplet of IgG-FITC (3.4 µL of a 200 µg/mL solution) was supplied to the NC membrane slides using a Nordson EFD needle and the spreading and penetration of the drop was captured at 100 frames per second (fps) (see Figure 5.2-A). The video was analyzed in ImageJ software and the change in contact angle (θ) at various time intervals was calculated.
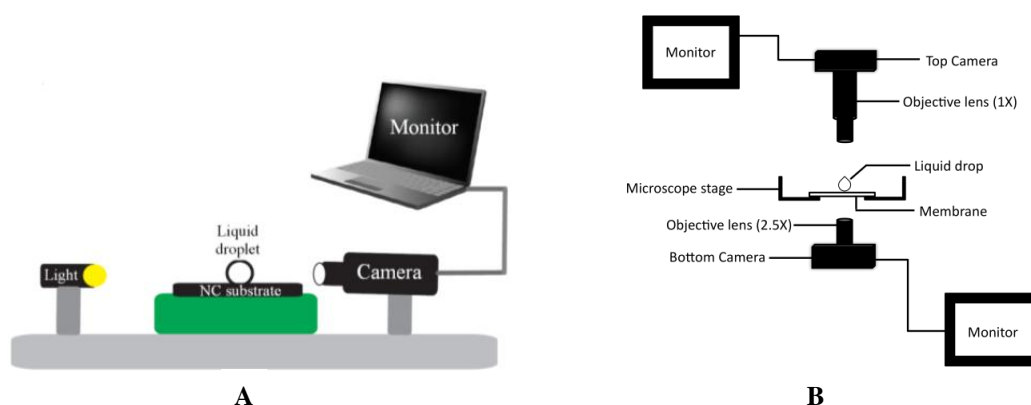

Figure 5.2 Schematic representation of the setup with a (A) "side view" high speed camera. (B) An integrated "top" and "bottom" view high speed cameras.

The spreading of the droplet on the top and bottom surfaces of the NC membrane pad and the penetration of the liquid in the nitrocellulose membrane was monitored simultaneously from the top and bottom sides by using two high speed cameras (25 fps) installed on the same microscope (Axiovert 200 MAT, Carl Zeiss B.V., Sliedrecht, The Netherlands). The top camera (uEye, UI-1240LE-M-GL, IDS Imaging Development Systems GmbH, Obersulm, Germany) was installed with a 1x objective lens whereas the bottom camera (MotionPro HS-4, Redlake MASD Inc., San Diego, CA, USA) was equipped with a 2.5x magnification lens. The schematic overview of the setup is shown in Figure 5.2-B. A droplet (250 nL) of IgG-FITC (200 µg/mL) was injected (using a 0.1-1.0 µL pipette) onto the various NC membrane slides The data obtained

from the top camera was analyzed by ImagePro software whereas that obtained from the bottom camera was analyzed by Motion Studio software (2.10.05, IDT).

5.3 Results and Discussion

5.3.1 CLSM analysis

The morphology of the inkjet printed spots on various NC membrane slides was characterized by CLSM (at 10x magnification) and the distribution of the biomolecules in the NC membranes by creating horizontal slices and vertical concentric rings of the embedded spot using 'Z' stack analysis at 100x magnification lens (oil immersion) (as explained in Figure 5.1-A). A similar type of slicing technique ('Z' stacking) by CLSM was used to investigate the in-depth penetration of colloidal solutions (ink) on a paper substrate[17] and the distribution of inkjet printed antibodies across NC substrates[18].

5.3.1.1 Distribution of fluorophore-labeled biomolecules in the NC membrane slides

The morphology of the IgG-FITC spots at 10x magnification was comparable for FAST and Unisart slides (see Figure 5.3-A, C). As concluded from the concentric ring analysis these spots had a "doughnut" shape indicating a non-homogeneous distribution of the biomolecules. In contrast, spots of IgG-FITC on the Oncyte-Avid slide showed a more uniform fluorescence morphology, indicating a more homogeneous distribution (see Figure 5.3-A).

Data obtained from 'Z' stacking analysis of the FAST slide membrane revealed that the mean fluorescence intensity of IgG-FITC lowered at increasing depth of the respective slices. The concentric ring analysis showed that a higher fluorescence intensity was observed in the outer ring as compared to the more inner rings (doughnut shape). In the deeper slices (between 4 and 6 μm) fluorescence was primarily observed for the outer ring (edges) whereas less or no fluorescence was detected in the inner rings (see Figure 5.3-B, FAST). In the

lowest slices no fluorescence could be detected at all. Similar results were observed for the Unisart slide, where the fluorescence intensity distribution in each of the slices also had a "doughnut shaped" morphology (see Figure 5.3-B, Unisart). Contrary to the doughnut shape observed for the IgG-FITC spots on the FAST and Unisart slides, a more uniform and homogeneous distribution of the biomolecules was observed on the Oncyte-Avid slide as judged from the concentric ring analysis (see Figure 5.3-B, Oncyte-Avid).
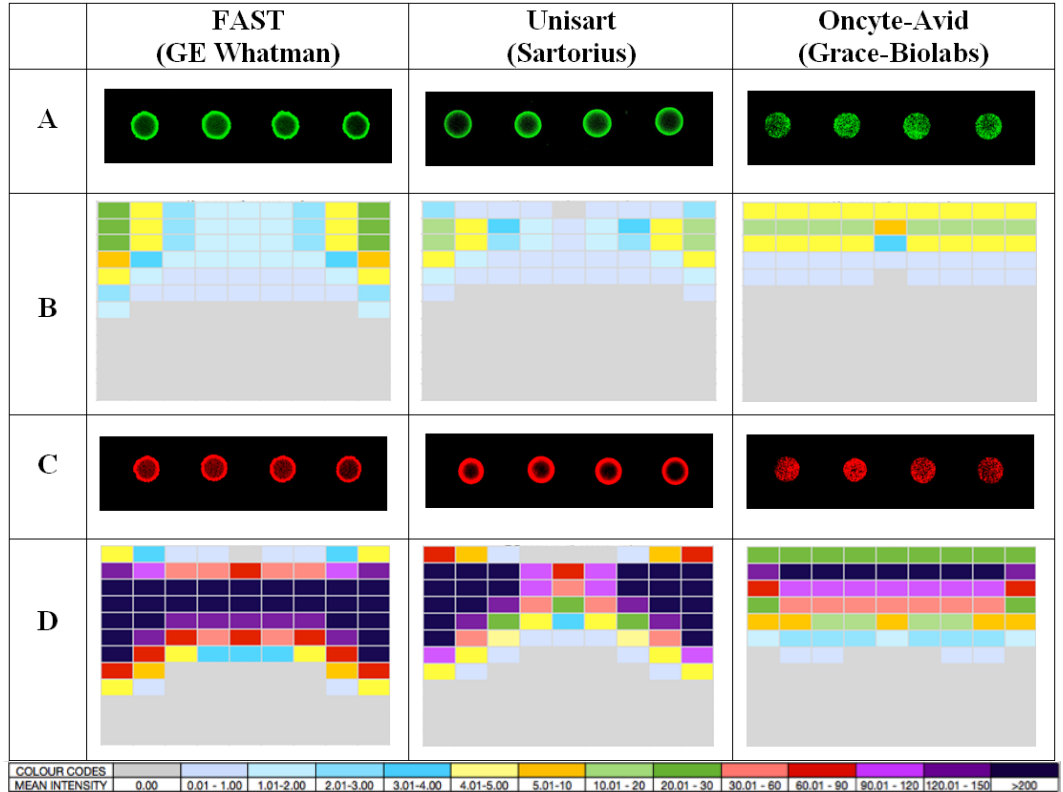

	FAST (GE Whatman)	Unisart (Sartorius)	Oncyte-Avid (Grace-Biolabs)
A			
B			
C			
D			

COLOUR CODES / MEAN INTENSITY: 0.00 | 0.01 - 1.00 | 1.01-2.00 | 2.01-3.00 | 3.01-4.00 | 4.01-5.00 | 5.01-10 | 10.01 - 20 | 20.01 - 30 | 30.01 - 60 | 60.01 - 90 | 90.01 - 120 | 120.01 - 150 | >200

Figure 5.3 (A) CLSM images of IgG-FITC spots on various NC membrane slides. (B) 'Z' stack data for distribution of IgG-FITC spot across various NC membrane slides. (C) CLSM images of BSA-Alexa spots on various NC membrane slides. (D) 'Z' stack data for distribution of BSA-Alexa spot across various NC membrane slides.

We also investigated and compared the morphology and distribution pattern of another biomolecule, i.e., BSA-Alexa-643. The morphology of the spots of BSA-Alexa-643 on the FAST and Unisart membrane slides was similar to those of

IgG-FITC, i.e. a "doughnut-shaped" appearance, independent of the gain setting used. The gain setting was chosen such that a clear background was obtained against which the features of the spot were clearly distinguishable. The 'Z' stacking and concentric ring analyses data showed that in each slice the outer rings had a higher fluorescence indicating a non-homogeneous distribution of BSA-Alexa-643. However, on the Oncyte-Avid slide, the spot morphology and distribution of the BSA-Alexa molecules as judged from the surface fluorescence (10x magnification) were much more homogeneous. In addition, this more uniform fluorescence intensity distribution was observed in each of the slices as obtained by the 'Z' stacking analysis, and was in line with the data obtained for IgG-FITC (see Figure 5.3-C, D).

5.3.1.2 Distribution and functionality of anti-FITC IgG across various NC membrane slides

Based on the principle of the Nucleic Acid Microarray Immuno Assay, NAMIA[1, 7, 8], a real one-step diagnostic assay was performed on the various NC membrane slides. Anti-FITC antibodies specific for the FAM tag were printed onto the various nitrocellulose membrane slides. A 60 min incubation with a PCR amplicon containing a FAM-label at one end and biotin at the other end[8] and streptavidin-Alexa-633 were used in this one-step assay (see Figure 5.4-A). The final signal distribution of the assay can be taken as the distribution of functional primary anti-FITC antibody molecules. Therefore, we analyzed the fluorescent signal in the 'Z' stacking mode by applying the concentric ring model.

Five NAMIA spots were scanned at 10x magnification in order to calculate the average total intensity (product of average mean intensity and spot area). Based on total intensity data, it was found that the fluorescence intensity of the anti-

FITC antibody was higher on the Unisart slide as compared to the FAST and Oncyte-Avid slides (see Figure 5.4-B).
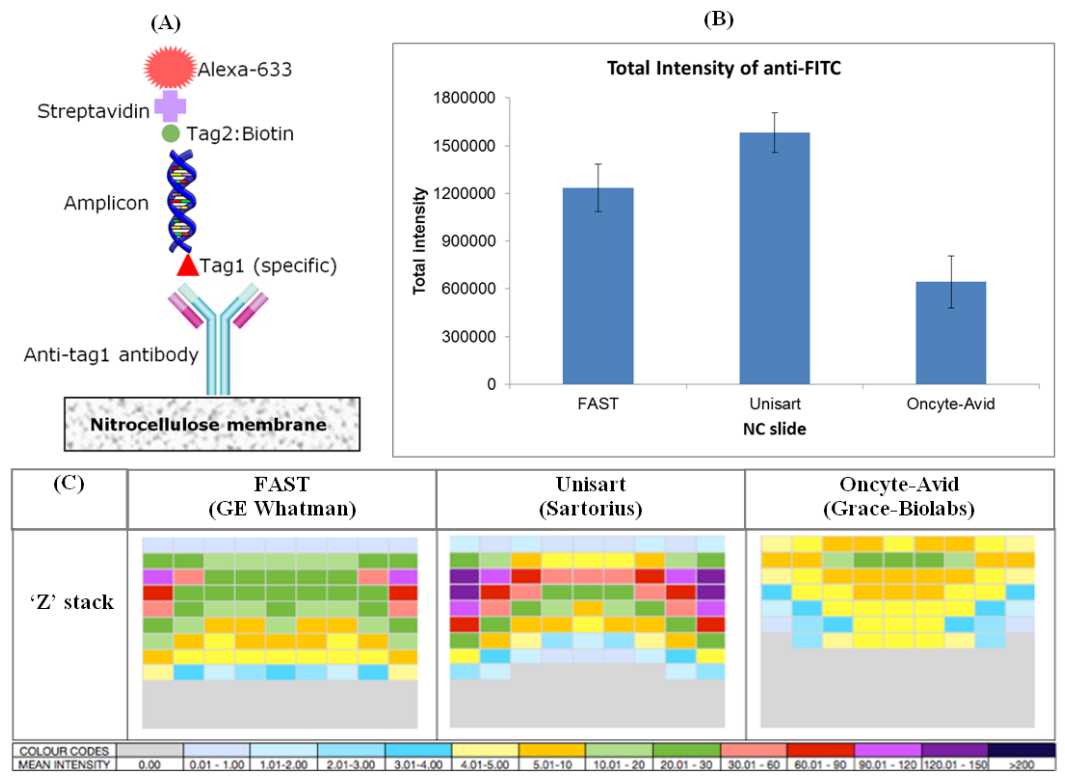

Figure 5.4 (A) Schematic representation of NAMIA. (B) CLSM (10x magnification) data showing total intensity of anti-FITC antibody on various NC membrane. (C) CLSM (100x) data showing distribution and functionality of anti-FITC antibody through various sections of NC membrane slides as analysed by the concentric ring model.

The 'Z' stacking of the NAMIA spots followed by the investigation of the mean fluorescence intensity distribution with the concentric-ring format revealed that in the FAST slide, the distribution of the anti-FITC IgG molecules was non-homogeneous; a higher mean fluorescence signal was observed for the outer rings as compared to the inner rings (see Figure 5.4-C). This was in line with the data observed for the model biomolecules IgG-FITC and BSA-Alexa.

Based on the final signal distribution of the primary anti-FITC IgG molecules, the distribution profile on the Unisart slide was comparable to that of the FAST slide, i.e., a non-homogeneous distribution of the signal. The overall signal of

the assay was slightly higher on the Unisart slide as compared to the other two slides, which suggests that the functionality of the anti-FITC biomolecules was better on the Unisart slide (see Figure 5.4-B, C). These observed differences may be due to the variation in the substrate properties of the porous membranes, which plays a role in the distribution of the inkjet printed spots[10].

On the Oncyte-Avid slide the spot morphology and the distribution of the anti-FITC IgG molecules was different from that on the FAST and Unisart slides. Analysis of the signal distribution in the various slices showed that the outer rings had a lower signal than the inner rings. Thus, the spot morphology showed a "reverse-doughnut-like" appearance (Figure 5.4-C). Comparison of all the analyses of the 'Z' slices (see Figures 5.3 and 5.4) revealed that the biomolecules did not penetrate throughout the whole membrane but bound to the upper part of the NC pads which is in agreement with a prior study by van Lieshout *et al.*[18].

5.3.2 Analysis of the droplet behaviour and flow in the NC membrane slides using high-speed cameras

To analyse whether the difference in spot morphology between FAST, Unisart and Oncyte-Avid was due to a variation in wettability, a droplet was placed on the NC membrane and the behaviour was tested by assessing the contact angle using a 'side-view' high speed camera. Furthermore, the fluid flow dynamics in these membranes were also investigated by analysing the increase of the size of the wet spot on both the top and bottom layer of the membrane by positioning high-speed-cameras at opposite ends of the membrane ('top and bottom view') (see Figure 5.2).

5.3.2.1 Change in the contact angle of the droplet (Side view)

To further understand the behaviour of the droplet on the porous nitrocellulose membranes, we first studied the surface hydrophobicity of these membranes by

monitoring the change in contact angle (θ) using a 'side-view' high speed camera (HSC).

When a drop of IgG-FITC was suspended onto the surface the initial contact angles on the three NC membrane pads were very similar i.e., 94°±0.3°, which showed that the membranes had a similar surface hydrophobicity (see Figure 5.5). However, striking differences were observed in the transient wetting of the membranes, i.e., the change in the contact angle (θ) over time. On the FAST slide the initial contact angle (t_{0sec}) of ~93.7° reduced to 64.2° within one second. The droplet continued to spread in the membrane as reflected by a gradual decrease of the contact angle. At t_{4sec} the membrane pad was completely saturated with liquid and the contact angle was recorded to be 47.4° (see Figure 5.5-FAST). A similar change in contact angle was observed on the Unisart slide as well (see Figure 5.5-Unisart).
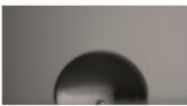
	FAST (GE Whatman)	Unisart (Sartorius)	Oncyte-Avid (Grace-Biolabs)
0	$\theta = 93.7°$	$\theta = 94.1°$	$\theta = 94.2°$
1	$\theta = 64.2°$	$\theta = 59.5°$	$\theta = 79.3°$
2	$\theta = 60.9°$	$\theta = 55.8°$	$\theta = 79.2°$
3	$\theta = 50.2°$	$\theta = 55.0°$	$\theta = 79.1°$

Figure 5.5 Change in contact angle monitored by a 'side-view' HSC for a droplet of IgG-FITC in PBS (pH7.4).

The wettability dynamics of the Oncyte-Avid slide were much slower as compared to the FAST and Unisart slides since the change in the contact angle (θ) at t_{1sec} was only 14.9° (see Figure 5.5-Oncyte-Avid). Earlier, Starov *et al.* investigated the imbibition of a liquid on porous substrates[19] in detail. They showed that the droplet upon contacting the substrate first spread to a maximum and then shrunk again. However, in our case, due to the small volume of the NC pad underneath the droplet as compared to the drop volume (3.4 μL), the pad was saturated with the liquid within 3 seconds. Hence, we could not reproduce the observations as made by Starov *et al.*[19].

5.3.2.2 Spreading and penetration of the liquid droplet in the NC membrane pads monitored with top and bottom cameras

We also had a closer view on the dynamics of the liquid droplet in the NC membrane slides. The spreading and penetration of the liquid was monitored simultaneously on the top and the bottom surface of the membrane using two high-speed-cameras installed on the same microscope.

When a droplet of IgG-FITC was pipetted onto the surface of the FAST slide, it spread immediately and diffused through the membrane with a t_{pen} = 0.48 s. Comparison of the spot radius on the top and bottom surfaces showed that the fluid spread more quickly in the top layer of the membrane than in the bottom layer (see Figure 5.6-A).

On the Unisart slide a similar pattern was observed as on the FAST slide, but in a more dynamic way. The droplet spread very rapidly on the top side of the membrane as compared to the bottom side (see Figure 5.6-B). On the Unisart membrane t_{pen} was 0.88 s, which may indicate that on the Unisart slide the horizontal spreading of the liquid was favoured as compared to the vertical movement, i.e., the penetration of the liquid. On this slide, the entire pad was saturated in less than 15 s as compared to 25 s required to saturate the NC pad

on the FAST slide (V=250 nL). As with the FAST slide this may indicate that the biomolecules are forced to move with the solvent front to the edges of the spot resulting in a doughnut-shaped appearance.
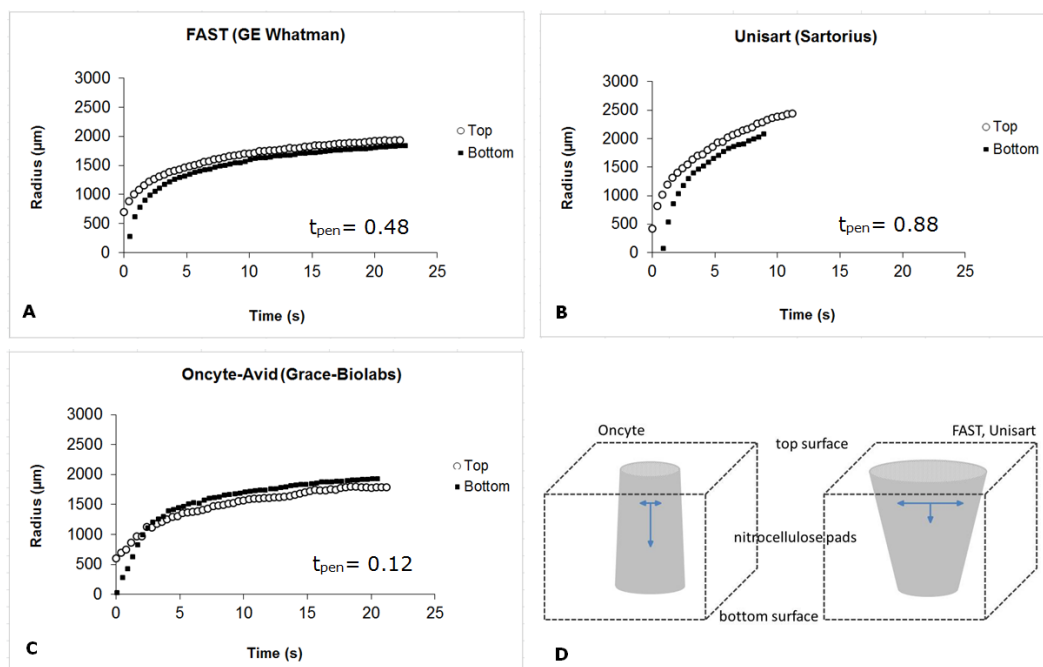

Figure 5.6 The spreading of a droplet of IgG-FITC monitored simultaneously by top and bottom camera on various NC membrane slides. (A) FAST (GE Whatman), (B) Unisart (Sartorius) (C) Oncyte-Avid (Grace-Biolabs). The t_{pen} was recorded for each NC membrane slide. (D) Schematic representation for the flow of liquid in the various NC membranes

In contrast to the FAST and Unisart slides, penetration of liquid was much faster in the Oncyte-Avid slide, i.e., t_{pen} = 0.12 s. As shown in Figure 5.6-C, at a given point in time the radius of the spreading liquid was somewhat larger at the bottom than at the top of the membrane. Obviously, in this membrane the liquid droplet penetrates vertically into the membrane with such a speed that after approximately two seconds the radius of the droplet at the bottom surface is only slightly larger than at the top surface. The biomolecules move along with this vertical flow meanwhile adhering to the inner matrix of the NC

membrane in a cylinder-like format having a radius that is comparable to the ones of the spreading droplet on the top and bottom surfaces. The speed of the horizontal spreading of the liquid (see the tangent at the initial and later time-points of the Top droplet; Figure 5.6-C) is clearly lower than that for the FAST and, even more so the Unisart membrane. The more prominent vertical liquid flow in this confined volume may result in more homogeneously distributed biomolecules in the porous NC membrane of the Oncyte-Avid slide. However, in the FAST and Unisart membranes the upside down cone-like format of the liquid penetration is representative of a more prominent horizontal as compared to the vertical speed (see Figure 5.6-D). Consequently, the biomolecules are driven to the edge of the expanding liquid cone in the membrane resulting in a doughnut-like morphology of the final signal of the spot.

Indeed, by analysing the signal intensity distribution profile (concentric rings) on the FAST and Unisart slides a higher signal was observed for the outside rings of the spots than for the center part. As shown in Figure 5.5, the change in contact angle (θ) was faster and the edges of the droplet on these membranes had a smaller contact angle, which is in line with a more hydrophilic surface and also illustrates the more prominent horizontal movement of the liquid as compared to the Oncyte slide. As explained previously by Deegan[15, 16] a higher evaporation rate[20] occurs at the edges of droplets and, as explained by Ressine *et al.*[6], the internal convection taking place within the droplet also drives biomolecules in the droplet to the edges, especially in droplets with a low contact angle. These combined effects promote the accumulation of the biomolecules in the outer region of the spot, which is visible as a 'coffee-stain' or 'doughnut-like shape'.

However, on the Oncyte-Avid slides, the larger contact angle and the lesser change in the first seconds would result in an internal convection that promotes a more homogeneous distribution of the biomolecules[6], further supported by the more prominent vertical movement. Indeed, this was observed and is supported by Tekin *et al.*[21]; a larger contact angle of a spot may result in a lessened doughnut-effect as compared to droplets with a lower contact angle (θ)[10, 22]

It has been reported that the incorporation of various additives like Triton-X 100[23], DMSO[24], betaine[25], polyvinyl alcohol[26] in the printing buffer may help to overcome the non-homogenous distribution of biomolecules in porous substrates. It is well-known that additives are used in the production process of nitrocellulose diagnostic membranes[27] and that the particular additive or additive mix used substantially influences the performance of the immunoassay as done with this particular membrane. Without additives and depending on the immunoassay format one commercial membrane may be superior in a lateral flow assay, whereas another one could be better for an incubation-type assay. Therefore, in using a particular membrane one should always study whether additives would improve the performance of the assay that is being developed. In an ongoing study we are evaluating the influence of a tri-block copolymer of a central hydrophobic and two external hydrophilic polymer parts (see Chapter 6). Such a compound could potentially help to achieve the correct orientation of proteins to ensure optimal functionality, for example the binding capacity of antibodies[28].

5.4 Conclusions

The spot morphology of inkjet printed biomolecules showed different distribution patterns in various NC membrane slides. The spot homogeneity was more uniform on Oncyte-Avid (Grace-Biolabs), whereas on the FAST (GE

Whatman) and Unisart (Sartorius) slides, an irregular distribution of the biomolecules was observed resulting in doughnut-shaped spots. The differences in spot morphology and biomolecule distribution could be partly explained by different substrate properties, notably their hydrophobicities and fluid flow dynamics. To our knowledge this is the first time that fluid dynamics in diagnostic membranes have been analyzed by using high-speed cameras.

References

1. P. S. Noguera, G. A. Posthuma-Trumpie, M. van Tuil, F. J. van der Wal, A. d. Boer, A. P. H. A. Moers and A. van Amerongen, *Analytical Chemistry*, 2011, **83**, 8531-8536.

2. B. A. Stillman and J. L. Tonkinson, *BioTechniques*, 2000, **29**, 630-635.

3. P. T. Charles, C. R. Taitt, E. R. Goldman, J. G. Rangasammy and D. A. Stenger, *Langmuir*, 2003, **20**, 270-272.

4. M. Moschallski, J. Baader, O. Prucker and J. Rühe, *Analytica Chimica Acta*, 2010, **671**, 92-98.

5. S. Y. Kim, J. Yu, S. J. Son and J. Min, *Ultramicroscopy*, 2010, **110**, 659-665.

6. A. Ressine, G. r. Marko-Varga, T. Laurell and M. R. El-Gewely, in *Biotechnology Annual Review*, Elsevier, 2007, vol. Volume 13, pp. 149-200.

7. L. H. Mujawar, W. Norde and A. van Amerongen, *Analyst*, 2013, **138**, 518-524.

8. L. H. Mujawar, A. van Amerongen and W. Norde, *Talanta*, 2012, **98**, 1-6.

9. D. A. Fici, W. McCormick, D. W. Brown, J. E. Herrmann, V. Kumar and Z. L. Awdeh, *Journal of Immunological Methods*, 2010, **363**, 60-66.

10. C. Steinhauer, A. Ressine, G. r. Marko-Varga, T. Laurell, C. A. K. Borrebaeck and C. Wingren, *Analytical Biochemistry*, 2005, **341**, 204-213.

11. P. Knight, A. Sreekumar, J. Siddiqui, B. Laxman, S. Copeland, A. Chinnaiyan and D. Remick, *Shock*, 2004, **21**, 26-30.

12. E. J. Irvine, A. Hernandez-Santana, K. Faulds and D. Graham, *Analyst*, 2011, **136**, 2925-2930.

13. J.-G. Walter, F. Stahl, M. Reck, I. Praulich, Y. Nataf, M. Hollas, K. Pflanz, D. Melzner, Y. Shoham and T. Scheper, *Eng. Life Sci.*, 2010, **10**, 103-108.

14. V. Dinca, A. Ranella, M. Farsari, D. Kafetzopoulos, M. Dinescu, A. Popescu and C. Fotakis, *Biomedical Microdevices*, 2008, **10**, 719-725.

15.   R. D. Deegan, O. Bakajin, T. F. Dupont, G. Huber, S. R. Nagel and T. A. Witten, *Nature*, 1997, **389**, 827-829.

16.   R. D. Deegan, O. Bakajin, T. F. Dupont, G. Huber, S. R. Nagel and T. A. Witten, *Physical Review E*, 2000, **62**, 756.

17.   A. Isogai, M. Naito, Y. Ozaki, H. Nagashima and T. Enomae, *Journal of Imaging Science*, 2011, **55**, 20201-20208.

18.   R. M. L. van Lieshout, T. van Domburg, M. Saalmink, R. Verbeek, R. Wimberger-Friedl, M. P. van Dieijen-Visser and C. Punyadeera, *Analytical Chemistry*, 2009, **81**, 5165-5171.

19.   V. M. Starov, S. A. Zhdanov and M. G. Velarde, *Langmuir*, 2002, **18**, 9744-9750.

20.   M. Ikegawa and H. Azuma, *JSME International Journal, Series B: Fluids and Thermal Engineering*, 2004, **47**, 490-496.

21.   E. Tekin, P. J. Smith and U. S. Schubert, *Soft Matter*, 2008, **4**, 703-713.

22.   W. Kusnezow and J. D. Hoheisel, *Journal of Molecular Recognition*, 2003, **16**, 165-176.

23.   Y. Deng, X. Y. Zhu, T. Kienlen and A. Guo, *Journal of the American Chemical Society*, 2006, **128**, 2768-2769.

24.   M. K. McQuain, K. Seale, J. Peek, S. Levy and F. R. Haselton, *Analytical Biochemistry*, 2003, **320**, 281-291.

25.   F. Diehl, S. Grahlmann, M. Beier and J. D. Hoheisel, *Nucleic acids research*, 2001, **29**.

26.   P. Wu and D. W. Grainger, *Journal of Proteome Research*, 2006, **5**, 2956-2965.

27.   A. L. Ahmad, S. C. Low, S. R. A. Shukor and A. Ismail, *Journal of Applied Polymer Science*, 2008, **108**, 2550-2557.

28.   A. Wolter, R. Niessner and M. Seidel, *Analytical Chemistry*, 2007, **79**, 4529-4537.

Influence of Pluronic F127 on the distribution and functionality of inkjet printed biomolecules

Abstract

The distribution of inkjet printed biomolecules in porous nitrocellulose substrates often results in a non-homogeneous spot morphology commonly referred to as 'doughnut-shaped' spots. We have studied the influence of Pluronic F127 (an amphiphilic surfactant) on the functionality of inkjet printed primary antibody molecules and on the final diagnostic assay result by performing a one-step diagnostic assay in the nitrocellulose substrate. The primary antibody was printed with and without Pluronic, followed by the addition of double-labelled amplicons as antigen molecules and a fluorophore-labelled streptavidin as detection conjugate. The distribution of the fluorescence intensity down into the nitrocellulose substrate was investigated by confocal laser scanning microscopy in 'Z' stacking mode. Each horizontal slice was further analyzed by applying a concentric ring format and the fluorescence intensity in each slice was represented in a colour-coded way. The mean and total fluorescence intensity of the diagnostic assay (fluorescent streptavidin) showed a peak at 0.2% (w/v) Pluronic F127. In addition, an improved spot morphology was observed also peaking at the same Pluronic concentration. Subsequently, we investigated the direct influence of Pluronic F127 on the location of the primary antibody molecules by labeling these molecules with the fluorophore Alexa-488. Our results show that, upon increasing the concentration of Pluronic F127 in the printing buffer, the spot diameter increased and the number of primary antibody molecules bound in the spot

area gradually decreased. We conclude that a particular ratio between primary antibody and Pluronic F127 molecules in combination with available substrate binding capacity results in an optimal orientation, i.e. F*ab*-UP, of the primary antibody molecules. Consequently, an increased number of antigen molecules (in our case the labelled amplicons) and of the fluorescent detection conjugate (streptavidin) will give an optimal signal. Moreover, distribution of the primary antibody molecules was more homogeneous at the optimal Pluronic F127 concentration, contributing to the better spot morphology observed.

6.1 Introduction

Non-contact arraying is a modern tool for printing biomolecules[1] on a range of porous and non-porous substrates. Researchers have shown that high quality microarrays are produced on porous substrates like nitrocellulose[2], porous silicon[3], alumina[4] and hydrogels[5] as compared the non-porous substrates like glass[6] and polystyrene[7]. On porous substrates a lower limit of detection can be obtained as compared to non-porous substrates[8]. The 3-D matrix of the porous substrates[9] enables more molecules to bind as projected per unit surface area and this results in a better signal-to-noise (S/N) ratio[10]. Of all the available porous substrates, the nitrocellulose membrane have been used extensively in diagnostic applications[2, 11, 12] for producing biochips[13].

It has been commonly observed that, upon printing, biomolecules often distribute non-homogeneously which results in 'doughnut-shaped' spots, also referred to as the 'coffee-stain' effect[14-16]. Researchers have successfully demonstrated that for DNA microarrays, incorporation of various additives like DMSO[17], polyvinyl alcohol[18], betaine[19] and Triton-X 100[20] can result in a more homogeneous spot morphology. However, the chemical aspects of DNA microarrays cannot be easily translated to the production of protein

microarrays due to the fundamental biophysical and biochemical differences between these two classes of biological substances.

Recently, Norde and Lyklema have shown that Pluronic molecules may also help to achieve a preferred orientation of deposited antibodies[21]. Pluronic F127 is an amphiphilic non-ionic surfactant which belongs to a class of polymers called as poloxamers[22]. It is a tri-block copolymer with repeating polyoxyethylene-polyoxypropylene-polyoxyethylene (PEO-PPO-PEO) units where the central part (PPO) is hydrophobic, whereas the ends (PEO) are amphiphilic in nature. Therefore, we have studied the influence of Pluronic F127 (an amphiphilic surfactant) on the functionality of inkjet printed primary antibody molecules, the final diagnostic assay result and on the spot morphology using slides with nitrocellulose membrane pads. Moreover, it has been used for inkjet printing applications before[23, 24].

We have assessed the influence of various concentrations of Pluronic F127 (0 to 1% (w/v)) on the spot morphology and functionality of the primary antibody (anti-FITC). Using a non-contact inkjet printer, primary anti-FITC antibodies were printed on nitrocellulose membrane slides and the functionality of the primary antibodies was investigated by performing a one-step diagnostic antibody assay based on the binding of a double-labeled amplicon (FITC- and biotin-labeled), as was reported for the nucleic acid microarray immunoassay (NAMIA)[2, 6, 7]. The distribution as well as the functionality of the primary antibody was judged from the distribution of the fluorescence signal of the final assay. Using confocal laser microscopy the NAMIA spots were sliced horizontally ('Z' stack method) and the signal distribution profile in each slice was calculated using a concentric ring format. The results are presented in a color-coded format. Additionally, we also investigated the direct influence of

the amphiphilic surfactant (Pluronic F127) on the distribution of the primary antibody molecules that had been labeled with Alexa-488.

6.2 Materials and methods

6.2.1 Reagents

Pluronic F127 was purchased from Sigma Aldrich (St. Louis, MO, USA) and a 1% (w/v) stock solution was prepared in 150 mM phosphate buffered saline (PBS, pH 7.4). Running buffer (100 mM borate buffer containing 1% BSA and 0.05% Tween-20) was used as a diluent for the conjugates/labels and also during the intermediate washing steps.

6.2.2 Biomolecules

Anti-fluoroisothiocynate (FITC) was purchased from Bioconnect (Huissen, The Netherlands), The DNA templates for *Corynebacterium bovis* were provided by the Animal Health Service, Deventer, (The Netherlands).

6.2.3 Substrates for printing biomolecules

Nexterion nitrocellulose membrane coated slides in 16-pad format were purchased from Schott AG (Mainz, Germany). The dimension of each pad was 6x6 mm, whereas the thickness was ~11 μm.

6.2.4 Labelling of the primary anti-FITC antibody

The primary anti-FITC antibody molecules were labelled with Alexa-488 fluorophore using an Alexa Fluor 488 antibody labelling kit (Invitrogen, Oregon, USA). The labelling procedure was carried out as described by Invitrogen and the concentration of the fluorophore-conjugated antibody (anti-FITC-Alexa-488) was measured using a Nanodrop-1000-v3.6 spectrophotometer (Wilmington, DE, USA).

6.2.5 Printing of antibodies on NC membrane slides

Anti-FITC and Alexa-488 conjugated anti-FITC antibodies were diluted (200 μg/mL) in various Pluronic F127 concentrations (0%, 0.01%, 0.05%, 0.1%, 0.2%, 0.4, 0.8% 1.0% w/v) and loaded into the wells of a Genetix microplate (384 wells). The diluted antibodies were printed on the nitrocellulose membrane pads using a non-contact inkjet printer, sciFLEXARRAYER S3 (Scienion AG, Berlin, Germany). The printer was placed in a hood to maintain constant temperature and humidity. Spotting of the biomolecules was performed at room temperature and ~70% humidity. The voltage and pulse of the piezo dispensing capillary (PDC) was optimized to print a droplet of ~250 pL throughout the experiment. The slides were stored overnight in a sealed Al pouch.

6.2.6 PCR reaction

DNA template from *Corynebacterium bovis* was amplified using primers Cb-F2 and Cb-R3 according to a published protocol[7]. The PCR protocol was optimized to 30 minutes using Phire Hot Start polymerase (Finnzymes) and the Piko thermal cycler (Finnzymes). The forward primer was labeled with a FAM tag and the reverse primer with biotin. The amplification resulted in a double stranded amplicon with at each end a tag, FAM or biotin. Gel electrophoresis confirmed that the amplicon obtained after PCR had the correct band length[25].

6.2.7 Nucleic acid microarray immunoassay (NAMIA)

To investigate the influence of Pluronic F127 in the printing buffer of the primary anti-FITC antibody a one-step diagnostic assay was performed on the NC membrane slides based on the principle of the Nucleic Acid Microarray Immuno Assay, NAMIA[6, 7]. Anti-FITC antibodies (specific for the FAM tag) were diluted in various concentrations of Pluronic F127 and printed onto the NC membrane slides. The test was performed as a short incubation (60 min) of

the PCR amplicon containing the FAM and the biotin labels and streptavidin-Alexa-633 (see Figure 6.1). The fluorescence intensity of the signal was related to the functionality of the primary anti-FITC antibody molecules with respect to the Pluronic F127 concentration in the printing buffer.
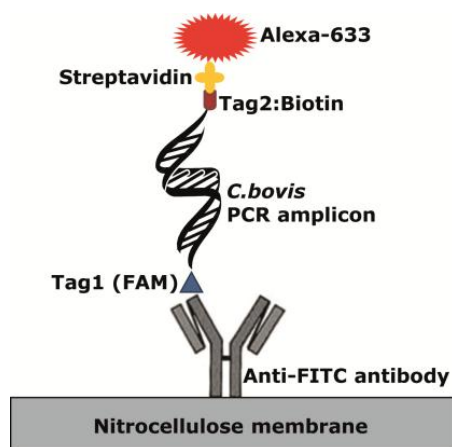

Figure 6.1 Schematic representation for detection principle of NAMIA.

6.2.8 Confocal laser scanning microscopy (CLSM)

The spot morphology and the distribution of the biomolecules in the porous NC membranes were analyzed by confocal laser scanning microscopy (CLSM; Carl Zeiss Axiovert 200 microscope, Zeiss, Jena, Germany), equipped with a LSM 5 Exciter. The fluorophore labeled spots were first scanned at a 10x magnification (overall surface fluorescence), where the configuration of the objective was LD Plan-Neofluar 10x/0.30 Korr M27. For Alexa-633 conjugated NAMIA spots, the He-Ne laser set at 633 nm was used, whereas for the Alexa-488 conjugated anti-FITC antibodies an Ar laser was used set at 488 nm. The size of the pinhole was 182 µm and the transmission was 11%. The dimension of the scanner was X: 1270 µm and Y: 1270 µm.

The distribution of the fluorescence intensity down into the NC membrane was studied by 'Z' stacking using an oil-immersion lens (100x magnification). The

configuration of the objective was LD Plan-Neofluar 100x/0.6 Korr Ph2 M27 and the dimensions of the scanner were X: 127.0 μm and Y: 127.0 μm, respectively. Each spot of biomolecule on NC membranes was sliced horizontally into 12 slices with a thickness of 1 μm per slice (Figure 6.2-A) (see Chapter 5). Such slicing technique has been already used in the past to investigate the penetration of colloidal ink in paper substrates[26] and to study the distribution of antibodies in NC membrane slides[27]. Furthermore, each slice was divided in five concentric-rings[28] (the thickness of each ring was constant and was equal to the radius of the inner ring). The mean intensity of each ring was determined to assess the (in)homogeneity of the spots (Figure 6.2-B) (see Chapter 5).
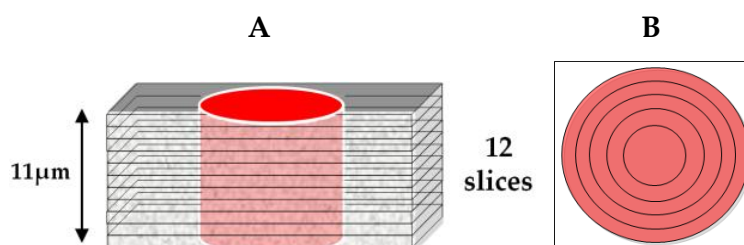

Figure 6.2 (A) Schematic representation of the 'Z' stacking method. (B) Schematic view of the 5 concentric ring model to calculate the distribution of the mean intensity of the concentric rings in each slice of the spot.

6.3 Results and Discussion

6.3.1 Influence of Pluronic F127 in the printing buffer of the primary anti-FITC antibody molecules on the final diagnostic assay signal

In order to investigate the influence of Pluronic F127 on the functionality of the primary anti-FITC antibody, a diagnostic antibody assay was performed based on the principle of NAMIA (see Figure 6.1)[6,7]. The final assay signal was scored on the basis of the fluorescence of the bound secondary conjugate, streptavidin. With increasing concentration of Pluronic in the printing buffer, the spot radii of the NAMIA spots also increased from 58 to 83 μm (see Figure 6.3-A). The property of a surfactant to enhance the spreading and uniform distribution of a

droplet on a substrate surface has also been reported by Dugas *et al.*[29]. They showed that during evaporation of a droplet in the presence of surfactant, the hydrodynamic flow causes the accumulation of the surface active agents at the periphery of the droplet. This increased concentration lowers the evaporation on the edge of the droplet, thus assisting in an uniform spot deposition throughout the droplet area.
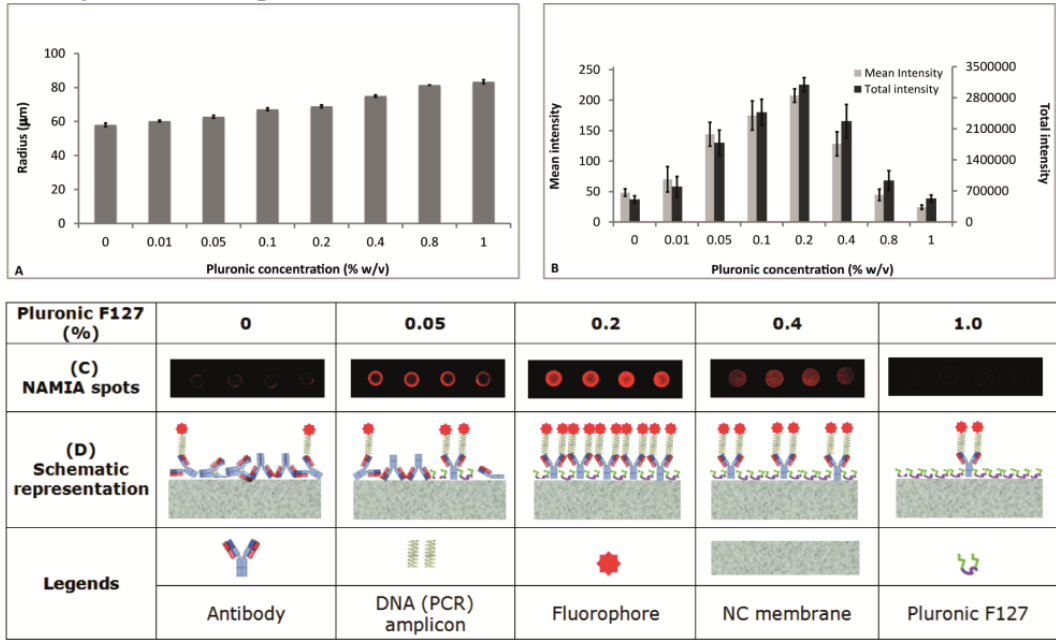

Figure 6.3 Influence of Pluronic F127 on the (A) final spot radius upon printing the primary anti-FITC antibody with pluronic, (B) mean and total signal intensity of the diagnostic assay. (C) CLSM (10x) images of the assay spots. A schematic illustration to explain the influence of Pluronic on the final assay signals is given in (D).

The fluorescence intensity of the assay spots was influenced by the concentration of Pluronic. In the absence of Pluronic (i.e., only PBS in the printing buffer of the primary antibody), the fluorescence signal intensity was low and the spot morphology was doughnut-like (see Figure 6.3-B,C). However, in the presence of Pluronic in the printing buffer, the mean and total fluorescence intensity increased and the doughnut spot morphology was substantially suppressed when the Pluronic concentration was increased to

0.2%. A further increase in the concentration of Pluronic up to 0.4% resulted in a similar spot morphology, but the mean and total fluorescence intensity of the spot was less than that observed for the 0.2% spot. At 1% Pluronic the fluorescence intensity of the spot was almost vanished (see Figure 6.3-B,C).

Wolter *et al.*[30] also observed a similar enhancement in the signal due to incorporation of Pluronic F127. The signal enhancement on a non-porous substrate was mainly due to improved stabilization of protein molecules in the presence of Pluronic F127. However, they noticed excessive spreading of the spots on non-porous substrates, which was further improved by addition of trehalose. We have used a similar approach for improvement of the signal on porous substrate but in addition to this we also studied the distribution of the signal for a diagnostic assay into the three dimensional matrix of the nitrocellulose substrate and the possible mechanism for signal improvement.

In any immunoassay, the correct orientation of the antibody molecule is crucial as it plays a role in defining the final assay signal. The primary antibodies upon printing on NC membranes may adopt 'Side-ON', 'Flat-ON', 'F*ab*-UP' and 'F*ab*-DOWN' orientations[31, 32]. When the antibody molecule deposits in a Side-ON or Flat-ON orientation and, even more so, in a F*ab*-DOWN orientation, fewer F*ab* binding sites are available for binding antigen molecules. However, in the F*ab*-UP orientation maximum accessibility of the antigen binding sites is ensured[33]. Thus, in the absence of Pluronic the printed anti-FITC antibody molecules may orient themselves more or less randomly at the NC surface, that is in any of the before mentioned orientations. In the presence of Pluronic, this polymer competes with the antibodies for binding to the substrate surface. Consequently, the density of the antibody molecules at and under the spot is lowered, which would result in a reduced fluorescence intensity of the anti-FITC assay. However, because the Pluronic molecules tend to bind to the

surface through their central apolar PPO part, leaving their two terminal polar PEO parts dangling in the solution, antibody molecules most likely dock in the interstitial spaces between the adsorbed Pluronic molecules. At a particular Pluronic concentration these interstitial spaces may be confined such that they prohibit Side-ON, Flat-ON and F*ab*-DOWN orientations of the antibodies, but allow accommodation of the less bulky part of the antibody, its F*c* part, resulting in a F*ab*-UP orientation. Docking of the F*c* part of the IgG molecule into the PEO layer will more easily occur when the thickness of the brush (~5.5 nm for Pluronic F127)[34] does not exceed the length of F*c* part (7.7 nm)[35]. Thus, the adsorbed Pluronic molecules may act as a sieve to force the antibody molecules to adsorb via their F*c* part and with their binding sites away from the surface so that they are accessible by the antigen molecules. This sieving effect and hence, the fluorescence intensity of the assay is enhanced with increasing coverage of the NC surface by Pluronic up to a certain degree (i.e., 0.2%) beyond which the Pluronic molecules are too densely packed to allow for sufficient antibody molecules to be incorporated (i.e., 0.4% and higher). As a result, a lower fluorescence intensity of the assay spots was observed when the Pluronic concentration was 0.4% and higher. The interaction of the protein molecules with the PEO brushes has been discussed in detail by Norde and Lyklema[21]. This has been schematically illustrated in Figure 6.3-D, which may at least partly, explain the differences observed in the fluorescence signals between spots of which the primary anti-FITC antibody was printed with different concentrations of Pluronic F127.

6.4.2 Influence of Pluronic F127 in the printing buffer of the primary anti-FITC antibody molecules on their distribution and on the final diagnostic assay signal

We also indirectly analyzed the distribution of the primary anti-FITC antibody molecules down into the NC membrane using a 'Z' stacking mode (slicing of spots) of the CLSM (100x magnification) to measure the final spot fluorescence. This kind of slicing technique to study the distribution of the inkjet printed antibodies down into the NC substrate has been used in the past by Lieshout *et al.*[27]. In addition, we applied a concentric ring model to measure the fluorescence in rings across the spot in order to assess its morphology.

In the absence of Pluronic F127, the distribution of the fluorescence intensity of the final spot in the subsequent slices was non-homogeneous, thus resembling a doughnut-shape distribution, i.e., higher intensity at the edges than in the center. As indirectly judged from the final spot fluorescence it was also observed that in the absence of the amphiphilic surfactant the biomolecule penetrates only up to 6 μm deep in the NC membrane. This shows that upon inkjet printing most of the NC volume beneath the spot was still unoccupied by any biomolecule (see Figure 6.4). As discussed in section 6.3.1 the low fluorescence signals in the absence of Pluronic in the slices just below the surface could be well explained by assuming orientations of the antibody molecules that restrict the accessibility of the antigen binding sites by the antigen.

Incorporation of Pluronic (0.01%) in the printing buffer resulted in an increase of the fluorescence intensity of the final assay spot in each slice, along with deeper penetration of the antibody molecules into the membrane. With a further increase in the Pluronic concentration (0.05% and 0.1%) the fluorescence intensity in the horizontal slices not only increased, but was also found to be

more homogeneously distributed. The best homogeneous fluorescence intensity distribution was observed throughout all the slices of the assay spots when the anti-FITC antibody was printed with 0.2% Pluronic. Further increase in the Pluronic concentration resulted in spots with a diameter larger than the dimensions of the CLSM scanner, frustrating 'Z' stacking analysis for the spots printed with higher Pluronic concentration (i.e., above 0.2%). However, based on spot images it can be concluded that the morphology of the spots was less homogeneous as compared to the spots of which the primary antibodies had been printed with 0.2% Pluronic (see Figures 6.3-C and 6.4).
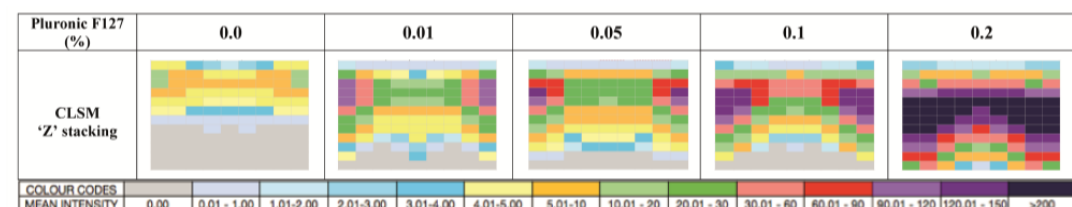

Figure 6.4 CLSM (100x) data showing distribution and functionality of anti-FITC antibody through various sections of NC membrane slides as analyzed by the concentric ring model and presented in a color-coded format.

6.3.3 Direct influence of Pluronic F127 on the distribution of primary antibody molecules

In order to investigate the effect of Pluronic 127 on the distribution of the primary antibody molecules, we printed Alexa-488 conjugated primary anti-FITC antibody molecules in various Pluronic concentrations and analyzed the fluorescence intensity of these fluorophore conjugated primary antibodies.

With increasing concentration of Pluronic, the spot radii of the Alexa-488 conjugated primary anti-FITC antibody molecules also increased (see Figure 6.5-A) as was observed for the final assay spots (compare with Figure 6.3-A). However, the fluorescence intensity of the Alexa-488 conjugated primary antibody molecules was highest in the absence of Pluronic and continued to

decrease with increasing Pluronic concentration; an inverse relationship was observed between Pluronic concentration and mean fluorescence intensity (see Figure 6.5-B). However, the total fluorescence intensity slightly increased when the Pluronic concentration was raised from 0% to 0.05 %, but beyond 0.05% the trend for the total fluorescence intensity was similar to that observed for the mean intensity. When the concentration of Pluronic was 0% and 0.05% the mean intensity was highest whereas for higher Pluronic concentration (up to 1%), the fluorescence intensity was very low.
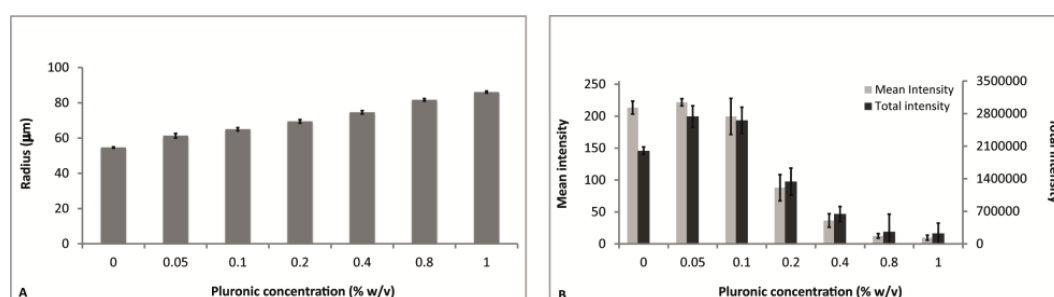

Figure 6.5 Influence of Pluronic F127 on the (A) Spot radius of the anti-FITC-Alexa-488 antibody, (B) Mean intensity for anti-FITC-Alexa-488 antibodies printed at various Pluronic concentrations.

This gradual decrease in fluorescence intensity of the primary antibody molecules is in contrast to the distribution profile of the final assay spots having the highest fluorescence at a Pluronic concentration of 0.2%. From our results we have to conclude that the presence of Pluronic in the printing buffer has an effect on the orientation of the primary antibody molecules. We hypothesize that a particular ratio between primary antibody and Pluronic F127 molecules in combination with available substrate binding capacity triggers an optimal orientation, i.e., F*ab*-UP, of the primary antibody molecules. Consequently, an increased number of antigen molecules (in our case the labelled amplicons) and of the fluorescent detection conjugate (streptavidin) will bind, resulting in an optimal signal. Moreover, the distribution of the primary antibody molecules

was more homogeneous at the optimal Pluronic F127 concentration, contributing to the better spot morphology observed.

6.4 Conclusions

Incorporation of the amphiphilic surfactant, Pluronic F127, in the printing buffer improves the functionality and also the distribution of primary antibodies in porous NC substrates. CLSM data (10x) confirmed that in the presence of Pluronic F127 a more homogeneous morphology was obtained and that the biomolecules distributed more uniformly down into the NC membrane (confirmed by 'Z' stack analysis). A diagnostic assay on top of these primary antibodies with antigen and fluorophore-labeled streptavidin showed that the mean fluorescence intensity was best at a the concentration of 0.2% Pluronic F127 in the printing buffer. It is concluded that at this optimal concentration Pluronic F127 molecules induced the preferred orientation of the primary antibody molecules, i.e., F*ab*-UP, resulting in an improved final assay signal.

References

1.   J. B. Delehanty and F. S. Ligler, *Analytical Chemistry*, 2002, **74**, 5681-5687.

2.   P. S. Noguera, G. A. Posthuma-Trumpie, M. van Tuil, F. J. van der Wal, A. d. Boer, A. P. H. A. Moers and A. van Amerongen, *Analytical Chemistry*, 2011, **83**, 8531-8536.

3.   A. Ressine, G. r. Marko-Varga, T. Laurell and M. R. El-Gewely, in *Biotechnology Annual Review*, Elsevier, 2007, vol. Volume 13, pp. 149-200.

4.   S. Y. Kim, J. Yu, S. J. Son and J. Min, *Ultramicroscopy*, 2010, **110**, 659-665.

5.   J. C. Miller, H. Zhou, J. Kwekel, R. Cavallo, J. Burke, E. B. Butler, B. S. Teh and B. B. Haab, *Proteomics*, 2003, **3**, 56-63.

6.   L. H. Mujawar, W. Norde and A. van Amerongen, *Analyst*, 2013, **138**, 518-524.

7.   L. H. Mujawar, A. van Amerongen and W. Norde, *Talanta*, 2012, **98**, 1-6.

8. M. Reck, F. Stahl, J. G. Walter, M. Hollas, D. Melzner and T. Scheper, *Biotechnolgy Progress*, 2007, **23**, 1498-1505.

9. M. Dufva, *Biomolecular Engineering*, 2005, **22**, 173-184.

10. J.-G. Walter, F. Stahl, M. Reck, I. Praulich, Y. Nataf, M. Hollas, K. Pflanz, D. Melzner, Y. Shoham and T. Scheper, *Eng. Life Sci.*, 2010, **10**, 103-108.

11. J. Petrik, *Transfusion Medicine*, 2006, **16**, 233-247.

12. T. Kukar, S. Eckenrode, Y. Gu, W. Lian, M. Megginson, J.-X. She and D. Wu, *Analytical Biochemistry*, 2002, **306**, 50-54.

13. B. A. Stillman and J. L. Tonkinson, *BioTechniques*, 2000, **29**, 630-635.

14. R. D. Deegan, *Physical Review E*, 2000, **61**, 475.

15. R. D. Deegan, O. Bakajin, T. F. Dupont, G. Huber, S. R. Nagel and T. A. Witten, *Nature*, 1997, **389**, 827-829.

16. R. D. Deegan, O. Bakajin, T. F. Dupont, G. Huber, S. R. Nagel and T. A. Witten, *Physical Review E*, 2000, **62**, 756.

17. M. K. McQuain, K. Seale, J. Peek, S. Levy and F. R. Haselton, *Analytical Biochemistry*, 2003, **320**, 281-291.

18. P. Wu and D. W. Grainger, *Journal of Proteome Research*, 2006, **5**, 2956-2965.

19. F. Diehl, S. Grahlmann, M. Beier and J. D. Hoheisel, *Nucleic acids research*, 2001, **29**.

20. Y. Deng, X. Y. Zhu, T. Kienlen and A. Guo, *Journal of the American Chemical Society*, 2006, **128**, 2768-2769.

21. W. Norde and J. Lyklema, *Advances in Colloid and Interface Science*, 2012, **179–182**, 5-13.

22. M. Bohorquez, C. Koch, T. Trygstad and N. Pandit, *Journal of Colloid and Interface Science*, 1999, **216**, 34-40.

23. A. Kosmala, Q. Zhang, R. Wright and P. Kirby, *Materials Chemistry and Physics*, 2012, **132**, 788-795.

24. B. Fousseret, M. Mougenot, F. Rossignol, J.-F. Baumard, B. Soulestin, C. Boissière, F. Ribot, D. Jalabert, C. Carrion, C. Sanchez and M. Lejeune, *Chemistry of Materials*, 2010, **22**, 3875-3883.

25. K.-H. Lee, J.-W. Lee, S.-W. Wang, L.-Y. Liu, M.-F. Lee, S.-T. Chuang, Y.-M. Shy, C.-L. Chang, M.-C. Wu and C.-H. Chi, *J Vet Diagn Invest*, 2008, **20**, 463-471.

26. A. Isogai, M. Naito, Y. Ozaki, H. Nagashima and T. Enomae, *Journal of Imaging Science*, 2011, **55**, 20201-20208.

27. R. M. L. van Lieshout, T. van Domburg, M. Saalmink, R. Verbeek, R. Wimberger-Friedl, M. P. van Dieijen-Visser and C. Punyadeera, *Analytical Chemistry*, 2009, **81**, 5165-5171.

28. L. H. Mujawar, A. A. Maan, M. K. I. Khan, W. Norde and A. van Amerongen, *Analytical Chemistry*, 2013, **85**, 3723-3729.

29. V. Dugas, J. Broutin and E. Souteyrand, *Langmuir*, 2005, **21**, 9130-9136.

30. A. Wolter, R. Niessner and M. Seidel, *Analytical Chemistry*, 2007, **79**, 4529-4537.

31. M. E. Wiseman and C. W. Frank, *Langmuir*, 2012, **28**, 1765-1774.

32. W. Norde and D. Gage, *Langmuir*, 2004, **20**, 4162-4167.

33. A. K. Trilling, J. Beekwilder and H. Zuilhof, *Analyst*, 2013.

34. M. R. Nejadnik, A. L. J. Olsson, P. K. Sharma, H. C. van der Mei, W. Norde and H. J. Busscher, *Langmuir*, 2009, **25**, 6245-6249.

35. L. F. Pease, J. T. Elliott, D.-H. Tsai, M. R. Zachariah and M. J. Tarlov, *Biotechnol. Bioeng.*, 2008, **101**, 1214-1222.

7

Rapid mastitis detection assay on porous nitrocellulose membrane slides

Abstract

We have developed a rapid mastitis detection test based on the immobilization of tag-specific antibody molecules, the binding of double-tagged amplicons and as a secondary signal a conjugate of black carbon nanoparticles having molecules of a fusion protein of neutravidin and alkaline phosphatase at their surface. The antibodies were inkjet printed onto three different nitrocellulose membrane slides, Unisart (Sartorius), FAST (GE Whatman) and Oncyte-Avid (Grace-Biolabs) and the final assay signals on these slides were compared. The blackness of the spots was determined by flatbed scanning and assessment of the pixel grey volume using TotalLab image analysis software. The black spots could be easily read by the naked eye. We successfully demonstrated the detection of specific amplicons from mastitis causing pathogens in less than 3 hours. Using a similar protocol, we also showed that it was possible to detect specific amplicons from four different mastitis causing pathogens (6 strains) on the same pad. The influence of two different printing buffers, phosphate buffered saline (PBS, pH 7.4) and carbonate buffer (CB, pH 9.6) on the functionality of the primary antibodies was also compared.

7.1 Introduction

The application of antibody microarrays as a tool to detect pathogens is well known for the detection of food pathogens[1-3]. To produce microarrays various porous substrates like nitrocellulose[4], hydrogels[5], porous-silica[6] and alumina[7] have been used to produce high quality microarrays. As compared to non-porous substrate like glass[8] and polystyrene[9], these porous substrates provide a 3-D network[10] that increases the effective surface area to bind the capture biomolecule[5] resulting in increased signals and signal-to-noise (S/N) ratios[11]. Porous nitrocellulose membrane coated slides[4, 12] have been used extensively to produce biochips for diagnostic applications[13-15]. It has been shown previously that the assays performed on these substrates have a lower limit of detection as compared to 2-D substrates[16].

Mastitis is one of the most common intramammary diseases in dairy animals and can be caused by a wide range of pathogens[17]. We have used a mastitis detection test as a model to study microarray diagnostics in 3-dimensional nitrocellulose membranes. In the past, various mastitis detection methods such as the California mastitis test (CMT)[18], an ELISA for the laboratory detection of *Staphylococcus aureus*[19], and a PCR for the rapid diagnosis of *Escherichia coli*, *Staphylococcus aureus* and *Streptococcus agalactiae* have been reported [17]. For *Mycoplasma bovis* a real time PCR has been demonstrated by Cai and coworkers [20]. Advances in the field of biochips have also changed pathogen detection practices[21], disposable biochips have been developed by Moon and coworkers which can monitor the milk somatic cell count (SCC)[22]. We have developed a test method by combining a rapid PCR method with a user-friendly, nucleic acid microarray immunoassay (NAMIA) with colorimetric detection. This detection principle was also used by Lee *et al.*[23] for a biochip to detect various pathogens. Using a non-contact inkjet printer, a set of tag-specific antibodies

were printed on nitrocellulose membrane coated slides from three different manufacturers (GE Whatman, Sartorius and Grace-Biolabs). Following a PCR reaction with tagged primers, the double-tagged amplicons were sandwiched between the printed tag-specific antibodies and a carbon nanoparticles conjugate with a fusion protein between alkaline phosphatase and neutravidin in an one-step incubation. The final assay signal could be further enhanced by a short incubation with an alkaline phosphatase substrate solution resulting in a chromogenic precipitate on the sample spots. The NAMIA signal was read by a flatbed scanner[24] and the scanned images could be further analyzed by TotalLab image analysis software to measure the signal intensity in pixel grey volume (PGV).

7.2 Materials and methods

7.2.1 Reagents

Nanoparticles of carbon-alkaline phosphatase-neutravidin conjugates were prepared as described by Noguera *et al.*[14]. The substrate for the alkaline phosphatase was from Sigma (SigmaFAST BCIP/NBT). Streptavidin-Alexa-633 conjugate for labelling the biotinylated proteins was obtained from Invitrogen. Phosphate buffered saline (PBS), 150 mM, pH 7.4 and carbonate buffer (CB), (100 mM), pH 9.6 were prepared in Milli-Q water. Running buffer (100mM borate buffer containing 1% BSA and 0.05% Tween20) was used as a diluent for the conjugates / labels and also during the intermediate washing steps.

7.2.2 Biomolecules

Anti-Digoxigenin was purchased from Roche Diagnostics GmBH (Mannheim, Germany), anti-Fluoroisothiocynate from Bioconnect (Huissen, The Netherlands) and anti-Dinitrophenyl and anti-Texas red from Invitrogen (Oreagon, USA). Immunopure biotinylated bovine serum albumin (BSA-biotin)

was purchased from Thermo scientific (Rockford, USA). The DNA templates for the six different mastitis causing pathogens, *Staphylococcus aureus*, *Corynebacterium bovis*, *Mycoplasma bovis*, and *Streptococcus agalactiae*, *dysgalactiae* and *uberis* were provided by the Animal Health Service (GD) (Deventer, The Netherlands).

7.2.3 Substrates for printing biomolecules

Nitrocellulose (NC) membrane coated slides in a 16 pad format were used from three different manufacturers; Sartorius-Stedim Biotech, Göttingen, Germany (Unisart), Grace- Biolabs, Oregon, USA (ONCYTE® AVID 16) and GE-Whatman, Freiburg, Germany (FAST slide 16). The dimension of each pad was 6x6 mm whereas the thickness of FAST and Unisart slide was ~11 μm and that of Oncyte-Avid slide was ~9 μm, respectively.

7.2.4 Atomic force microscopy

The surface characteristics (topography and roughness) of various NC membranes was investigated by atomic force microscopy (Asylum MFP-3D, Santa Barbara, CA, USA) by scanning an area of 100 μm using tapping-mode (in air).

7.2.5 Printing

Anti-DIG, anti-DNP, anti-FITC, and BSA-biotin (positive control) were diluted in PBS (pH 7.4) or CB (pH 9.6) to 200 μg/mL, whereas anti-TR was diluted to a concentration of 500 μg/mL. The diluted sample (20 μL) was loaded into the wells of a Genetix microplate (384 wells). The biomolecules were printed on the three nitrocellulose membrane slides with a non-contact inkjet printer, sciFLEXARRAYER S3 (Scienion AG, Berlin, Germany). The printing of the biomolecules was performed at room temperature and at 70% humidity. Throughout the experiments, the robotic printer was programmed to print a droplet of ~250 pL. After printing, the NC substrates were dried under

controlled temperature (37°C) and humidity (~70%) in the Scienion sciProCLIMATE (Berlin, Germany) for 1 hour. The slides were stored overnight in a sealed aluminium pouch with a silica desiccant.

7.2.6 PCR reaction

The PCR protocol was optimized to 30 minutes using the Phire Hot Start polymerase (Finnzymes) and the Piko thermal cycler (Finnzymes). The PCR tube contained 0.4 µl Phire Hot Start DNA Polymerase, 1x Phire reaction buffer (final concentration $MgCl_2$: 1.5 mM), 200 µM dNTPs, 0.5 µM of each forward and reverse primer and 2 µl template in a total volume of 20 µl. The protocol consisted of an initial denaturation step at 98 ºC for 30 s followed by 35 cycles at 98°C for 5 s, 60°C for 5 s, 72°C for 10 s, and a final extension step at 72°C for 1 min. DNA templates for *Streptococcus agalactiae*, *dysgalactiae*, and *uberis* were amplified using primers SU-F2 and SU-R (2). *Staphylococcus aureus*, *Corynebacterium bovis*, and *Mycoplasma bovis* templates were amplified using primers[23] Au-F and Au-R, Cb-F2 and Cb-R3, Mb-F and Mb-R, respectively. Forward primers were labeled at the 5'-end with discriminating tags, digoxigenin (DIG), dinitrophenyl (DNP), Fluorescein amidite (FAM; bound by the anti-FITC antibody) and texas red (TR) (See Table 7.1). All reverse primers were labeled at the 5'-end with biotin. After the completion of the PCR reaction, and if specific template material was present, a double stranded amplicon was produced with two tags at each end. Gel electrophoresis confirmed the amplicons obtained after PCR reaction had correct band length[23].

Table 7.1 List of antibodies against mastitis causing pathogens with the set of primers showing the tags at the forward (F) and reverse (R) primer

Specific antibody	Micro organism	Primer	Sequence (5'- 3')	Forward tag	Amplicon size (bp)
Anti-DIG	*Staphylococcus*	Au-F	TTCGTACCAGCCAGAGGT	DIG	227
	aureus	Au-R	TTCAGCGCATCACCAAT	Biotin	
Anti-DNP$_1$	*Streptococcus*	SU-F2	AGCCGCCTAAGGTGGGAT	DNP	211
	agalactiae	SU-R	ATGGAGCCTAGCGGGATC	Biotin	
Anti-DNP$_2$	*Streptococcus*	SU-F2	AGCCGCCTAAGGTGGGAT	DNP	210
	dysgalactiae	SU-R	ATGGAGCCTAGCGGGATC	Biotin	
Anti-DNP$_3$	*Streptococcus*	SU-F2	AGCCGCCTAAGGTGGGAT	DNP	230
	uberis	SU-R	ATGGAGCCTAGCGGGATC	Biotin	
Anti -FITC	*Corynebacterium*	Cb-F2	CGTGCTTTAGTGTGTGCG	FAM	652
	bovis	Cb-R3	GGCACGGAAATCGTGGAAG	Biotin	
Anti -TR	*Mycoplasma*	Mb-F	GCTTCAGTATTTTGACGG	TR	302
	bovis	Mb-R	GGTTTAGCTCCATAACCAGA	Biotin	

7.2.7 Flatbed scanning

Spots stained by carbon conjugates were scanned on an Epson flat-bed scanner (Seiko Epson, Nagano, Japan) with a resolution of 128600 dpi and 16 bit grey-scale and the images were saved as TIFF-files. Spot intensities were scored as pixel gray volumes (PGV) as obtained by image analysis software (TotalLab, Nonlinear Dynamics, Newcastle upon Tyne, UK). The average PGV for five sample spots was measured and the coefficient of variation was calculated. Similarly, the background signal was also assessed by measuring the average PGV for five blank spots and its influence on the assay signal (signal-to-noise; S/N ratio) was studied.

7.4 Results and Discussion

7.4.1 Surface topography and roughness (AFM study)

We investigated the surface characteristics of the NC membranes from the three manufacturers, Sartorius (Unisart), Grace-Biolabs (Oncyte-avid), and GE

Whatman (FAST) by atomic force microscopy (Asylum MFP-3D, Santa Barbara, CA, USA). The surface topography of the bare NC membrane was analyzed (tapping-mode in air). The topography of the FAST slide was found to be irregular with high RMS roughness value (185 nm) as compared to the Oncyte-Avid slide (70 nm) and the Unisart slide (27 nm). The Unisart slide was found to be smoother in topography as compared to the other two NC membrane slides (see Figure 7.1).
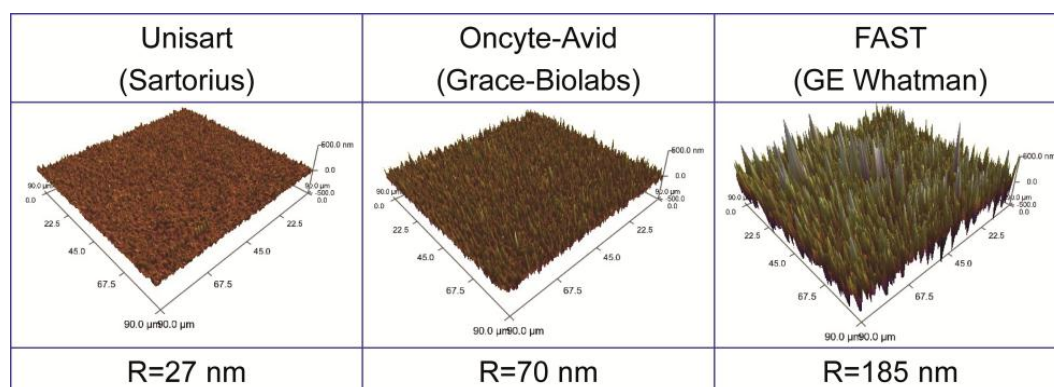

Unisart (Sartorius)	Oncyte-Avid (Grace-Biolabs)	FAST (GE Whatman)
R=27 nm	R=70 nm	R=185 nm

Figure 7.1 Surface topography (3-D) and roughness (R) of bare Unisart (Sartorius), Oncyte-avid (Grace-Biolabs), and Fast (GE Whatman) nitrocellulose membrane slides.

7.4.2 Nucleic acid microarray immunoassay (NAMIA)

The detection of various amplicons by the specific antibodies was determined by a Nucleic Acid Microarray ImmunoAssay (NAMIA)[4, 8, 9]. In this assay the double-labeled amplicons were sandwiched in an one-step incubation between the specific antibodies and carbon nanoparticles having alkaline phosphatase - neutravidin fusion protein molecules bound to their surface (see Figure 7.2).

The appearance of the black carbon nanoparticles on the immobilized antibody spots indicated the presence of amplicons with the respective anti-antibody tag at one end and biotin on the other end, and hence, the presence of the pathogen connected to this specific tag. The signal could be further amplified by a short incubation (5 minutes) with an alkaline phosphatase substrate solution that was

converted into precipitable dye molecules. The dark-black spots could be easily read by the naked eye.
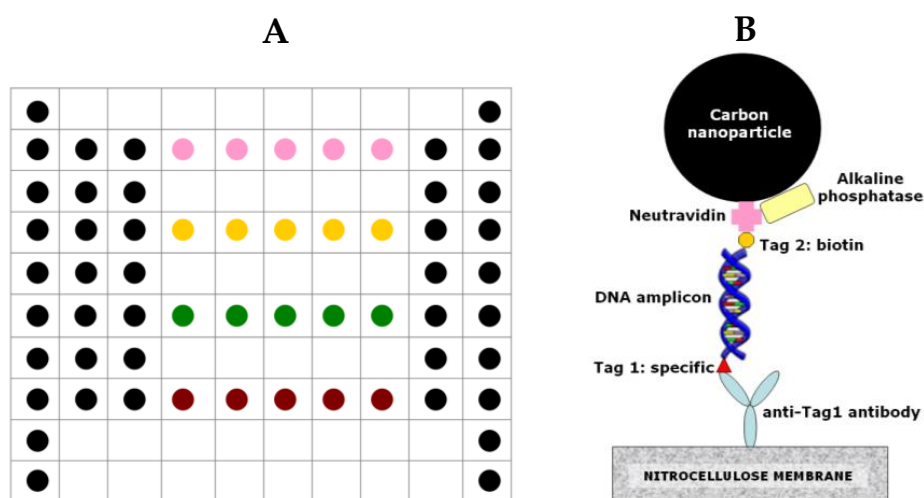

Figure 7.2 (A) Layout of mastitis microarray, ● Anti- DIG, ● Anti- DNP, ● Anti-FITC, ● Anti-TR and ● BSA-biotin (control). (B) Schematic representation for detection principle of NAMIA.

The NAMIA for mastitis detection showed that the PCR amplicon - carbon conjugate mixture bound specifically to the respective tag-specific antibodies and that no cross-reaction or non-specific binding of the amplicons was observed (Figure 7.3-top:Single amplicon detection). All the four antibodies (anti-DIG, anti-DNP, anti-FITC and anti-TR) showed a positive reaction against their respective mastitis pathogens with a good signal to noise ratio (S/N). The main advantage of this enhancement method was that the NAMIA spots (black-coloured sample spots) could be easily read by the naked eye without any high-tech readers. The use of such carbon nanoparticles (CNPs) functionalised with an alkaline phosphatase-neutravidin conjugate in developing a NAMIA had been successfully reported by Mujawar *et al.*[8, 9]. Also Noguera *et al.* used a similar technique, in that case for the detection of Shiga virulence factors[14].

Furthermore, we prepared in-house pooled PCR amplicon sample mixtures, and incubated the NC pads with these samples along with the carbon conjugate label. We found that we could easily and correctly detect multiple mastitis causing pathogens on the same pad (see Figure 7.3-A, B, C: Multiple amplicon detection). Further extension of this model would be to print more tag-specific antibodies and simultaneously detect more than six mastitis-causing pathogens in a given sample at the same time. The total assay time required for the specific detection of mastitis causing pathogen was less than 3 hours.
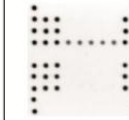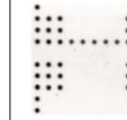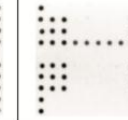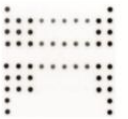
SINGLE AMPLICON DETECTION						
Anti-tag antibody	Anti-DIG	Anti-FITC	Anti-TR	Anti-DNP$_1$	Anti-DNP$_2$	Anti-DNP$_3$
Pathogen	*Staphylococcus aureus*	*Corynebacterium bovis*	*Mycoplasma bovis*	*Streptococcus agalactiae*	*Streptococcus dysagalactiae*	*Streptococcus uberis*
NAMIA results						

Figure 7.3 (top) A typical NAMIA result on the FAST slide showing positive results of single amplicon detection for anti-DIG *(S.aureus)*, anti-FITC *(C.bovis)*, anti-TR *(M.bovis)*, DNP$_1$ *(Strep.aga)*, DNP$_2$ *(Strep dys)*, DNP$_3$ *(Strep.ube).* Multiple amplicon detection of (A) *S.aureus* and *Strep.aga* (B) *S.aureus*, *Strep.dysgalactiae* and *C.bovis* (C) *S.aureus, Strep.ube, C.bovis and M.Bovis.*

7.4.3 NAMIA on various nitrocellulose substrates

A comparative study of the mastitis NAMIA was conducted on three different nitrocellulose membrane slides, Unisart (Sartorius), Oncyte-avid (Grace-Biolabs), and FAST (GE Whatman). On these NC membranes we also compared the influence of two different printing buffers, PBS (pH 7.4) and CB (pH 9.6) on

the functionality of the tag-specific antibodies. The printing protocol, microarray format and labelling procedure was similar to that explained before. In addition, the influence of alkaline phosphatase substrate solution on the PGV amplification (S/N ratio) and the background signal was studied and compared on different NC membrane slides.

In the absence of substrate incubation, the carbon labelled tag-specific antibodies showed a similar signal on all the NC membranes except for the anti-FITC antibody of which the signal was slightly higher as compared to other antibodies (see Figure 7.4-A, B).

Following a short incubation (5 min) with alkaline phosphatase solution, the PGV of the sample spots increased five-fold as compared to the PGV in the absence of substrate. However the PGV for anti-TR was lower than that for the other tag-specific antibodies (see Figure 7.4-C, D). The signal (PGV) for all the tag-specific antibodies was higher when PBS (pH 7.4) was used as the printing buffer as compared to CB (pH 9.6) (See Figure 7.4-C, D). The influence of various printing buffers on the functionality of antibodies bound to porous NC substrates has been well documented by Karoonuthaisiri et al.[25]. Also these authors found that a superior S/N ratio was obtained on NC substrates when PBS (pH 7.4) was used as a printing buffer.

We have used three different slides with similar surface chemistry (i.e., nitrocellulose), but our results show that irrespective of the printing buffer used for depositing antibodies onto various NC membrane slides, the absolute PGV values were higher on FAST and Oncyte-Avid slides as compared to Unisart slides. The observed differences in the signal may be due to the variation in the membrane properties like roughness, morphology and pore size, which influences the protein binding to the substrate. As shown in figure 7.1, the morphology as well as the surface roughness of the various NC membrane

slides were found to be different from one another. The higher surface roughness for FAST and Oncyte-Avid slides will increase binding capacity per surface area. Indeed, Kim *et al.* have shown that the immobilization of protein molecules improved with increasing surface roughness since higher roughness increased the surface area for protein immobilization[7].
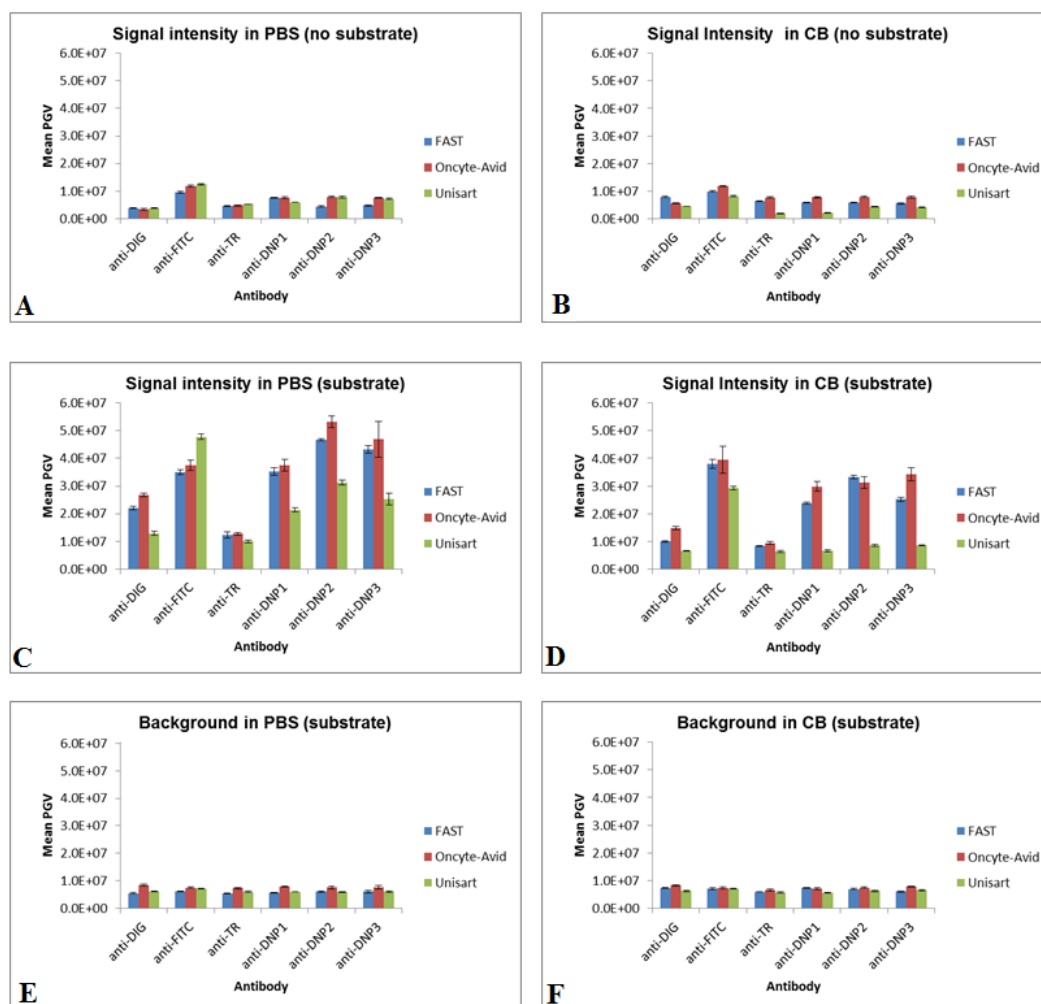

Figure 7.4 Average pixel gray volume for five spots was on various NC membrane slides for (A) Signal intensity in PBS (without substrate), (B) Signal intensity in CB (without substrate), (C) Signal intensity in PBS (with substrate), (D) Signal intensity in CB (with substrate), (E) Background signal in PBS (with substrate), (F) Background signal in CB (with substrate).

It has been known that additives are incorporated during production of nitrocellulose membranes[26], which may also influence the performance of the immunoassay. Moreover, Ahmad *et al.* have also shown that the binding of the protein molecules is influenced by membrane morphology[27].

The order of the functionality of the tag-specific antibodies in PBS (pH 7.4) on the FAST and the Oncyte-Avid slides was anti-DNP>anti-FITC>anti-DIG>anti-TR and on the Unisart slide the trend was anti-FITC>anti-DNP>anti-DIG>anti-TR. In addition, on all the NC membrane slides, the background signal was approximately similar and the background PGV values were much lower than the final assay signal, indicating good signal-to-noise ratios (see Figure 7.4-E, F).

Upon printing biomolecules bind efficiently to the nitrocellulose matrix and maintain a good functionality[11, 28]. The influence of the 3-D matrix on the assay signal has been well explained by Dufva *et al.*[10]. It was also reported that on such porous substrates, the loss of biomolecules upon rinsing was less[15] as compared to non-porous substrates. Comparison with a similar NAMIA test on glass slides[8] (having a range of hydrophobic surfaces) and polystyrene[9] (HTA slides) reported by Mujawar *et al.* learns that on the porous nitrocellulose substrate the S/N ratio is superior to that on non-porous substrates. The larger surface area of the 3-D substrates prevents aggregation[29] of printed protein molecules as compared to non-porous substrates, which signifies the importance of porous NC substrates for diagnostic applications.

7.5 Conclusions

We have developed a rapid (less than 3 hours) mastitis detection test for four pathogenic microorganisms (6 strains) based on the immobilization of tag-specific antibody molecules, the binding of double-tagged amplicons and as a secondary signal conjugate black carbon nanoparticles having molecules of a

fusion protein of neutravidin and alkaline phosphatase at their surface. The antibodies were inkjet printed onto three different nitrocellulose membrane slides, Unisart (Sartorius), FAST (GE Whatman) and Oncyte-Avid (Grace-Biolabs) and final assay signals were compared by flatbed scanning and assessment of the pixel gray volume. Phosphate buffered saline, pH 7.4, appeared to be a better printing buffer for a better functionality of the primary antibodies as compared to carbonate buffer, pH 9.6.

References

1. A. M. Foudeh, T. Fatanat Didar, T. Veres and M. Tabrizian, *Lab on a Chip*, 2012, **12**, 3249-3266.

2. M. Kostrzynska and A. Bachand, *Canadian Journal of Microbiology*, 2006, **52**, 1-8.

3. M. Seidel and R. Niessner, *Analytical and Bioanalytical Chemistry*, 2008, **391**, 1521-1544.

4. P. S. Noguera, G. A. Posthuma-Trumpie, M. van Tuil, F. J. van der Wal, A. d. Boer, A. P. H. A. Moers and A. van Amerongen, *Analytical Chemistry*, 2011, **83**, 8531-8536.

5. J. C. Miller, H. Zhou, J. Kwekel, R. Cavallo, J. Burke, E. B. Butler, B. S. Teh and B. B. Haab, *Proteomics*, 2003, **3**, 56-63.

6. A. Ressine, G. r. Marko-Varga, T. Laurell and M. R. El-Gewely, in *Biotechnology Annual Review*, Elsevier, 2007, vol. Volume 13, pp. 149-200.

7. S. Y. Kim, J. Yu, S. J. Son and J. Min, *Ultramicroscopy*, 2010, **110**, 659-665.

8. L. H. Mujawar, W. Norde and A. v. Amerongen, *Analyst*, 2012.

9. L. H. Mujawar, A. van Amerongen and W. Norde, *Talanta*, 2012, **98**, 1-6.

10. M. Dufva, *Biomolecular Engineering*, 2005, **22**, 173-184.

11. J.-G. Walter, F. Stahl, M. Reck, I. Praulich, Y. Nataf, M. Hollas, K. Pflanz, D. Melzner, Y. Shoham and T. Scheper, *Eng. Life Sci.*, 2010, **10**, 103-108.

12. B. A. Stillman and J. L. Tonkinson, *BioTechniques*, 2000, **29**, 630-635.

13. J. Petrik, *Transfusion Medicine*, 2006, **16**, 233-247.

14. P. S. Noguera, G. A. Posthuma-Trumpie, M. van Tuil, F. J. van der Wal, A. d. Boer, A. P. H. A. Moers and A. van Amerongen, *Analytical Chemistry*, **83**, 8531-8536.

15. T. Kukar, S. Eckenrode, Y. Gu, W. Lian, M. Megginson, J.-X. She and D. Wu, *Analytical Biochemistry*, 2002, **306**, 50-54.

16. M. Reck, F. Stahl, J. G. Walter, M. Hollas, D. Melzner and T. Scheper, *Biotechnolgy Progress*, 2007, **23**, 1498-1505.

17. M. T. Koskinen, J. Holopainen, S. Pyörälä, P. Bredbacka, A. Pitkälä, H. W. Barkema, R. Bexiga, J. Roberson, L. Sølverød, R. Piccinini, D. Kelton, H. Lehmusto, S. Niskala and L. Salmikivi, *Journal of Dairy Science*, 2009, **92**, 952-959.

18. S. Pyorala, *Veterinary Research*, 2003, **34**, 565-578.

19. L. K. Fox and D. S. Adams, *Journal of Veterinary Medicine, Series B*, 2000, **47**, 517-526.

20. H. Y. Cai, P. Bell-Rogers, L. Parker and J. F. Prescott, *Journal of Veterinary Diagnostic Investigation*, 2005, **17**, 537-545.

21. J. L. Garcia-Cordero, A. J. Ricco and D. Li, Springer US, 2008, pp. 962-969.

22. J. S. Moon, H. C. Koo, Y. S. Joo, S. H. Jeon, D. S. Hur, C. I. Chung, H. S. Jo and Y. H. Park, *Journal of Dairy Science*, 2007, **90**, 2253-2259.

23. K.-H. Lee, J.-W. Lee, S.-W. Wang, L.-Y. Liu, M.-F. Lee, S.-T. Chuang, Y.-M. Shy, C.-L. Chang, M.-C. Wu and C.-H. Chi, *J Vet Diagn Invest*, 2008, **20**, 463-471.

24. M. Lönnberg and J. Carlsson, *Analytical Biochemistry*, 2001, **293**, 224-231.

25. N. Karoonuthaisiri, R. Charlermroj, U. Uawisetwathana, P. Luxananil, K. Kirtikara and O. Gajanandana, *Biosensors and Bioelectronics*, 2009, **24**, 1641-1648.

26. A. L. Ahmad, S. C. Low, S. R. A. Shukor and A. Ismail, *Journal of Applied Polymer Science*, 2008, **108**, 2550-2557.

27. A. L. Ahmad, S. C. Low, S. R. A. Shukor and A. Ismail, *Journal of Immunoassay and Immunochemistry*, 2011, **33**, 48-58.

28. E. J. Irvine, A. Hernandez-Santana, K. Faulds and D. Graham, *Analyst*, 2011, **136**, 2925-2930.

29. P. Arenkov, A. Kukhtin, A. Gemmell, S. Voloshchuk, V. Chupeeva and A. Mirzabekov, *Analytical Biochemistry*, 2000, **278**, 123-131.

8

General Discussion

In this chapter we discuss the theme of the thesis with respect to the learning aspects of the project, the utilization of results for inkjet printing (including recommendations) and the possible challenges for the future. The chapter concludes with a summary of the thesis.

8.1 General discussion

Ever since the printing technique was used, various modes of contact and non-contact printing techniques for deposition of (bio)molecules have been demonstrated. The advancement towards non-contact inkjet printing technology was a boon to molecular biologists, in particular diagnostic researchers, since it became possible to study complex biological systems using a very small volume of biomolecules. In bioassays, the distribution of printed biomolecules on the substrate surface and their functionality are the key issues to be investigated. This brings us to the aim of this project: elucidating the queries on distribution and functionality and how our findings can be utilized in the diagnostic area.

8.1.1 Learning aspects and utilization of results for inkjet printing applications

The progress of the inkjet printing technology made the application of DNA microarrays a common practice, but the production of functional microarrays for more complex and fragile molecules like proteins is still a big challenge. The charge-dependent behaviour of protein molecules in various solvents and onto different substrate surfaces makes the process of printing protein molecules more complicated. Upon deposition these biomolecules tend to undergo conformational changes[1], which may result in reduced functionality, essentially more easily as compared to DNA molecules. Therefore, to produce functional microarrays, it is important to suppress conformational alterations in the deposited biomolecules by optimizing the printing conditions. On the other hand, the application of inkjet printing for producing microarrays in diagnostic research[2] contrived researchers to produce biochips on cheap and inexpensive sources of substrates like polystyrene[3] and glass[4].

8.1.1.1 Non-porous substrates

In order to print protein molecules on such non-porous substrates, several parameters like the composition and pH of the printing buffer, substrate hydrophobicity and substrate chemistry play an important role in the distribution and functionality of the printed biomolecule. For protein applications, phosphate buffered saline, PBS, (pH 7.4) is commonly used, but it has been realized that the high saline content of PBS causes salt crystallization and spot smearing[5], which affects the spot morphology and, in turn, the bioassay signal distribution[3]. These issues were eliminated by choosing an appropriate printing buffer, in our case carbonate buffer, CB, (pH 9.6), which ensures high quality printed spots with good signal-to-noise (S/N) ratio[3].

The wettability of non-porous substrate is another important variable that influences the distribution of inkjet printed biomolecules and the signal-to-noise ratio of the bioassay. On pristine glass, the hydrophilicity of the substrate results in low binding and irregular spot morphology. However, this problem could be rectified by printing the biomolecules on glass substrates that were modified by reducing their hydrophilicity. Increasing the substrate hydrophobicity improved the binding of the biomolecules. However, the distribution and functionality of the printed biomolecules is not directly proportional to the degree of hydrophobicity. For an optimal distribution and superior S/N ratio, the substrate should be of intermediate hydrophobicity (i.e., a water contact angle (θ) ~75°)[4]. On the other hand, even though substrates had similar hydrophobicities, the surface chemistry also plays a role in the distribution of the inkjet printed biomolecules. As explained in Chapter 3, the hydrophobicities of HMDS and polystyrene slides were similar, but the signals, as measured by confocal laser scanning microscopy (CLSM) and TotalLab analysis, showed that the biomolecules printed on HTA polystyrene slides

resulted in a superior spot morphology and higher S/N ratio as compared to those on silanized glass.

Another important parameter that influences the distribution of inkjet printed biomolecules onto a substrate surface is the rate of evaporation of the droplet deposited on the surface. Explanation provided by Deegan *et al.*[6] showed the importance of evaporation and its influence on the formation of doughnut-shaped spots. At low relative humidity, the droplet is pinned on the surface and a higher evaporation rate at the edges of the drop causes internal convection due to which more mass migrates to the edge resulting in a doughnut-shaped spot. However, when a similar droplet is allowed to evaporate at a higher relative humidity, the slower rate of evaporation causes less convection allowing the dissolved biomolecules more time to get adsorbed onto the substrate surface in a more even distribution. An optimal distribution of the biomolecules in the spot can be obtained by evaporating the inkjet printed droplets at a relative humidity close to ~70%. Hence, without the incorporation of any additives, the spot morphology of inkjet printed microarrays can be improved by choosing the right conditions such as the buffer, the surface characteristics and the relative humidity.

8.1.1.2 Porous substrates

Moving from non-porous substrates to a porous substrate, like nitrocellulose (NC), leads to a significant change in the distribution and functionality of biomolecules. The 3-D matrix of nitrocellulose membranes imparts a high surface to volume ratio[7] due to which more biomolecules bind per unit volume as projected per unit surface area. It was observed that both the signal and the signal-to-noise ratio are superior as compared to non-porous substrates. However, on NC membrane pads produced by different manufacturers, e.g., GE Whatman (FAST), Sartorius (Unisart) and Grace-Biolabs (Oncyte-Avid),

spot morphologies of the inkjet printed microarrays were observed to be different. While manufacturing NC membranes, wetting agents are being incorporated and these additives play a role in the spreading of the drop on the substrate and the distribution of the biomolecules in the membrane. High-speed camera analysis confirmed that the spreading of liquid on/in Oncyte-Avid NC membranes was slower as compared to the FAST and Unisart slides. Due to this slow wetting the biomolecules moved along the contact line slowly and deposited more homogenously within a confined space, whereas in FAST and Unisart membranes, due to the fast spreading of the liquid drop, a higher number of biomolecules travelled along with the liquid flow towards the edges. The influence of hydrophobicity of porous substrates in suppressing the non-homogenous distribution has been explained by Ressine *et al.*[5, 8]. Even though the NC membranes on Oncyte-Avid slides showed slow spreading, the penetration of the liquid was faster than in the FAST and Unisart slides, due to which the biomolecules penetrated deeper into the Oncyte-Avid membrane and were distributed in more layers of the NC matrix.

To prevent doughnut-shaped spot morphology of inkjet printed antibody microarrays it is very important to understand how printing conditions with respect to buffer pH, relative humidity and substrate hydrophobicity influence the characteristics of inkjet printed biomolecules and, hence, of spots on substrate surfaces. It is known that incorporation of additives into the printing buffer assists in more uniformly distributing inkjet printed biomolecules in a spot[9, 10]. However, these additives may also have a negative influence on the functionality of the printed biomolecule. It has been shown that microarrays produced in the presence of the amphiphilic surfactant Pluronic F127 not only showed improved spot homogeneity, but also resulted in signal enhancement of the bioassay[11]. A possible explanation for the improved signal of the bioassay could be the proper orientation of the deposited antibody molecules as

described by Norde and Lyklema[12]. In their hypothesis the polypropylene oxide (PPO) part of the Pluronic molecule binds to the NC matrix whereas the two polyethylene oxide (PEO) parts form brush-like structures. At an optimum concentration, the density of Pluronic molecules on the surface is tuned such that the space between two Pluronic molecules allows docking of the F*c* part of the IgG molecule, whereas this is impossible for the more bulky (F*ab*)$_2$ region, thus resulting in a upright orientation i.e., F*ab*-UP. Consequently, the accessibility of the F*ab* sites to the incoming antigens is increased and this will also improve the sensitivity of the bioassay. The influence of Pluronic F127 to improve the bioassay signal (i.e., S/N ratio) was also demonstrated by Wolter *et al.*[13]. A superior S/N ratio was observed when the concentration of Pluronic F127 was 0.2 % (w/v), i.e., when the surface coverage by the Pluronic molecules is sufficient to orient most of the antibody molecules in the F*ab*-UP orientation.

In view of the foregoing considerations we arrive at the following recommendations:

- For producing microarrays on polystyrene-based substrates, the use of carbonate buffer, CB (pH 9.6) is to be preferred over more commonly used phosphate buffered saline, PBS (pH 7.4).

- For producing biochips on non-porous substrates like glass, intermediate water wettability (θ~75°) promotes a more homogenous distribution, resulting in a higher signal-to-noise ratio.

- Homogeneity of spot morphology can be optimized by drying the printed microarrays at a relative humidity of 60-70%.

- Spot homogeneity of inkjet printed biomolecules on NC membranes can be improved by producing microarrays on substrates with a low wettability.

- Pluronic F127 as additive serves two main objectives: a more homogenous spot morphology and an improved signal-to-noise ratio.

8.1.3 Future challenges

While working on this project, we came across some observations, which may be carried forward as a new step in the inkjet printing research. As already shown in Chapter 2, upon printing, the biomolecules in the drying droplet accumulate in multilayers on top of the surface. These multilayer stacks tend to be washed away upon rinsing, leaving behind a monolayer that is adsorbed onto the substrate surface. Hence, a significant amount of the precious biomolecules is wasted. It would be worth to investigate the maximum concentration required for printing in order to prevent the formation of multilayers and, thereby, loss upon rinsing. Moreover, if an inkjet printed platform would not be rinsed before addition of the sample with the antigens, a lot of antigen molecules could bind to printed biomolecules in the multilayer stacks and be removed in the first wash step. This would lead to a substantial decrease in assay sensitivity. It further underpins the importance of optimizing the concentration of biomolecules in the inkjet printed droplet.

'Z' stack analysis of the microarray spots down into the ~11 µm thick membranes showed that the printed biomolecules were confined in the top layers of the NC matrix (i.e., biomolecules penetrate only 6-7 µm) leaving 40% of the space unoccupied (see Chapter 5). One can optimize the concentration of the printed biomolecule with respect to the thickness of the membrane pads so that the space is more effectively occupied and investigate the influence on the signal and sensitivity of the bioassay.

As we observed that microarrays printed on various nitrocellulose membrane slides showed differences in the spot morphology, our study can be carried forward by testing NC membrane substrates of various porosities and

chemistries (including additives). The next step is to study the distribution of printed biomolecules as a function of substrate porosity and chemistry. Unfortunately, chemistries are generally not disclosed by the companies manufacturing nitrocellulose membranes.

References

1.   R. A. Vijayendran and D. E. Leckband, *Analytical Chemistry*, 2000, **73**, 471-480.

2.   M. Hartmann, J. Roeraade, D. Stoll, M. F. Templin and T. O. Joos, *Analytical and Bioanalytical Chemistry*, 2009, **393**, 1407-1416.

3.   L. H. Mujawar, A. van Amerongen and W. Norde, *Talanta*, 2012, **98**, 1-6.

4.   L. H. Mujawar, W. Norde and A. van Amerongen, *Analyst*, 2013, **138**, 518-524.

5.   A. Ressine, G. r. Marko-Varga, T. Laurell and M. R. El-Gewely, in *Biotechnology Annual Review*, Elsevier, 2007, vol. Volume 13, pp. 149-200.

6.   R. D. Deegan, O. Bakajin, T. F. Dupont, G. Huber, S. R. Nagel and T. A. Witten, *Nature*, 1997, **389**, 827-829.

7.   M. Dufva, *Biomolecular Engineering*, 2005, **22**, 173-184.

8.   A. Ressine, D. Finnskog, G. Marko-Varga and T. Laurell, *NanoBiotechnology*, 2008, **4**, 18-27.

9.   V. Dugas, J. Broutin and E. Souteyrand, *Langmuir*, 2005, **21**, 9130-9136.

10.   Y. Deng, X. Y. Zhu, T. Kienlen and A. Guo, *Journal of the American Chemical Society*, 2006, **128**, 2768-2769.

11.   M. E. Wiseman and C. W. Frank, *Langmuir*, 2012, **28**, 1765-1774.

12.   W. Norde and J. Lyklema, *Advances in Colloid and Interface Science*, 2012, **179–182**, 5-13.

13.   J.-G. Walter, F. Stahl, M. Reck, I. Praulich, Y. Nataf, M. Hollas, K. Pflanz, D. Melzner, Y. Shoham and T. Scheper, *Eng. Life Sci.*, 2010, **10**, 103-108.

Summary

Inkjet printing is an efficient technique to deposit a range of colloidal particles onto substrate surfaces. In the last few decades, the application of inkjet printing has been employed in diagnostic research to apply biomolecules onto porous and non-porous substrates. Due to the influence of various parameters like the solvent composition, the rate of evaporation and the substrate properties (wettability and porosity) on the distribution and functionality of the inkjet printed biomolecules it is a fascinating research area and also the main focus of this thesis. This dissertation addresses the above-mentioned queries, which have been reported after careful experimentation, and interpretation of the results based on various physical, chemical, analytical and microscopic analyses.

In **chapter 2** we studied the influence of printing buffers on spot morphology and functionality of inkjet printed biomolecules on a non-porous polystyrene substrate. Spots of biotinylated protein molecules printed in PBS showed a tailing appearance commonly called 'spot-smearing' whereas those in CB were more regular and compact. The irregular spot morphology appeared to be mainly due to the presence of a high NaCl content in the PBS buffer. The high salt content resulted in a co-crystallization with the biomolecules, this being the main reason for spot-smearing. Obviously, this is unacceptable in diagnostic research, as a non-homogeneous signal distribution reduces the (data) output quality. Based on our experimental data we recommend that, upon printing onto a hydrophobic substrate, the printing buffer should be carbonate buffer (CB) (pH 9.6). This results in a more even spot morphology with a superior signal to noise ratio as compared to PBS. On hydrophobic polystyrene substrates, we also compared the performance of a nucleic acid microarray immunoassay (NAMIA) with different buffers. Here too, higher signal intensity

and superior spot quality was achieved when CB (pH 9.6) was used instead of PBS (pH 7.4) as a printing buffer.

In **chapter 3** we examined the influence of the hydrophobicity of non-porous substrates on the distribution of inkjet printed biomolecules. Furthermore, the influence of the hydrophobicity on the functionality of the adsorbed biomolecules was studied. Following inkjet printing of biotinylated BSA and IgG on a series of hydrophobic glass (θ ~49°-103°) and polystyrene substrates, the distribution of these biomolecules, the total fluorescence intensity and the spot uniformity were analyzed by confocal laser scanning microscopy. The functionality of the printed biomolecules was judged by performing a two-step diagnostic antibody assay. Results showed that the distribution of printed biomolecules and the signal of the assay were superior on HTA polystyrene slide and the glass substrate silanized with PhECS (θ ~75°) as compared to glass slides with other hydrophobicities. These results can be used to rationalize and optimize the development of diagnostic protein microarrays.

In **chapter 4** we studied the effect of the rate of evaporation on the distribution of the inkjet printed biomolecules on a non-porous substrate. Fluorophore-labeled biomolecules were printed and dried at various relative humidities ranging from ~40% to ~80%, respectively. It was observed that at a low humidity, the printed biomolecules were non-homogeneously distributed, thus resulting in doughnut-shaped spots. With increasing relative humidity, a more homogeneously distributed spot morphology was achieved. The best morphological results were obtained at a relative humidity of 70%, but with respect to mean and total fluorescence intensities we concluded that the optimum relative humidity for printing biomolecules onto non-porous substrates is between 60-70%. The experimental results confirmed the data from

a numerical simulation of the influence of the relative humidity on the mass distribution of inkjet-printed biomolecules on non-porous substrates.

In **chapter 5** our studies related to the distribution of inkjet printed biomolecules on porous nitrocellulose substrates are discussed. Slides from three different manufacturers, namely Oncyte-Avid (Grace-Biolabs), FAST (GE Whatman) and Unisart (Sartorius), were compared. The distribution and spot homogeneity was more uniform on Oncyte-Avid (Grace-Biolabs), as compared to the FAST (GE Whatman) and Unisart (Sartorius) slides, on which doughnut-shaped spots were observed. The differences in spot morphology and biomolecule distribution could be partly explained by different substrate properties, i.e., wettability and fluid flow dynamics. Using high-speed cameras the behavior (spreading and penetration) of a sessile droplet on the porous substrates could be monitored.

Chapter 6 presents the application of the amphiphilic surfactant Pluronic F127 to overcome a non-homogenous distribution of inkjet printed antibodies and to enhance a preferred orientation of the deposited IgG molecules. CLSM data (10x) confirmed that in the presence of Pluronic F127 the biomolecules distributed more uniformly across and down into the NC membrane (confirmed by 'Z' stack analysis) yielding a more homogeneous spot morphology. Based on a diagnostic antibody assay it was shown that the mean fluorescence intensity enhanced by four times when the concentration of Pluronic F127 in the printing buffer was 0.2% (w/v). It was concluded that incorporation of Pluronic F127 in the printing buffer not only improves the distribution, but also helps the antibody molecules to achieve the preferred orientation i.e., *Fab*-UP. Thus the accessibility of the incoming antigen to the F*ab* sites is increased which improves the signal of the bioassay.

In **chapter 7** we present a biochip for a diagnostic application, the design of which is based on results discussed in the foregoing chapters. We showed that it is possible to specifically detect six mastitis causing pathogens in less than 3 hours with a Nucleic Acid Microarray ImmunoAssay (NAMIA). Tag-specific antibodies were printed on various Oncyte-Avid (Grace-Biolabs), FAST (GE Whatman) and Unisart (Sartorius) nitrocellulose membranes, mounted on slides, and a two-step assay was performed using carbon nanoparticles conjugated to a fusion protein of neutravidin and alkaline phosphatase. A superior S/N ratio was observed on FAST and Oncyte-Avid slides when PBS (pH 7.4) was used as a printing buffer.

Acknowledgement

It's hard to find words and more harder to put into sentence for all of those who have contributed their time, hard-work, patience and helped me to finish this thesis.

First of all I would like to dedicate this thesis to my father who had a dream of seeing me with a doctorate degree, *'Papa this is for you'*. I would like to thank my darling Banoma who stood as a solid rock during these period. I want to extend my deepest gratitude to my dear Courtmamu, Ammi, Khala and Chacha for always remembering me in your prayers. My sweet Aapa, Dr. Sami, your moral support always made me feel comfortable. Shanu and Sidraah, your funny acts made me forget all my worries whenever I met you or heard about you.

I want to express my sincere gratitude for my both supervisors; Prof. Willem Norde and Dr. Aart van Amerongen for their immense support and faith. Willem, your calm attitude made me feel very relax and helped me to express my views in front of you. Dear Aart (Sahib), for me you are a sharp and creative scientist and I will always admire you for this. Every time I used to ask for 5 minutes (for discussion) but it used to always much more than that. I thank you for all the time and efforts you spend in the success of this project.

A special thanks to Prof. Hans Kuerten, Hans Dijk, Frits Dijksman, Isakandar Gandasasmita, Anke Pierik, Rik De Wijn and Herman Wijshoff from the STW user committee, whose valuable suggestion helped me to improve the quality of my thesis. And I would also like to extend my gratitude for Daniel Siregar for helping me with modeling related studies.

I would like to thank the members of my second home, Fysko, where I spend most of my time. Josie, your smiling face was the first thing I used to see whenever I entered the department and I thank you for your encouragement.

Remco, thanks for helping me with the reflectometer and goniometer and thanks for Mara as well for helping me with ordering of the chemicals. I would also like to thank other faculty members for their valuable contribution during the group meetings and administrative staff for their help.

I would like to thank my FBR group members as well, Jan (for your helping nature and nice jokes, chats), Twan (for helping me with molecular biology stuffs), Truus (introducing me to the microarrayer). I would also like to thank Heelen, Marjo, Louise, Lucienne for their kind support.

Life is not complete in Wageningen without friends and I was lucky enough to have national and many international friends. I would like to thank Soumi (for being my paranymph) and Surender for encouraging me during these years. Saurabh, how can I forget the memorable Budapest trip? I had lots of nice moments with you and Shruti bhabhi. Dr. Thiyagarajan, you were a great support for me since whenever I needed any help, you were the first person to whom I approached, Thanks man…thanks a lot. And thanks to Smita bhabhi, Varsha and Dev (I enjoy his mischiefs). I would also like to thanks to Dr. Kakanth whom I respect for his ever-polite nature. I would also like to extend my thanks for my ORC friends, Sidhu, Satish, Umesh, Dr. Saurav and Nagendra for all the nice talks and chats in the corridor.

Dear Khanji, Maanji, Ustaad, Paai you were an integral part of my stay. Because of all of you, I never felt alone in Wageningen. I would also like to thank Masood, Shahji[2], Imran, Shahid for all the fun we had during playing cricket. Sami (FPE), thanks for always helping me in learning Turkish language, I will miss it.

Fysko being an international department made an easy circle of good colleagues/friends like Dimitry, Yunus, Armando with whom I spend most of my time while travelling and sport activities. I would like to mention special

About the author

Liyakat Hamid Mujawar was born in Wai (India) on 21st September, 1980. He completed his secondary school from Mumbra in 1996. and higher secondary studies from S.K. Somaiya College, Mumbai in 1998. Later in the same year he was admitted for the Bachelors programme of University of Mumbai and was graduated in 2001 with Microbiology and Biochemistry as his major subjects. Immediately after graduation he enrolled for MSc course (Biochemistry) at Seth G.S. Medical College (University of Mumbai) and was awarded MSc degree in June 2003. After post-graduation he worked for two years as a microbiologist in a pharmaceutical industry. But his interest towards applied research inspired him to join I.I.T. Bombay where he worked as a Research Assistant and was first introduced to the world of biosensors. He worked on disposable glucose biosensor and biosensor for *E.coli* monitoring in potable water. In the year 2009 he joined the Department of Physical Chemistry and Colloid Science at Wageningen University to work on STW funded PhD project under the supervision of Prof. Willem Norde and Dr. Aart van Amerongen. His doctorate thesis is about 'Biomolecule Substrate Topography of Inkjet Printed Structures'. The results of this research are presented in this thesis.

Liyakat can be reached through liyakat.mujawar@gmail.com.

List of Publications

This Thesis

- **L.H. Mujawar**, A. van Amerongen, W. Norde, Influence of buffer composition on the distribution of inkjet printed protein molecules and the resulting spot morphology, **Talanta**, 98 (2012) 1.

- **L.H. Mujawar**, W. Norde, A. van Amerongen, Spot morphology of non-contact printed protein molecules on non-porous substrates with a range of hydrophobicities, **Analyst**, 138 (2013) 518.

- **L.H. Mujawar**, A.A. Maan, M.K.I. Khan, W. Norde, A. van Amerongen, Distribution of Biomolecules in Porous Nitrocellulose Membrane Pads Using Confocal Laser Scanning Microscopy and High-Speed Cameras, **Analytical Chemistry**, 85 (2013) 3723.

- **L.H. Mujawar**, A. van Amerongen, W. Norde, Influence of Pluronic F127 on the distribution and functionality of inkjet printed biomolecules in porous nitrocellulose substrates. **(Submitted)**

- **L.H. Mujawar**, W. Norde, A. van Amerongen, Rapid mastitis detection assay on porous nitrocellulose membrane slides. **(Submitted)**

- **L.H. Mujawar**, J. G. M. Kuerten, D.P. Siregar, A. van Amerongen, W. Norde, Influence of the relative humidity on the morphology of inkjet printed spots on a non-porous substrate. **(Submitted)**

Other work

- M.K.I. Khan, **L.H. Mujawar**, M.A.I. Schutyser, K. Schroën, R. Boom, Deposition of Thin Lipid Films Prepared by Electrospraying, **Food and Bioprocess Technology** (2012) 1.
- A. A. Maan, S. Sahin, **L. H. Mujawar**, R. Boom and K. Schroën, **Journal of Colloid and Interface Science** (2013) dx.doi.org/10.1016/j.jcis.2013.04.036

Overview of completed training activities

Discipline specific

Advanced Soft Matter (2009)

Statistical thermodynamics (2011)

Conferences/ Symposia/ Congress

X[th] International Conference on AgriFood Antibodies, Wageningen, The Netherlands (2009)

Micro Nano Conference, Delft, The Netherlands (2009)

Rapid Methods Europe, Noordwijkerhout, The Netherlands (2010)

Biosensors 2010, Glasgow, UK (2010)

European Association Veterinary Laboratory Diagnosticians (EAVLD), Lelystad, The Netherlands (2010)

Rapid Methods Europe, Noordwijkerhout, The Netherlands (2011)

243rd ACS National Meeting , San Diego, California, USA (2012)

General courses

Philosophy and Ethics of Food Science and Technology (2009)

PhD competence assessment (2010)

Techniques for writing scientific and presenting scientific paper (2011)

Optionals

Fysko PhD trip to Singapore, Malaysia and Vietnam (2011)

Fysko group meetings (weekly)

STW project meetings (Bi-yearly)